To the Graduate Council :

I am submitting this dissertation written by Mohammed Abu-Shehadeh entitled " A Dynamic Model for the Advanced Neutron Source Reactor Including the Xenon Oscillation and the Utilization of Optimal Control as a Diagnostic Tool." I have examined the final copy of this dissertation for form and content and recommend that it be accepted in partial fulfillment of the requirements for the degree of Doctor of Philosophy, with a major in Nuclear Engineering.

R. Perez, Major Professor

We have read this dissertation
and recommend its acceptance :

L Z Miller

B R Upadhyaya

Accepted for the Council

Vice Provost and Dean of
The Graduate School

A Dynamic Model for the Advanced Neutron Source Reactor Including the Xenon Oscillation and the Utilization of Optimal Control as a Diagnostic Tool

A Dissertation
Presented for the
Doctor of Philosophy
Degree
The University of Tennessee, Knoxville

Mohammed Abu-Shehadeh
December 1989

Dedicated to

My mother, brothers, and sisters

Acknowledgment

The work presented in this dissertation was performed partly for the Engineering Physics and Mathematics Division and partly for the Instrumentation and Control Division of the Oak Ridge National Laboratory, which is operated by the Martin Marietta Energy System, under contract no. 41B-99732C, project authorization X68.

The author wishes to express his sincere appreciation to the following graduate committee and faculty members at the University of Tennessee for their constructive and useful suggestions in the preparation of this manuscript.

1. Dr. R. Perez (major advisor)
2. Dr. T. Kerlin (department head)
3. Dr. B. Upadhyaya
4. Dr. L. Miller
5. Dr. R. Uhrig
6. Dr. L. Dodds
7. Dr. V. Protopopescu

Special appreciation and respect to Dr. Felix Difilippo (ORNL), for his invaluable ideas, support, cooperation, guidance and patience in the course of this study. Special thanks to Jose March-Leuba (ORNL) for his scientific and technical help.

Abstract

The research performed in this Ph.D. dissertation has been in support of the Advanced Neutron Source Reactor (ANS), a national experimental facility to be built at the Oak Ridge National Laboratory (ORNL). The goal of this work was to calculate kinetic parameters and develop algorithms for the setting-up of an appropriate control architecture for the ANS reactor.

One-and two-dimensional static calculations were performed using the BOLD VENTURE computation system to obtain the global spatial dependence of the neutron flux throughout the reactor core and reflector. These calculations were used to determine the amount of built-in reactivity and control required to compensate for the excess reactivity contained in the initial fuel loading, to allow for flexible and safe reactor operation and to calculate reactor kinetic parameters (neutron lifetime and the effective delayed neutron fraction).

Regarding the development of support algorithms to be integrated in the control architecture of the ANS reactor, three issues appeared to be of crucial interest: (i) start-up and approach to criticality, (ii) xenon and samarium poisoning, and (iii) diagnostic tools for the unmeasurable quantities of the ANS reactor.

A two-Point-two-group kinetics model was developed to study the startup and criticality issues, which can be implemented as an on - line computer algorithm. This development was needed since

the disparity of neutron spectrum in the reflector and core makes the usual one point reactor kinetics approach a doubtful one, especially for severe reactor transients.

The xenon poisoning is a process of crucial relevance in view of the high neutron flux present in the ANS reactor. This process affects both the control algorithm, and more importantly the ability to restart the reactor after unanticipated shutdowns. It was found that the presence of samarium poisoning will stabilize the xenon oscillations, a certainly welcome result. Additionally, extensive calculations were performed of the after-shutdown reactivity due to xenon and samarium build-ups.

Diagnostics tools were developed, using optimal control techniques, to estimate the average thickness of aluminum oxide on the fuel plates, the average temperature of the fuel plates, which is not a measured state variable in the ANS reactor, and the coolant flow.

Table of Contents

List of Tables

List of Figures

Introduction

General Information

This research represents a part of the Advanced Neutron Source (ANS) project being conducted at Oak Ridge National Laboratory (ORNL). The Advanced Neutron Source is a new, national experimental facility being planned by ORNL in response to a recent study (Eastman-Seitz Committee, National Academy of Science)[27] which reflects the need for an intense steady-state source of neutrons and for associated experimental equipment. The design team at ORNL has identified the goals for the proposed facility. One of the most important goals of the design is to achieve an unprecedented thermal neutron flux for scattering experiments (0.5×10^{16} to 1×10^{16} $\frac{n}{cm^2 .sec.}$).

Although the largest field of research is expected to be neutron scattering, the production of isotopes (including transuranium isotopes for research) and the irradiation of engineering materials will also be important functions of the facility. At present the High Flux Isotope Reactor (HFIR) is the leading facility for isotope production; it is also used extensively for materials irradiation. The needs for these research areas are reflected in the goals for the global project:

(1) To design and construct the world's best research reactor for neutron scattering,

(2) To provide facilities for materials irradiation that are as good as or better than HFIR,

(3) To provide facilities for isotope production as good as or better than HFIR.

These goals have been translated, provisionally, into quantitative design criteria for the neutron source, which in ORNL's proposal is a reactor.

The most important design criterion is, of course, a very high neutron flux; thermal flux for the beam tubes, epithermal flux for isotope production, and fast flux for engineering materials irradiation.

In seeking an acceptable design, it was agreed upon that the proposed reactor should not depend on the success of radically new concepts or on the achievement of some major new technical advances in, for example, fuel or coolant technology. The designers have developed a preliminary reference design for the Advanced Neutron Source reactor[1,2].

The design of a nuclear reactor is an enormously complex task and involves the coordination of a remarkably diverse range of disciplines. Each major design feature of the reactor requires a separate and distinct design analysis.

Objectives and Organization

The goal of the present work is to study a subset of the required design objectives. This includes (a) optimization of design

parameters, (b) determination of kinetic parameters and control actions, (c) study of short-term transients, (d) study of long-term transients, and (e) development of diagnostics algorithms.

In chapter I a description of the fuel element design, core composition and core arrangement[1,2] is given. In chapter II the one-dimensional static calculations are utilized to optimize the core lifetime (CLT), by surveying some of the reference design parameters, such as the thickness of D_2O reflector and H_2O biological shield, the volume of the central island region, and the thickness of the target aluminum cylinder located between the two fuel annuli. In chapter III two-dimensional static calculations are utilized to determine the amount of negative reactivity or control required to compensate for the excess reactivity contained in the initial fuel loading in the ANS reactor. The excess reactivity will be controlled with several control mechanisms including control rods and burnable poison. The two-dimensional calculations are also used to determine two important kinetic parameters. These are the prompt-neutron lifetime l, and the delayed neutron fraction β. In chapter IV a Two-Point-Two-Group model of the ANS reactor will be developed. This model together with a One-Point-One-Group model is used to study the short-term transient response of the ANS reactor. These transients include the reactor startup and shutdown. The startup transient will be used to determine the effect of the source-removal time on the final power level, the effect of the reactivity amplitude on the power level will also be discussed. The shutdown transient will be used to study the

efficiency of each of the two control mechanisms by utilizing the Two-Point-Two-Group model. The long-term transients due to xenon and samarium buildup are discussed in chapter V. A dynamic model will be developed to study the nonlinear behavior of the system due to the xenon and temperature feedback effects. Finally, in chapter VI, the optimal control theory is used to develop diagnostics algorithms to estimate uncertain parameters, such as the heat transfer coefficient, and uncertain parts of the plant dynamics, such as the average fuel plate temperature and the coolant mass flow rate. An algorithm will also be developed for the problem of checking compliance in the reactivity inserting procedure.

Previous Work and Accomplishment

Previous work related to the development of algorithms for the study of short-term transients used the one-point reactor kinetics approach. Since the ANS reactor exhibits very dissimilar neutron spectra in the core and reflector, a new reactor kinetics model has been developed in chapter IV. The understanding of the effects of xenon and samarium poisoning on the ANS operation is a subject of fundamental importance. Previous work in this area[10,11,12,13,14] did not explicitly include the combined effects of xenon, samarium, and temperature feedbacks. Two major accomplishments of this work have been to show the stabilizing effect of the samarium reactivity feedback and the stability of the

system against spatial oscillations of the neutron flux. Finally, new diagnostics algorithms were developed for parameter tracking, state variable estimation, and as well as a reactivity meter for core diagnostics.

Chapter I

Reference Core Design

Static design is used to obtain the global spatial dependence of the neutron flux throughout the reactor core. This information is required for accurate predictions of the power distributions, excess reactivity, and other quantities. The three-dimensional BOLD VENTURE[28] computation system has been used to perform the static calculations. However, only one and two-dimensional calculations have been performed; since three-dimensional calculations are extremely expensive. The one-dimensional calculations have been utilized to survey some design parameters and to identify some constraints; in order to establish a reference design that provides a calculational base against which optimization calculations can be compared.

However, the two-dimensional calculations have been utilized to determine the amount of negative reactivity or control required to compensate for the excess reactivity contained in the initial fuel loading as well as to allow for flexible and safe reactor operation. One must allocate this reactivity among several different control mechanisms, including movable control rods and burnable poison. Therefore, an investigation involving the control rod material, location, and thickness has been performed. Also the control rod worth calculations were done. On the other hand the effect of burnable poison was determined. In addition, the 2-D calculations have been used to determine some of the most

important kinetics parameters of the reactor. Namely, the mean neutron lifetime l, and the delayed neutron fraction β. These parameters will be used in the study of the ANS reactor kinetics.

1.1 Core Design Requirements and Limitations[1]

The single most important factor in determining the value of a reactor for neutron scattering work is the thermal flux outside the core where beam tubes can be placed. The basic requirements of such a reactor are a high power level and a small external surface area to the core, because the flux is related both to the number of neutrons and to the area they must pass through. In fact, for cores of basically similar composition and geometry, the thermal flux in the reflector is approximately proportional to the neutron production rate (or power level) divided by the core surface area[1]. The surface area in turn is proportional to the two-thirds power of core volume, and the power per unit volume is the average power density:

$$\phi_{th} \propto P/A \propto P/V^{2/3} \propto P^{1/3}\left(\frac{P}{V}\right)^{2/3} \propto P^{1/3}\,(\overline{P})^{2/3}$$

P = power
V = core volume
ϕ_{th} = thermal flux
$\overline{P}$ = Average power density

This simple argument indicates that a high power is beneficial but that a high power density is even more beneficial.

However, a high power density means a small core volume and thereby a limited heat transfer surface is available within the core. Also, small core volume limits the amount of fuel that can be contained and therefore the length of the fuel cycle. Using a high density fuel form, however, such as the uranium silicides (U_3Si_2) developed by Argonne National Laboratory, this problem can be overcome. Other constraints include the formation of an oxide layer at the surface of the aluminum cladding. The effect of this oxide will be discussed in more details in Chapter VI.

The choice of reflector is not straightforward. Clearly, a material with a very low thermal absorption cross section is required, which rules out light water. The obvious choices include heavy water and beryllium. Calculations[1] indicate that a slightly higher thermal flux and longer core life could be obtained with a beryllium reflector than with a heavy water one, but that the thermal peak would be much narrower, making less volume available to accommodate the beam tubes. Furthermore, a very complicated, and presumably expensive beryllium shape would be needed to provide access for the various beam tubes and irradiation facilities. Therefore, heavy water has been the choice even though the investigation of the possibility of a combination of beryllium pieces (especially in the center of the core) and heavy water will continue.

1.2 Core Design

A reference core design that meets the objectives of the project for neutron flux, spectrum, and fuel life has been evolved. In this section, a detailed description of the core design is given.

1.2.1 Fuel Element. The fuel element consists of a convolute plate that is 1.27 mm thick. This includes the uranium-aluminum meat which is 0.762 mm thick, sandwiched between two aluminum clads with 0.254 mm thickness for each (see Figure 1.1).

The meat is composed of uranium silicide, U_3Si_2, in an aluminum matrix. The uranium is enriched to 93%. The aluminum matrix as well as the aluminum cladding are both 6061-T6 aluminum alloys. The maximum volume fraction of uranium in the meat is 0.45, with maximum void fraction of 0.10. The maximum uranium density is 4.8 g/ml of fuel meat. The choice of U_3Si_2 was based on the study of Argonne National Laboratory's reduced enrichment for research and test reactor program[7]. In-pile tests have shown that U_3Si_2 turns out to be very resistant to swelling and other undesirable effects during irradiation. In a high power density, and therefore, a high heat flux core, it is essential that the fuel have a high thermal conductivity. Therefore, the introduction of aluminum in the meet will help increase the thermal conductivity of the fuel. At high uranium loading (3 to 4 g/ml) the silicide offers a very great improvement over the oxide and aluminide forms presently used in most research reactors.

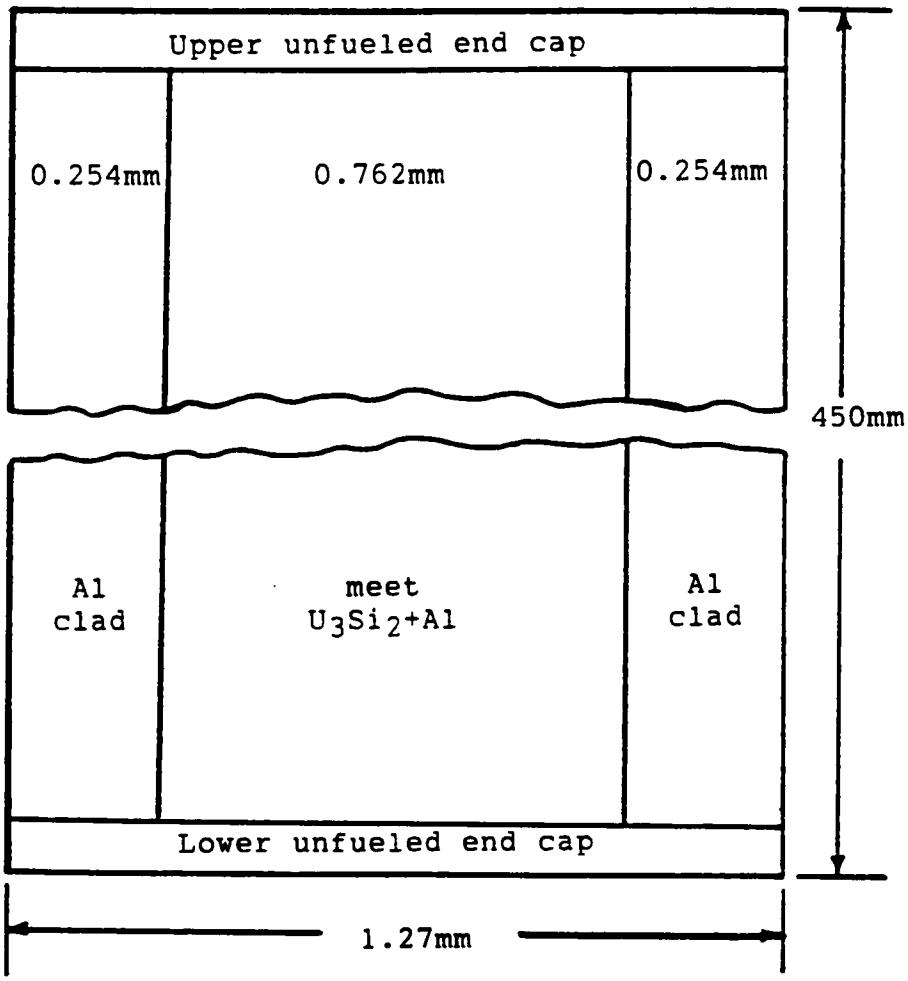

Fig.1.1 Fuel plate design.

1.2.2 Core Configurations. The fuel plates, in an involute shape, are arranged in two concentric annuli, thus only two different plate types are involved in the entire core. There are 1.27 mm coolant gaps between adjacent plates. Three aluminum cylinders are used to hold the plates in fixed positions in the two annuli. The innermost cylinder is 0.73 cm thick, the middle cylinder, which is shared by the two annuli, is 3.17 cm thick, and the third cylinder is 0.5 cm thick. The middle, 3.17 cm aluminum cylinder has axial holes which serve as irradiation positions. The inner fuel annulus is 5.11 cm thick and holds 176 plates, and the outer fuel annulus is 4 cm thick and holds 408 plates, figure 1.2 shows a cross section of the core region[3]. The total amount of U^{235} in the core is 24 kg. The innermost, 0.73 cm aluminum cylinder surrounds an island region which is mainly filled with D_2O coolant. Figure[2] 1.3 shows the core arrangement. The overall length of the core is 45 cm, including a 5 cm-long unfueled region at each end of the core.

The transuranium isotope production and engineering materials experiments require access to facilities with a high epithermal flux and a high fast flux, respectively, preferably with little contamination by thermal neutrons.

Choosing a small core volume and heavy water as the coolant ensures that most of the fission neutrons leave the core region before they are slowed down to epithermal or thermal energies. The core is surrounded by a reflector that completes the slowing

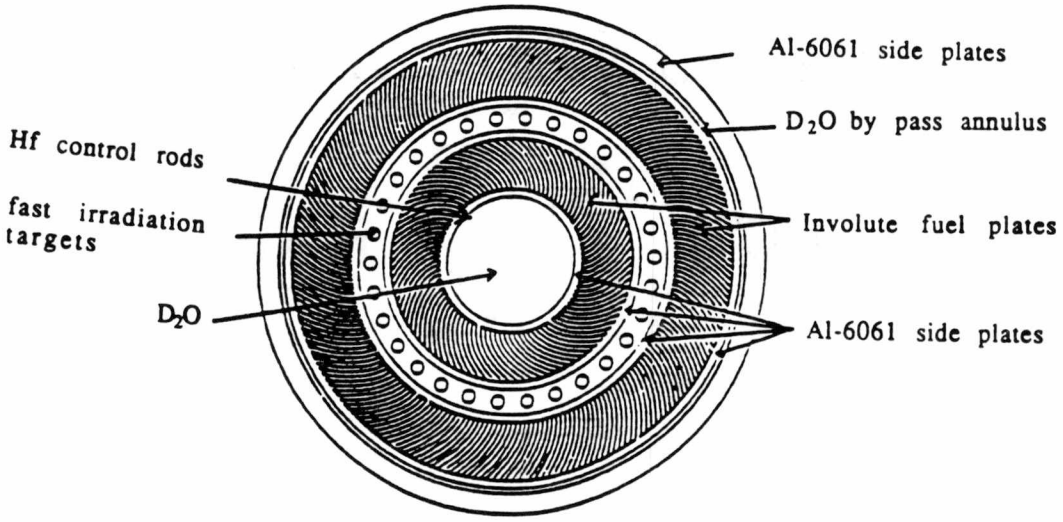

Fig.1.2 A cross section of the ANS reactor core .

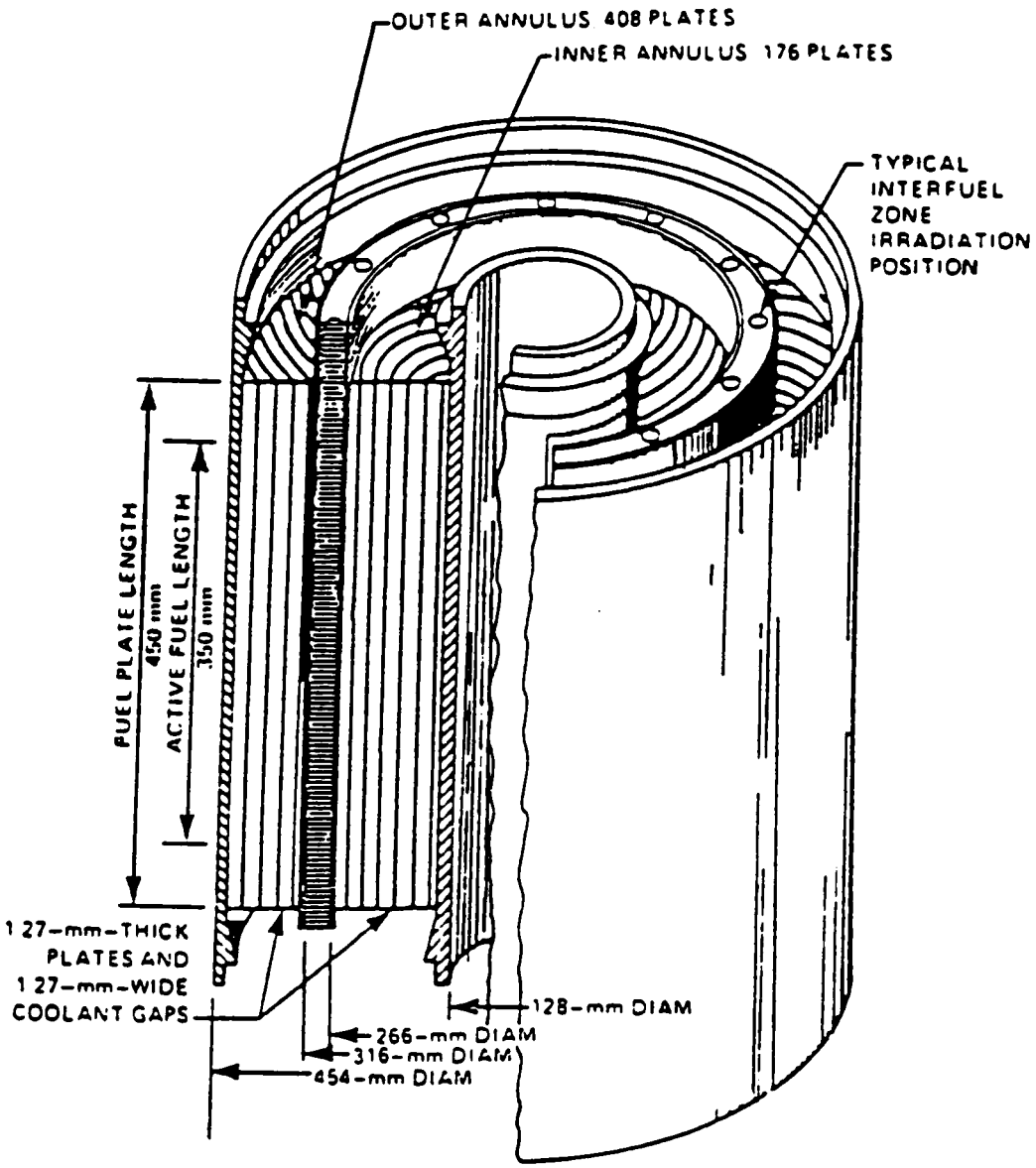

Fig.1.3 ANS reactor core arrangement.

down of neutrons and reflects some of them back into the core to maintain the chain reaction. A gradation therefore exists from a rather hard spectrum within and close to the core to a thermal spectrum out in the reflector, with a region in between that is rich in epithermal neutrons (Fig.1.4)[2] . The different requirements mandated by the three objectives can thus be met with a single reactor.

There may be some advantages in dividing the core into an upper and lower half[3] with a space in between for mixing of the coolant flow; beam tubes pointing at the space between the two core halves may gather a higher ratio of thermal-to-fast neutrons than beam tubes opposite to a fuel element. However, the horizontally divided core would probably be somewhat less neutronically efficient than a single core, requiring a higher power to produce the same flux. The actual core of the ANS reactor will adopt the most effective and efficient design that can be devised. However, in this research we focused our attention on the single core design; although, most of the analysis is also applicable to the split core design.

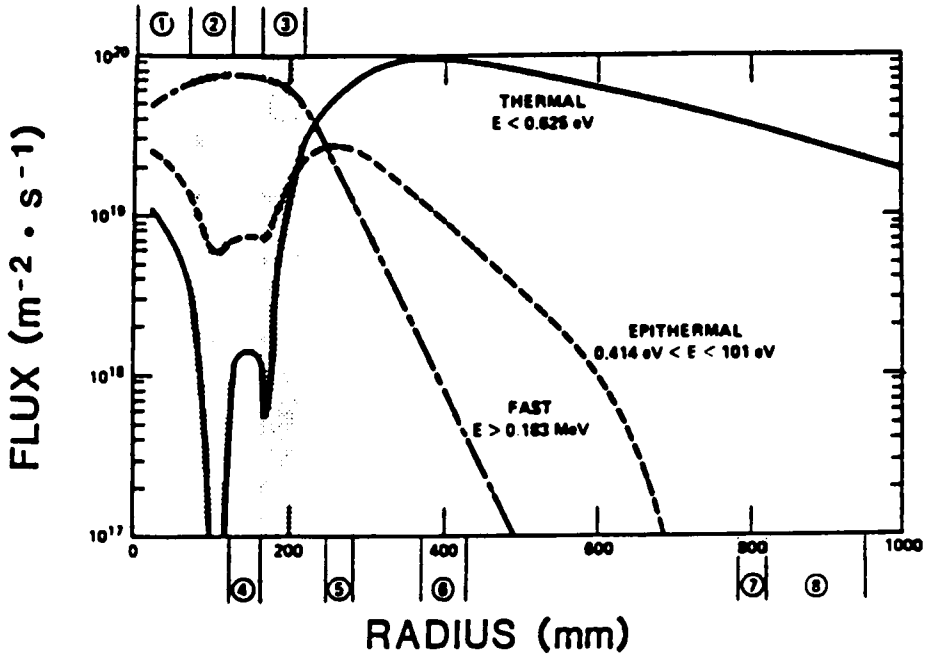

Fig.1.4 Unperturbed flux and irradiation position: reference core (1) Inner reflector, (2) fuel, (3) fuel, (4) interfuel irradiation positions , (5) epithermal peak irradiation positions, (6) beam tube entrance,(7) outer reflector thermal irradiation positions, (8) cold source location.

Chapter II

One-Dimensional Static Calculations

In the previous chapter a detailed description of the fuel element design, composition, and core arrangement was introduced.. Based on that arrangement, a reference design has been chosen; against which the optimization calculations have been performed. The main regions of the reference design are as follows:

(1) An island region filled with D_2O coolant, which constitutes the center of the reactor.

(2) An aluminum cylinder surrounding the central island. It will be referred to as *Al*1.

(3) An inner fuel annulus.

(4) An aluminum cylinder surrounding the inner fuel annulus; with vertical holes to be used as irradiation positions. It will be referred to as target aluminum.

(5) An outer fuel annulus.

(6) An aluminum cylinder surrounding the outer fuel annulus. It will be referred to as *Al*3.

(7) D_2O reflector region.

(8) H_2O biological shield region.

Figure 2.1 shows a cross-section of the main regions. The dimensions of these regions are given in Table 2.1.

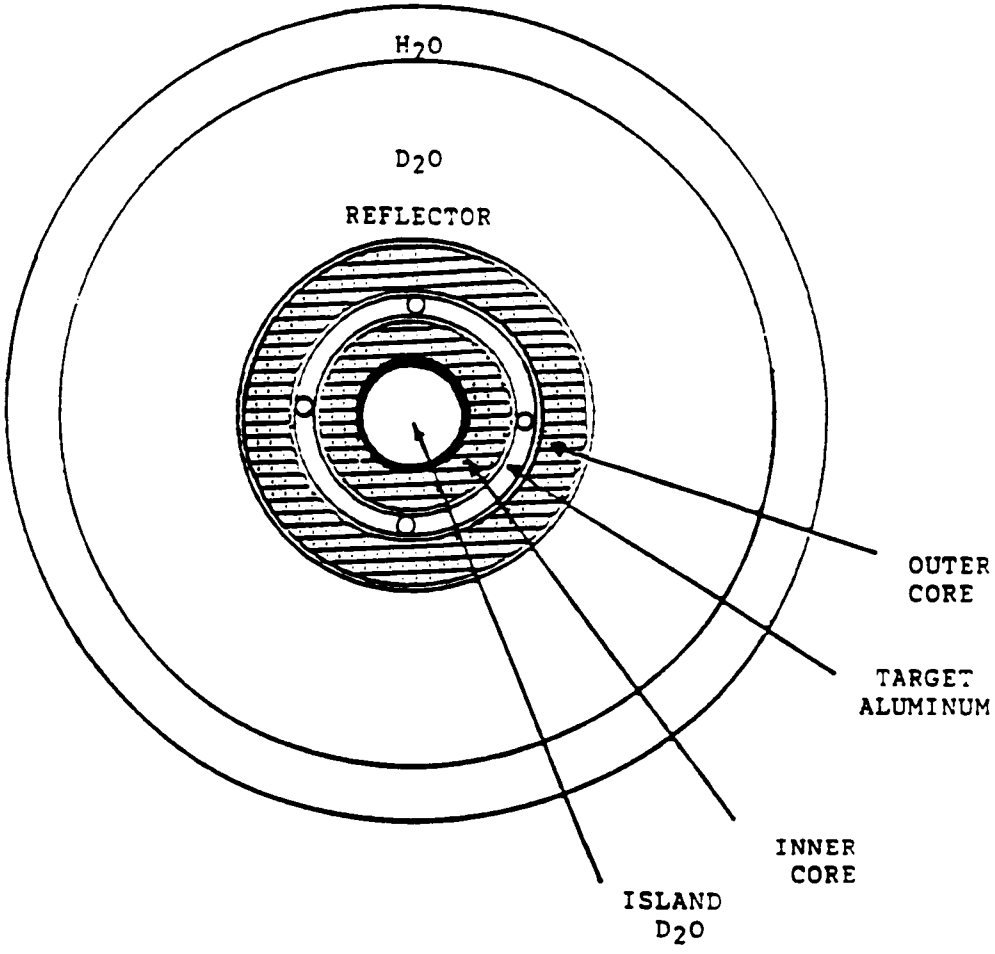

Fig.2.1 A cross section of the ANS reactor showing the main reactor regions.

The parameter to be optimized is the multiplication factor, K_{eff}, at the beginning of the core life time (BOL). Since the core life time depends on the amount of excess reactivity available at the beginning of life,.this will consequently affect the core life time(CLT). The goal is to obtain a thermal neutron flux of 1×10^{16} $\frac{n}{cm^2.sec}$ at the end of life(EOL) with a value of $K_{eff} = 1.0$. Therefore, the CLT has been normalized to an EOL $K_{eff} = 1$ and $\phi_{th} = 1 \times 10^{16}$ $\frac{n}{cm^2.sec}$.

Table 2.1 Dimensions of the reference core design

	Island	Al1	Core1	Al2	Core2	Al3	D_2O	H_2O
Thickness (cm)	10.28	0.73	5.11	3.17	4.03	.5	200	10
Volume (L)	4.55	1.03	11.9	12.5	23.05	3.49	46,909	6,580

The 1-D BOLD VENTURE computation system has been used to perform the neutronics calculations that will provide the value of K_{eff} at the BOL. Also burnup calculations have been performed to provide the value of K_{eff} and the flux level at selected time intervals during reactor operation. The value of K_{eff} was monitored as a function of burnup. The core life time is determined when the value of K_{eff} (as a function of burnup) reaches unity. The following parameters have been of special interest for the optimization process.

2.1 D_2O Reflector

To study the effect of D_2O reflector thickness on the CLT, the reference case thicknesses given by Table 2.1 were all kept constant. The thickness of D_2O reflector was the only variable. Figure 2.2(a) shows the change of K_{eff} (at BOL) as a function of D_2O reflector thickness. Figure 2.2(b) shows the change in CLT as a function of D_2O reflector thickness. The plots indicate that a change in D_2O reflector thickness from 100 cm to 200 cm produced 2.44% gain in K_{eff}, and 22.0% gain in the CLT. However, a change in D_2O reflector thickness from 200 cm to 300 cm produced only 0.54% gain in K_{eff}, and only 4.2% gain in the CLT. According to these results it was decided that a reflector thickness of 200 cm is a reasonable choice.

2.2 H_2O Biological shield

The reference case dimensions given in Table 2.1 were used. The thickness of H_2O region was the only variable. Figure 2.3 shows the effect of H_2O thickness on K_{eff} and CLT. The results indicate that a change in H_2O thickness from 0 to 10 cm produced 1% gain in K_{eff} and 8.5% gain in CLT. However, the plots also show that there is no change in either K_{eff} or CLT for H_2O thickness above 10 cm. Therefore, it was decided that 10 cm of H_2O is a reasonable choice.

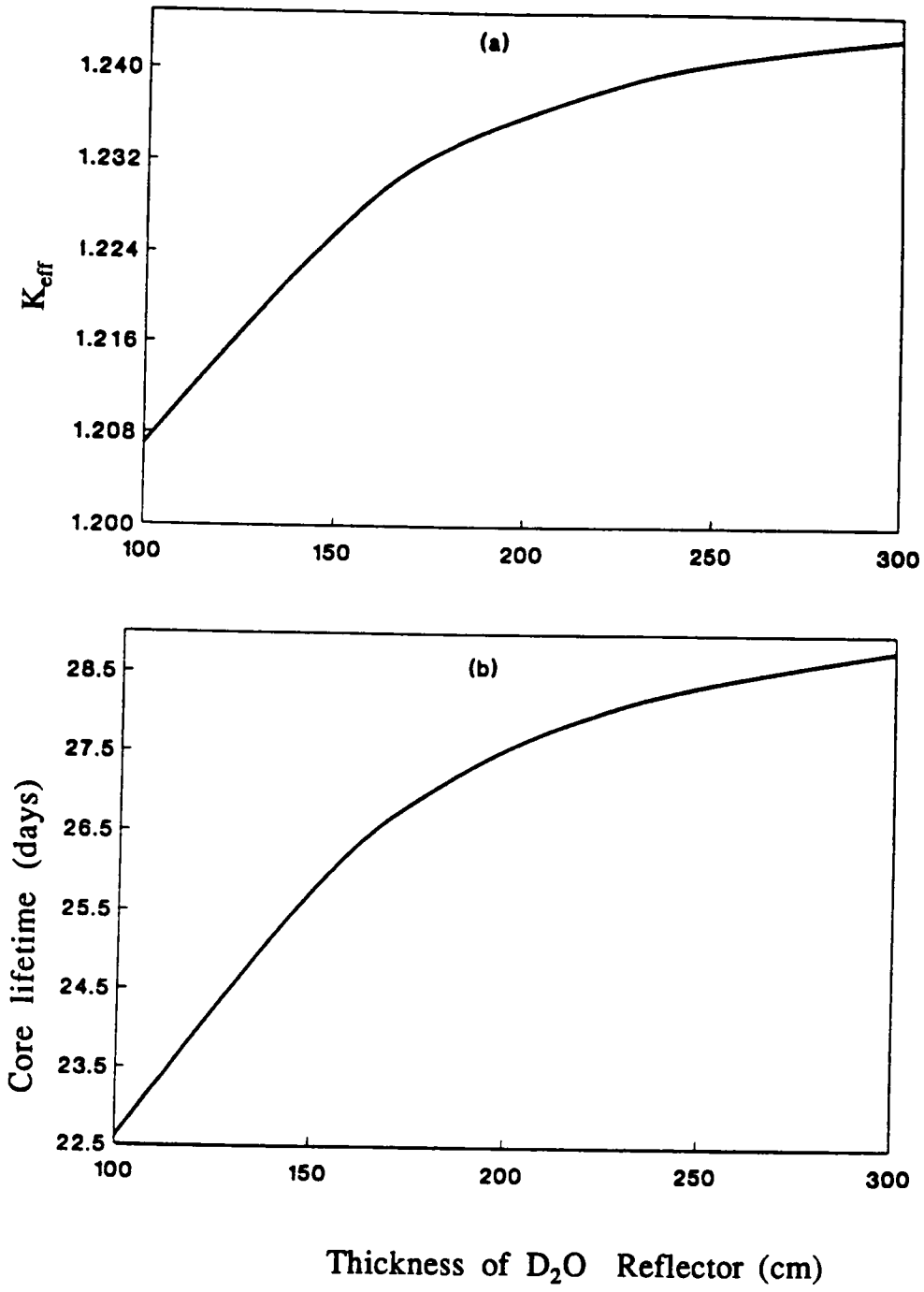

Fig.2.2 Effect of D_2O reflector on (a) K_{eff} and (b) core lifetime.

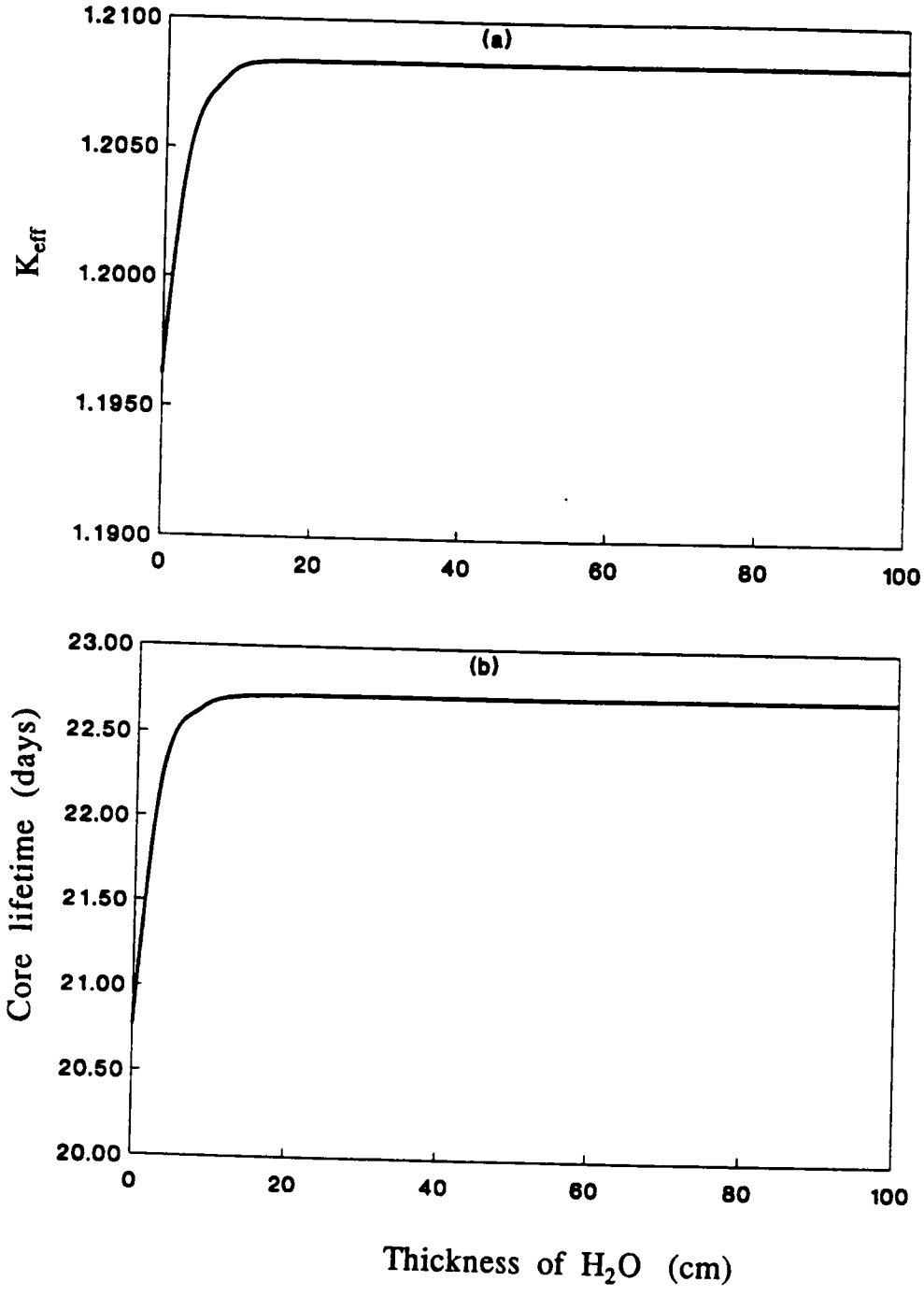

Fig.2.3 Effect of H_2O on (a) K_{eff} and (b) core lifetime.

2.3 Volume of Central Island

The effect of the volume of the central island on K_{eff} has been significant. To be consistent, the volumes of regions given in Table 2.1 for the reference case were kept constant. However, a change in the volume (or radius) of the island region results in a change in thicknesses in all regions although the regions' volumes were kept constant (consequently the total amount of U^{235} remained unchanged). Figure 2.4 shows that there is a monotonic increase in K_{eff} and CLT as the volume of the central island increases. The importance of the island region lies in the fact that it will be used to accommodate the regulating control rods. There is also the possibility of utilizing the island region as an irradiation position. The actual size of the island will depend on the type, shape, and positions of the control rods.

2.4 Target Aluminum

This is the aluminum cylinder between the two fuel annuli. Vertical holes made in this cylinder will be used as irradiation positions. Figure 2.5 shows the effect of the thickness of the target aluminum on K_{eff} and CLT. It is clear that the thickness of target aluminum has a negligible effect on both K_{eff} and CLT.

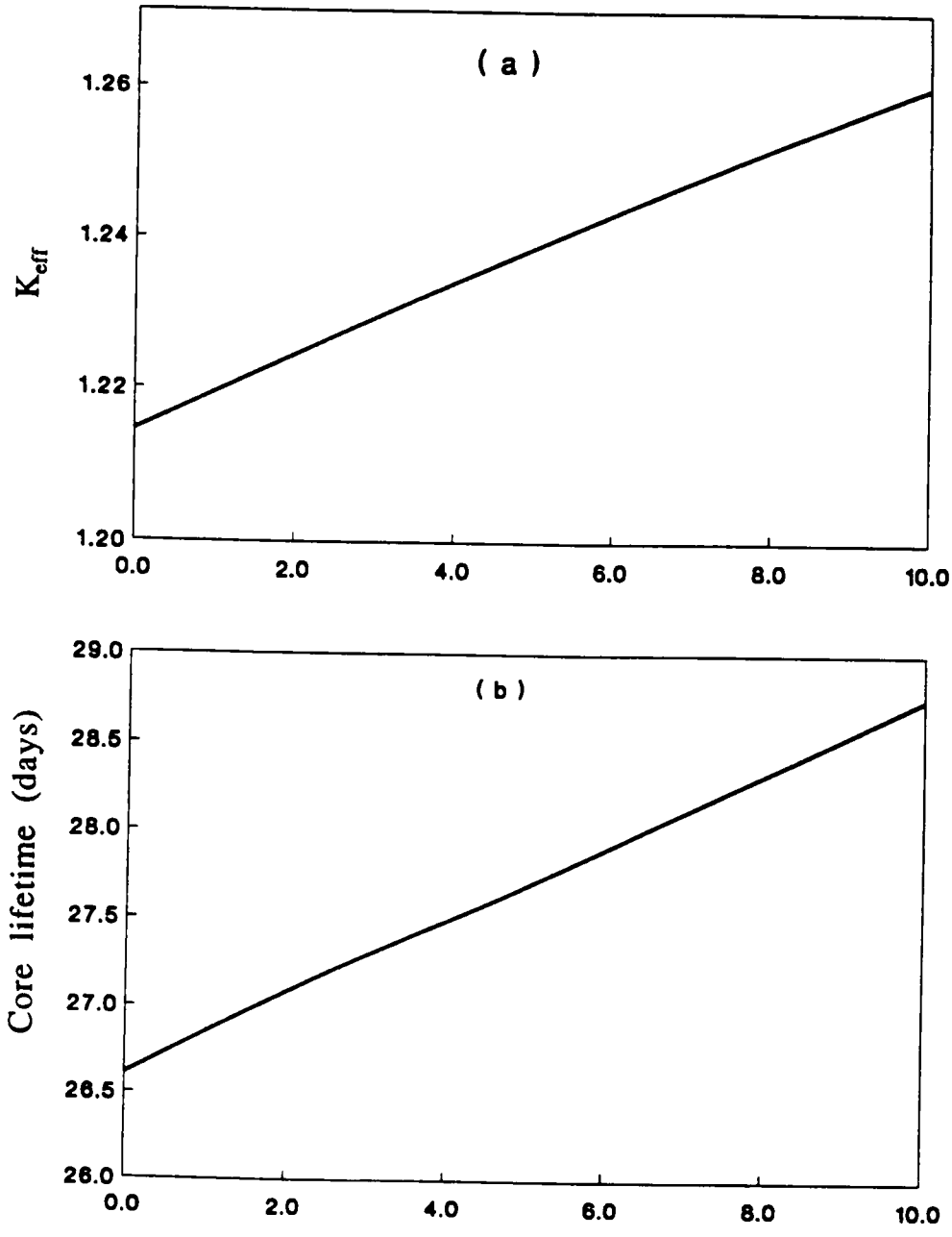

Fig.2.4 Effect of the volume of the island on (a) K_{eff} and (b) core lifetime.

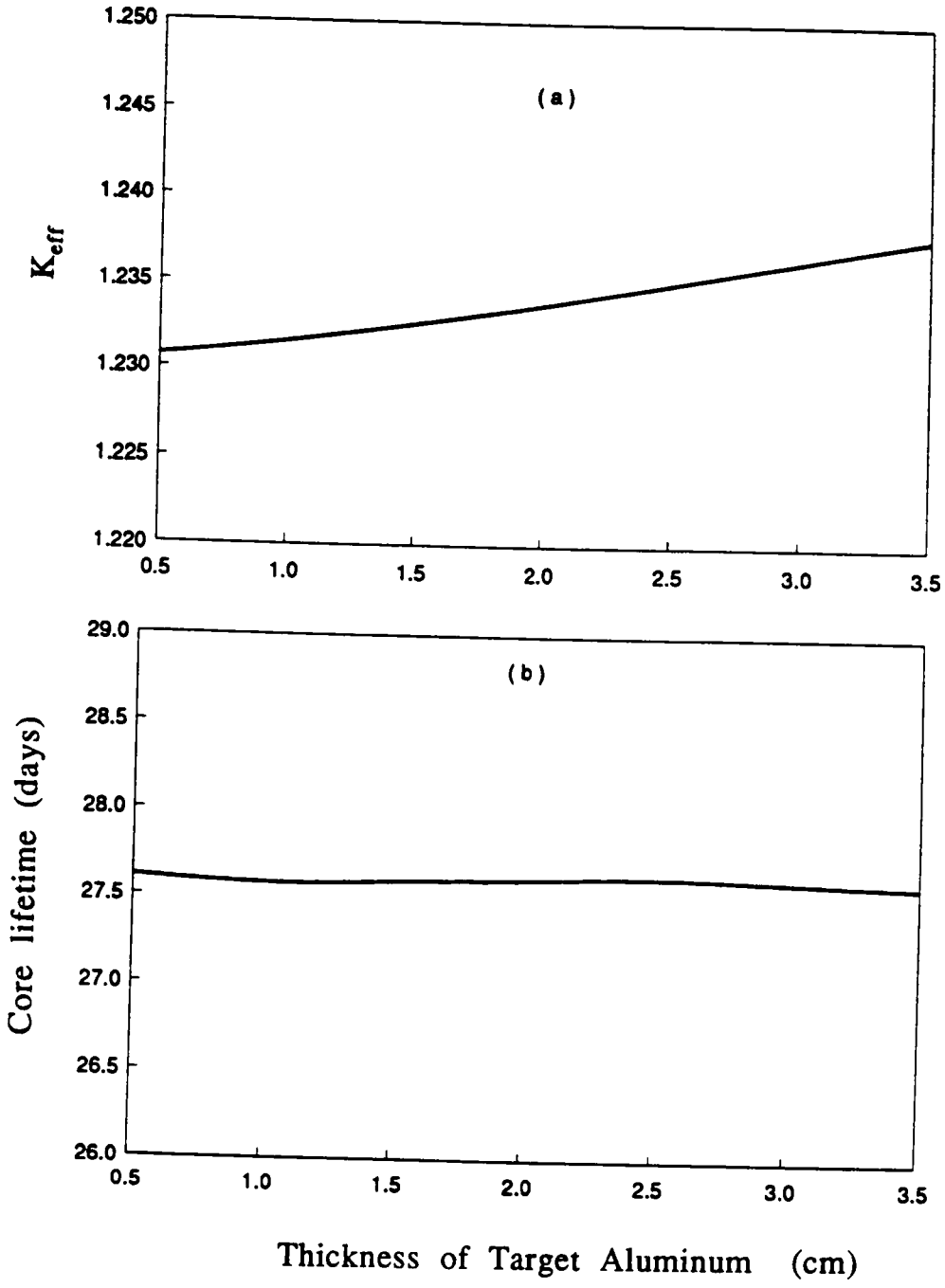

Fig.2.5 Effect of the thickness of target aluminum on (a) K_{eff} and (b) core lifetime.

Chapter III

Two-Dimensional Static Calculations

The 2-D calculations will be utilized to determine the amount of negative reactivity or control required to compensate for the excess reactivity contained in the initial fuel loading as well as to allow for flexible and safe reactor operation. One must allocate this reactivity among several different control mechanisms, including movable control rods and burnable poison. Therefore, an investigation involving the control rod material, location, thickness, and control rod worth calculations has been performed. On the other hand the effect of burnable poison will be determined. In addition, the 2-D calculations have been used to determine some of the most important kinetics parameters of the reactor. These are, the mean neutron lifetime l, and the delayed neutron fraction β.

3.1 Selection of Control Material and Control Design

The development of suitable control materials is of importance to high performance reactors; because control materials must not only meet the nuclear requirements for control of the reactor but must possess the necessary physical properties, radiation damage resistance, and corrosion resistance to the primary coolant. Control materials are used in reactor cores in two principal ways. One, the more conventional, is in control

rods ; the other as burnable poison which can be uniformly distributed within the fuel or placed in discrete locations in the reactor core. Each application raises its own peculiar problems. For control rods, often the only moving parts in the core, the control material must be able to resist shock, vibration, and wear. For burnable poison applications, the control material must not only have the necessary nuclear porperties but also the proper concentration so that the poison burns out at a rate which compensates for depletion of the fuel. Thus the development, selection, and application of control materials is a complex matter requiring judgment by the physicist, the mechanical designer, and the metallurgist. With the advent of higher power density, the requirements on control materials are becoming more stringent. Because of the basic requirement that such control materials have a high nuclear cross section for absorption of neurtons the number of suitable elements is limited. The additional requirements that these elements be capable of being incorporated into control rods with adequate mechanical strength and thermal stability further reduce the number of practical materials. The net result is that only two materials -hafnium, and boron- have been investigated.

3.1.1 Use of B^{10} to Reduce the Initial Excess Reactivity

The ANS cold and unpoisoned core multiplication factor K_{eff} is 1.1833. The large excess reactivity involved in the ANS design

cannot be compensated only with control rods due to space and practical limitations for worth of control rods. It is necessary then to control part of the excess reactivity with burnable poison.

The usefulness of a burnable poison lies largely in its ability to separate the endurance of a reactor from the reactivity worth of its control elements. If fuel and burnable poison are added in reactivity compensating amounts, and then this fuel is removed from the reactor through burnup and the poison is burned up in an exactly compensating fashion, then the control requirements are unaffected throughout the life of the reactor, and its endurance is determined solely by the amount of fuel and burnable poison added initially. Thus endurance is separated from control elements worth, provided only that the control elements are capable of meeting the initial control requirements.

Because of its high thermal neutron cross section, relatively predictable nuclear behavior, availability, and relatively low cost, boron has been one of the most widely utilized neutron-absorbing materials for nuclear reactors. These properties have made boron an excellent candidate for application in many reactors, as either a burnable poison, control, or shielding material.

Boron has two stable isotopes, B^{10} and B^{11}. From the standpoint of neutron absorption, only B^{10} is important. The absorption cross section for thermal neutrons is less than 0.5 barn for B^{11}, but is 3,840 barns for B^{10}. Natural boron contains 19.8 atom percent B^{10}.

Figure 3.1 shows the reduction of the multiplication constant

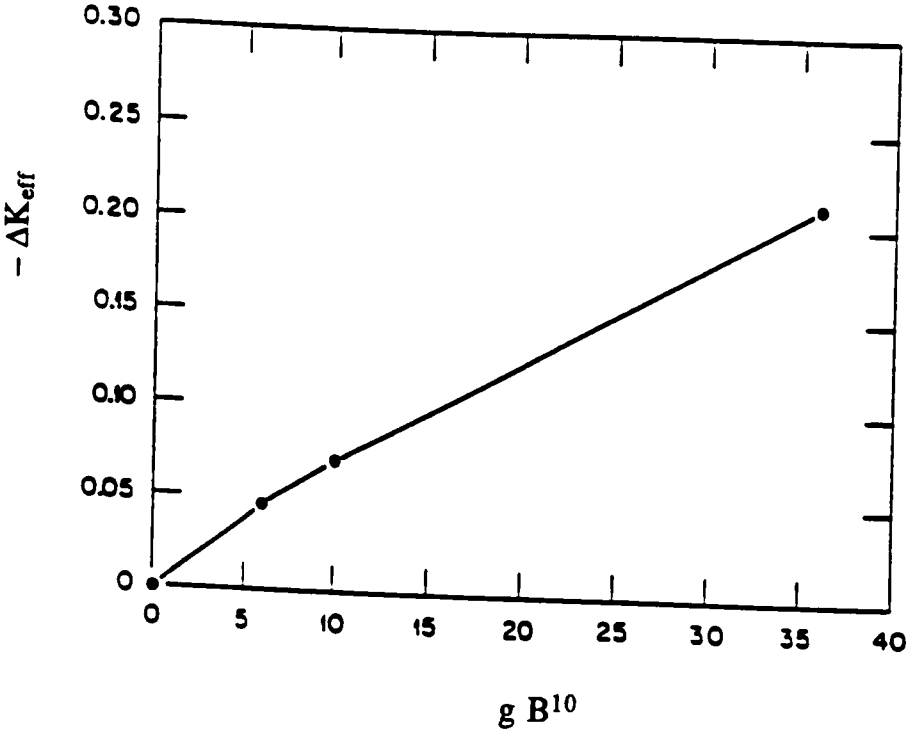

Figure 3.1 Change of the multiplication constant by adding uniformly B^{10} to the core (as a burnable poison).

by uniformly adding B^{10} to the core as a burnable poison. The initial amount of B^{10} as a burnable poison has to be chosen to minimize the effect of the residual amount of B^{10} at the end of the core life.

3.1.2 Regulating and Safety Control Rods Materials and Design

The design of control rods for reactors is a complicated problem for which there is no exact computational procedure.

Computations become more expensive as the complexity of the control mechanism is increased. For this reason a rather simplified approach has been adopted so as to obtain preliminary data which identify a range of interest. More complex and more accurate approach must be followed to determine the final control system design. However, this can be done when the characteristics of the system approach those desired. Once the desired performance characteristics of the reactor are established, it is possible to deduce the control requirements in terms of excess reactivity which must be controlled. Then the primary problem of control rod design is to find the number, placement, shape, and material of the control rods needed to make the reactor adequately subcritical when the rods are fully inserted.

As a simplified approach, two kinds of control rods were considered. The first to be located in the central cavity-island region-and to be used as a regulating rod. The other to be located

at the interface between the core and the radial reflector and to be used as a safety rod. A 2-D, (r,z), cylindrical geometry has been used to model the reactor; therefore, the rods take the shape of cylindrical shells. Also, it was assumed that in order to maintain a balanced power distribution, the control rods are moved symmetrically with respect to the midplane of the core.

Two materials have been considered for the design of the regulating control rod; these are boron and hafnium. The nuclear properties of boron were discussed in the previous chapter; however, those of hafnium will briefly be discussed presently.

Of the materials considered for control rod application, hafnium is the least complicated metallurgically. Pure hafnium has about the strength of zircaloy-2 and about one-third its corrosion rate in 500 to 600 °F water. Consequently, unlike boron, hafnium does not require any cladding or protective plating. Pure hafnium can be readily shaped and welded to itself. Since hafnium is a complex element having 6 stable isotopes and 59 known epithermal resonances[16], the precision with which the nuclear properties are treated varies with the application. The 6 isotopes, their natural abundance, and their thermal neutron cross sections are given in Table 3.1.

Table 3.1 Natural Abundance and Thermal Cross Section of the Hafnium Isotopes[16]

Isotopic mass no.	Natural Abundance(%)	Thermal x-sec. (b)
174	0.18	1,500 ± 1,000
176	5.15	15 ± 5
177	18.38	380 ± 30
178	27.08	75 ± 10
179	13.77	65 ± 15
180	35	14 ± 5

Figure 3.2 shows the worth of different rings of control rods. Rings 1 or 2 are located in the central cavity. Ring 1 is composed of 1 mm layer of natural boron sandwiched between two 1 mm thick aluminum cladding. Ring 2 is composed of a 0.5 cm thick pure hafnium. Ring 3 has the same composition as ring 1 and is located at the periphery of the core at the interface between the pressure vessel and the reflector. Figures 3.1 and 3.2 show that it might be possible to control the reactor using, for example, ring 2 as regulating rods, B^{10} as burnable poison, and ring 3 as safety rods.

Table 3.2 shows the change of K_{eff} as a function of the control rod position for ring 2. Table 3.3 shows the change of K_{eff} as a function of burnup. From these two tables a calibration curve, figure 3.3, for ring 2 control rod, can be constructed. This curve shows the position of the control rod that will make the reactor critical at any time during operation.

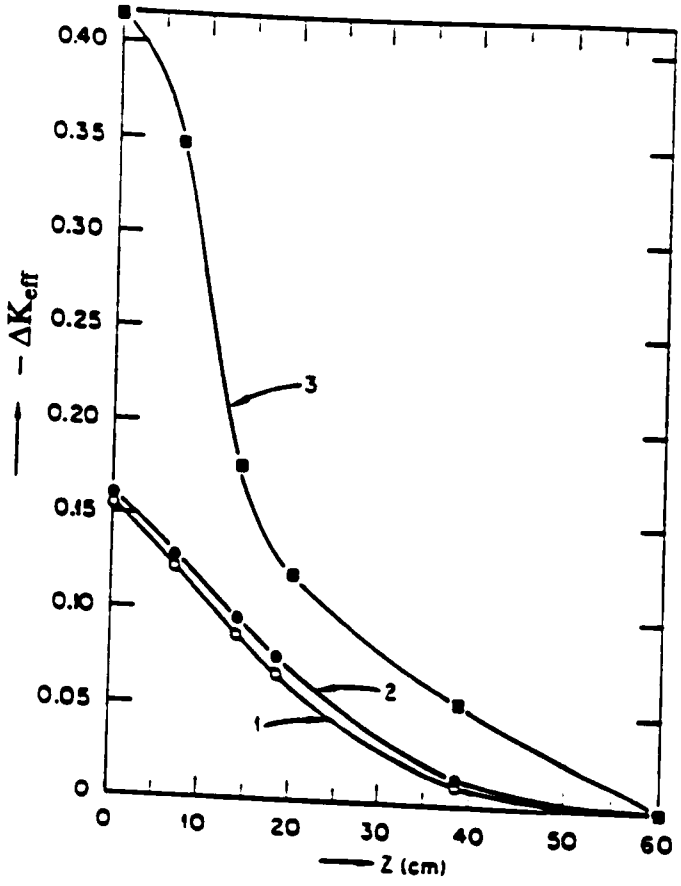

Figure 3.2 Worth of different rings of control rods.

Table 3.2 Change in K_{eff} as a result of Control Rod Position for Ring2

Z(cm)	K_{eff}	ΔK
0	0.9461	0.1672
7	0.9773	0.136
14	1.0105	0.1028
18.5	1.0303	0.083
38.5	1.0915	0.0218
∞	1.1133	0.0

Where Z = 0 corresponds to the fully inserted rod, Z = ∞ corresponds to the fully withdrawn rod, and $\Delta K = K_{z=\infty} - K_{eff}$.

Table 3.3 Change in K_{eff} as a Result of Burnup

Time (days)	K_{eff}	$\Delta K = K_{t=0} - 1$
0	1.1133	.1133
3.5	1.0888	.0888
7	1.0657	.0657
10.5	1.0372	.0372
14	1.0049	.0049

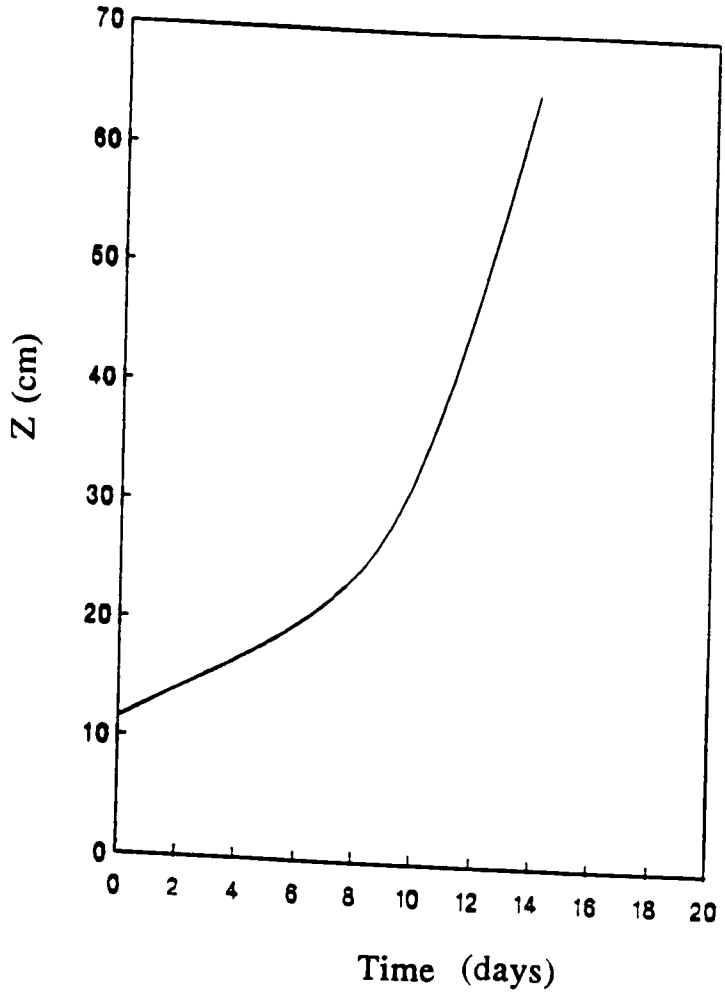

Figure 3.3 Calibration curve for ring 2 control rod.

3.2 Calculation of the Prompt-Neutron Lifetime

In the design of any new reactor an essential step is the determination of the reactor kinetics parameters. One of the most important parameters of reactor kinetics is the prompt-neutron lifetime l. Experimental measurements are usually carried out; the results are then compared with theory. To calculate the prompt neutron lifetime, the prompt-neutron decay constant α was first calculated. Then, a relationship between l and α allowed the calculation of l. In calculating α, the modal expansion of the neutron flux was assumed. The following analysis shows how these relations were developed. First consider the time-dependent one-group-diffusion equation for a nonmultiplying medium, the flux satisfies

$$\frac{1}{v}\frac{\partial \phi}{\partial t} = D\nabla^2 \phi - \Sigma_a \phi(r,t) \tag{3-1}$$

The time-independent equation is

$$D\nabla^2 \phi - \Sigma_a \phi(r) = 0 \tag{3-2}$$

consider the following modal expansion of the flux

$$\phi(r,t) = \Sigma \; A_i \Psi_i(r) e^{\alpha_i t} \tag{3-3}$$

For long times, the flux will approach the asymptotic form

$$\phi(\mathbf{r},t) = A_0\Psi_0(r)e^{\alpha_0 t} \qquad (3\text{-}4)$$

where $\Psi_0(r)$ is the fundamental mode of the flux.

Substitution of equation (3-4) into equation (3-1) yields the following equation for the fundamental mode

$$D\nabla^2\Psi_0(r) - (\Sigma_a + \alpha_0/v)\Psi_0(r) = 0 \qquad (3\text{-}5)$$

A comparison between equations (3-5) and (3-2) shows that the term in paranthesis $(\Sigma_a + \alpha_0/v)$ represents an effective total absorption cross section . Thus prompt-neutron decay can be associated with the presence of a uniformly distributed "1/v absorber" of macroscopic cross section α_0/v. This convenient equivalence permitted the use of the time-independent BOLD VENTURE code to calculate α (or the amount of 1/v absorber to be removed or added to the core) required to maintain the reactor prompt critical in the fundamental mode $\Psi_0(r)$. In order to develop a relation between α and l, the source-free point kinetics equations will be considered.

$$\frac{dn}{dt} = \frac{K_{eff}(1-\beta)-1}{l} n + \sum_i \lambda_i c_i \qquad (3\text{-}6)$$

$$\frac{dc_i}{dt} = \frac{K_{eff}\beta_i}{l} n - \lambda_i c_i = \dot{c}_i \qquad (3\text{-}7)$$

By definition

$$\alpha = \frac{1}{n}\frac{dn}{dt} = \frac{k_{eff}(1-\beta)-1}{l} + \frac{1}{n}\Sigma \lambda_i C_i \qquad (3\text{-}8)$$

From (3-7)

$$n = \frac{l}{K_{eff}\beta_i}\left(\dot{c}_i + \lambda_i c_i\right) \qquad (3\text{-}9)$$

Substituting (3-9) in (3-8) yields

$$\alpha = \frac{1}{n}\frac{dn}{dt} = \frac{K_{eff}(1-\beta_i)-1}{l} + \frac{K_{eff}\beta}{l}\sum \frac{a_i \lambda_i}{\lambda_i + \dot{c}_i/c_i} \qquad (3\text{-}10)$$

where

$$a_i = \beta_i/\beta \quad \text{and} \quad \beta=\Sigma \beta_i \qquad (3\text{-}11)$$

If we consider very large rates of reactivity insertion, then $\dot{c}_i/c_i >> \lambda_i$ and the instantaneous α becomes

$$\alpha = \frac{K_{eff}(1-\beta_i)-1}{l} \qquad (3\text{-}12)$$

This is the prompt-α observed after a sudden change of reactivity. Solving equation (3-12) for l yields

$$l = \frac{K_{eff}(1-\beta_i)-1}{\alpha} \qquad (3\text{-}13)$$

The BOLD VENTURE computation system has been used to calculate the value of K_{eff} for several core compositions. The neutron lifetime l was determined by computing the amount of 1/v absorber to be removed or added to reach a multiplication constant K_{eff} equal to $1 + \beta_{eff}$. The results of the calculations of l are shown in figure 3.4 as a function of K_{eff}. The curves show the differences in l when we change K_{eff} in different ways; curve 1 is for the case when K_{eff} changes because of different concentrations of B^{10} as a burnable poison, curve 2 corresponds to the case of a fixed amount of B^{10} (6g.), but with control rod movement (ring 2); and curve 3 corresponds to a sequence where K_{eff} changes because of different Xe^{135} concentrations at different power levels. The relation between l and K_{eff} is therefore not unique although figure 3.4 shows consistency within 10%.

In order to calculate the effective delayed neutron fraction β_{eff}, the perturbation code of the BOLD VENTURE computation system was supplied with the delayed neutron data given by table 3.4. The value of β_{eff} was found to be equal to 0.0072.

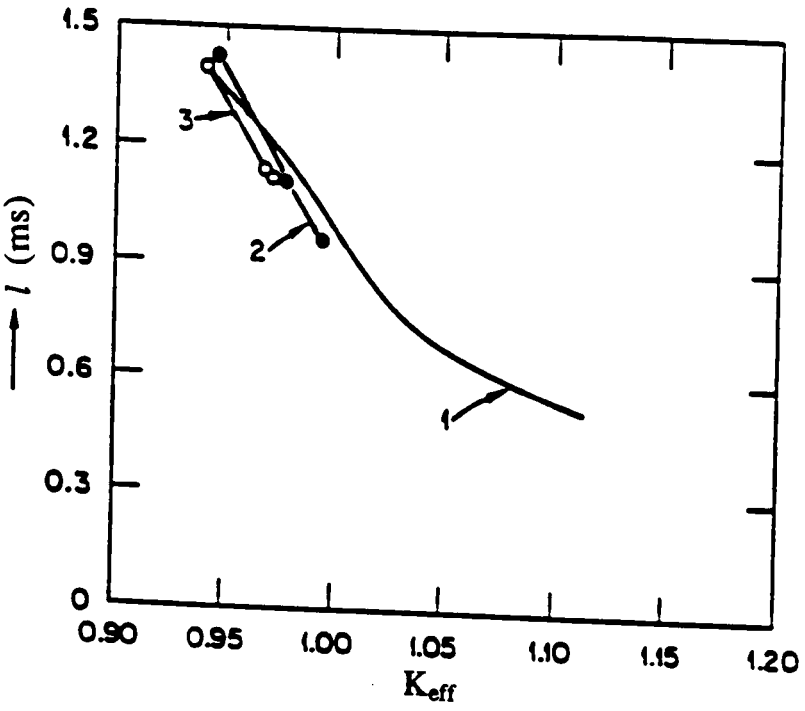

Figure 3.4 Neutron lifetime (l) as a function of the multiplication constant (K_{eff}). The different curves correspond to different ways of obtaining the same K_{eff}.

Table 3.4 Delayed- and Photo-Neutrons Data

1. Delayed Neutron Parameters. (Source: ENDF/B-V)

Group	a_i(Relative Abundance)	$\lambda_i(sec^{-1})$
1	0.038	0.01272
2	0.213	0.03174
3	0.188	0.116
4	0.407	0.311
5	0.128	1.40
6	0.026	3.87
	$\Sigma a_i = 1.000$	

2. Delayed photoneutrons from ^{235}U fission gammas on D_2O.

(Source: G.R. Keepin "Physics of Nuclear Kinetics", p.146).

Group	a_i(Relative Abundance)	$\lambda_i(sec^{-1})$
1	0.000496	6.26-7
2	0.00102	3.63-6
3	0.00320	4.37-5
4	0.0232	1.17-4
5	0.0205	4.28-4
6	0.0333	1.50-3
7	0.0695	4.81-3
8	0.2025	1.69-2
9	0.6461	2.77-1
	$\Sigma a_i = 1.000$	

Chapter IV

Reactor Transient Response

For a nuclear reactor to operate at a constant power level, the rate of neutron production via fission reactions should be exactly balanced by neutron absorption and leakage. Any deviation from this balance condition will result in a time-dependence of the neutron population and hence the power level of the reactor. This may occur for a number of reasons. For example, the reactor power level is required to be changed; this can be done by temporarily altering the core multiplication via control rod adjustment. Or there may be longer term changes in the core multiplication due to fuel depletion and isotopic buildup. More dramatic changes in multiplication might be caused by unforeseen accident situations, such as the accidental ejection of a control rod.

It is important to be able to predict the time behavior of the neutron population in a reactor core induced by changes in reactor multiplication. Here, our dominant concern will be the prediction of the time behavior of the neutron population in the ANS reactor for a given change in multiplication.

The principal applications of such an analysis are to study the operating transients in the reactor. We should distinguish between two different types of analysis depending on the time scale characterizing changes in the neutron population or core properties. For example, relatively short-term changes ranging from fractions of seconds up to minutes in length when analyzing

normal changes in reactor power level (e.g., startup or shutdown). By way of contrast, changes in core composition due to fuel burnup or isotope buildup usually occur over periods of days or months. Needless to say, the analysis required for each class of time behavior is quite different. In this chapter we will discuss the short-term transients. The long-term transients will be discussed in chapter V.

In order to study the kinetic behavior of the ANS reactor, two kinetics models have been developed. The first model is the One-Point-One-Group (1P1G), or what is known as the one point reactor kinetics model. The second is a Two-Point-Two-Group (2P2G) model. For comparison purposes, both models will be used in every power transient simulation with various ramp reactivity insertions.

A unique feature of the ANS reactor is that certain fission gammas create delayed photoneutrons in the D_2O reflector by (γ,n) reaction. Up to nine photoneutron groups and up to six delayed neutron groups were considered. A disadvantage of the 1P1G model is its inability to distinguish between transients induced by the regulating control rods and those induced by the safety control rods. Also, the 1P1G model cannot express the coupling effects between the core and the reflector; this is an important aspect of the ANS reactor since the photoneutrons are produced in the reflector while the delayed neutrons are produced in the core.

In the 2P2G model we have considered the reactor system that is composed of the core, i.e., the prompt and delayed neutron

source, and the D_2O reflector, i.e., the photoneutron source; whose intensity is proportional to the average neutron flux in the core. Neutron leakage and slowing down have been considered to have influence on the neutron density in reflector and core. We have taken as a model two homogeneous component reactor and applied the time-dependent two group diffusion theory for the system. A list of the symbols used in this chapter is given in Table 4.1.

The two kinetics models have been used to simulate several reactor transients. The transients that have been studied can be divided into two main categories. The first involves an extraneous source while the other does not. These transients can be induced by either the regulating control rods in the center of the core and hence the multiplication factors of the fast and thermal neutrons in the core were the control variables; or by the safety control rods, located between the core and the reflector, and hence the coupling coefficient between the reflector and the core was the control variable. As mentioned before, one of the disadvantages of the 1P1G model is that it cannot distinguish between the two control variables. Therefore, the effect of each of the control rods on the behavior of the reactor can be studied with the 2P2G model.

4.1 One-Point-One-Group Model

A number of questionable assumptions have entered into the derivation of the point kinetics equations, such as the one-speed

Table 4.1 A List of Symbols used in this chapter

Sym.	Description	Value
	I. State Variables	
	(1) 1P1G Model	
n	Total number of neutrons in the reactor.	
C_i^n	Total number of delayed neutron precursor atoms in the whole reactor.	
C_i^γ	Total number of photo neutron precursor atoms in the whole reactor.	
	(2) 2P2G Model	
N_{c1}	Total number of fast neutrons in the core.	
N_{c2}	Total number of thermal neutrons in the core.	
$N_{\gamma 1}$	Total number of fast neutrons in the reflector.	
$N_{\gamma 2}$	Total number of thermal neutrons in the reflector.	
C_i^n	Total number of delayed neutrons produced in the core.	
C_j^γ	Total number of photo neutrons produced in the reflector.	
	II. Constants and Parameters	
β^n	Delayed neutron fraction.	0.0072
β^γ	Photoneutron fraction.	0.00101
S_c	Extraneous source placed in the core.	
S_r	Extraneous source placed in the reflector.	
l_{c1}	Fast neutron lifetime in the core.	1.52 μsec.
l_{c2}	Thermal neutron lifetime in the core.	27.2 μsec.
l_{r1}	Fast neutron lifetime in the reflector.	10.52 μsec.
l_{r2}	Thermal neutron lifetime in the reflector.	10.45 msec.
l_{csl}	Slowing down time in the core.	37.2 μsec.
l_{rsl}	Slowing down time in the reflector.	10.52 μsec.

Table 4.1 continued.

Sym.	Description	Value
K_{c1}	Fast neutron multiplication constant in the core.	0.5639
K_{c2}	Thermal neutron multiplication constant in the core.	1.083
K_{cr}	Coupling coefficient between the core and the reflector, it is the fraction of neutrons that leave the core and go to the reflector. We assume that only fast neutrons migrate from the core to the reflector.	0.5785
K_{rc}	Coupling coefficient between the reflector and the core; it is the fraction of neutrons (assumed to be thermal) that migrate from the reflector to the core.	0.5251

diffusion approximation, and a time-independent spatial shape. In heavy-water-moderated systems the reactor kinetic equations must be extended to include contributions from the $D(\gamma, n)$ photoneutrons.

Then the reactor kinetic equations can be written

$$\frac{dn}{dt} = \frac{K_{eff}(1-\beta)-1}{l} n + \sum \lambda_i^n c_i^n + \sum \lambda_j^\gamma c_j^\gamma + S \qquad (4\text{-}1)$$

$$\frac{dc_i^n}{dt} = \frac{K_{eff}\,\beta_i^n}{l} n - \lambda_i^n c_i^n \qquad (4\text{-}2)$$

$$\frac{dc_i^\gamma}{dt} = \frac{K_{eff}\,\beta_j^\gamma}{l} n - \lambda_j^\gamma c_j^\gamma \qquad (4\text{-}3)$$

where $\beta = \Sigma \beta_i^n + \Sigma \beta_j^\gamma$

The above form of the model will be referred to as 1P1G-A. These equations can be written in a somewhat different form by introducing two definitions. First the mean neutron generation time is defined as

$$\Lambda = \frac{l}{K_{eff}} \qquad (4\text{-}4)$$

Next the reactivity, which measures the deviation of core multiplication from its critical value $K_{eff} = 1$, is defined as:

$$\rho = \frac{K_{eff} - 1}{K_{eff}} \qquad (4\text{-}5)$$

These definitions allow the writing of equations (4-1) to (4-3) in a slightly different form:

$$\frac{dn}{dt} = \frac{\rho - \beta}{\Lambda} n + \sum \lambda_i^n c_i^n + \sum \lambda_j^\gamma c_j^\gamma + S \qquad (4\text{-}6)$$

$$\frac{dc_i^n}{dt} = \frac{\beta_i^n}{\Lambda} n - \lambda_i^n c_i^n \qquad (4\text{-}7)$$

$$\frac{dc_j^\gamma}{dt} = \frac{\beta_j^\gamma}{\Lambda} n - \lambda_j^\gamma c_j^\gamma \qquad (4\text{-}8)$$

This form will be referred to as 1P1G-B. The results of the 1P1G model will be compared to those of the 2P2G model, and conclusions can be derived about the validity of the 1P1G model.

4.2 Two-Point-Two-Group Model

A characteristic of the ANS reactor is the strong coupling between two neutron fields with very different spectra: predominance of epithermal neutrons in the core and thermal neutrons in the reflector. Because there are large variations of neutron spectra within a few centimeters in a small core, the

validity of the one-point kinetic model was questionable. Therefore a two-point (core and reflector, c and r, respectively) and two-energy groups (fast and thermal, 1 and 2, respectively) model was developed to detect the conditions under which the 1P1G model is not valid. The equations for the core are:

$$\frac{dN_{c1}}{dt} = \frac{k_{c1}(1-\beta^n)-1}{l_{c1}} N_{c1} + \frac{k_{c2}(1-\beta^n)}{l_{c2}} N_{c2} + \sum \lambda_i^n c_i^n + S_c \qquad (4\text{-}9)$$

$$\frac{dc_i^n}{dt} = -\lambda_i^n c_i^n + \beta_i^n \left[\frac{k_{c1}}{l_{c1}} N_{c1} + \frac{k_{c2}}{l_{c2}} N_{c2} \right] \qquad (4\text{-}10)$$

$$\frac{dN_{c2}}{dt} = -\frac{N_{c2}}{l_{c2}} + \frac{N_{c1}}{l_{csl}} + k_{rc} \frac{N_{r2}}{l_{r2}} \qquad (4\text{-}11)$$

and for the reflector,

$$\frac{dN_{r1}}{dt} = -\frac{N_{r1}}{l_{r1}} + k_{cr} \frac{N_{c1}}{l_{c1}} + \sum \lambda_j^\gamma c_j^\gamma + S_r \qquad (4\text{-}12)$$

$$\frac{dc_j^\gamma}{dt} = -\lambda_j^\gamma c_j^\gamma + \beta_j^\gamma \left[\frac{k_{c1}}{l_{c1}} N_{c1} + \frac{k_{c2}}{l_{c2}} N_{c2} \right] \qquad (4\text{-}13)$$

$$\frac{dN_{r2}}{dt} = -\frac{N_{r2}}{l_{r2}} + \frac{N_{r1}}{l_{rsl}} \qquad (4\text{-}14)$$

The above form of the model will be referred to as 2P2G-A. Equation (4-9) was written under the assumption that the source of fast neutrons in the core is mainly the fission process and the

neutron decay of fission products; i.e. the fast neutrons coming from the reflector and the photoneutrons produced inside the core were ignored. Equation (4-10) is the balance equation of the delayed neutrons produced inside the core, and equation (4-11) is the balance equation of the thermal neutrons inside the core in which the sources of thermal neutrons are: the slowing down of fast neutrons inside the core and the fraction of thermal neutrons that enter the core from the reflector. Equation (4-14) states that the thermal neutrons in the reflector come mainly from the moderation process in the reflector; i.e., the thermal neutrons from the core were neglected. In summary, the coupling in the fast and thermal groups is produced by neutrons that go mainly from the core to the reflector and from the reflector to the core, respectively.

The equations of the 2P2G model can also be transformed into a slightly different form by introducing the following definitions:

Generation times

$$\Lambda_{c1} = \frac{l_{c1}}{K_{c1}} \quad , \quad \Lambda_{c2} = \frac{l_{c2}}{K_{c2}} \tag{4-15}$$

Reactivity

$$\rho_1 = \frac{K_{c1} - 1}{K_{c1}} \tag{4-16}$$

Introducing these definitions, the 2P2G model assumes the following form (which will be referred to as 2P2G-B):

$$\frac{dN_{c1}}{dt} = \frac{(\rho_1-\beta^n)}{\Lambda_{c1}} N_{c1} + \frac{(1-\beta^n)}{\Lambda_{c2}} N_{c2} + \Sigma \lambda_i^n c_i^n + S_c \qquad (4\text{-}17)$$

$$\frac{dc_i^n}{dt} = -\lambda_i^n c_i^n + \beta_i^n \left[\frac{N_{c1}}{\Lambda_{c1}} + \frac{N_{c2}}{\Lambda_{c2}} \right] \qquad (4\text{-}18)$$

$$\frac{dN_{c2}}{dt} = -\frac{N_{c2}}{\Lambda_{c2} k_{c2}} + \frac{N_{c1}}{l_{csl}} + \frac{N_{r2}}{l_{r2}} k_{rc} \qquad (4\text{-}19)$$

$$\frac{dN_{r1}}{dt} = -\frac{N_{r1}}{l_{r1}} + \frac{k_{cr}}{\Lambda_{c1} k_{c1}} N_{c1} + \Sigma \lambda_j^\gamma c_j^\gamma + S_r \qquad (4\text{-}20)$$

$$\frac{dc_i^\gamma}{dt} = -\lambda_i^\gamma c_i^\gamma + \beta_i^\gamma \left[\frac{N_{c1}}{\Lambda_{c1}} + \frac{N_{c2}}{\Lambda_{c2}} \right] \qquad (4\text{-}21)$$

$$\frac{dN_{r2}}{dt} = -\frac{N_{r2}}{l_{r2}} + \frac{N_{r2}}{l_{rsl}} \qquad (4\text{-}22)$$

This form of the model will be referred to as 2P2G-B and will be used if the generation times Λ_{c1} and Λ_{c2} are to be considered as constants.

The global multiplication constant k_{eff} is obtained in the usual way, i.e., by dividing the production terms in equations (4-9) through (4-14) by K_{eff} and setting the time derivatives equal to zero. The details are given in appendix A.1. The result is

$$K_{eff} = K_{c1} + K_{c2}\left[\frac{l_{c1}}{l_{csl}} + K_{rc}\,K_{cr}\,\frac{l_{r1}}{l_{rsl}}\right] + \beta^{\gamma}\,K_{c2}\,K_{rc}\,\frac{l_{r1}}{l_{rsl}} \qquad (4\text{-}23)$$

A spherical model of the ANS reactor was calculated with the transport code XSDRNPM; the summary tables of the output were used to compute the neutron lifetimes l's as the inverse of the corresponding reaction rates per neutron and the K's as ratios of production to destruction. Table[5] 4.2 summarizes the results for a reference case for which the overall K_{eff} = 0.9368.

Table 4.2

Two-Point-Two-Group Kinetics Parameters

K_{c1}= 0.5639	K_{c2} = 1.083
K_{rc} = 0.5251	K_{cr} = 0.5785
l_{c1}=1.52 μsec	l_{c2}=27.2 μsec
l_{r1}= 10.52 μsec	l_{r2}= 10.45 msec
l_{csl}= 37.2 μsec	l_{rsl}= 10.52 μsec

K_{eff} given by equation (4-23) can be expressed in terms of generation times by using the definitions given by equation (4-15). The result is

$$K_{eff} = K_{c1} + \frac{\Lambda_{c1}}{l_{csl}} S_p K_{c1}^2 + K_{c1} S_p K_{rc} K_{cr} \frac{l_{r1}}{l_{rsl}} + \beta^{\gamma} S_p K_{c1} K_{rc} \frac{l_{r1}}{l_{rsl}} \quad (4\text{-}24)$$

The two kinetics models which have been developed will be applied to several reactor transients of practical importance. Two types of transients have been considered. The first includes an extraneous source; the second does not. These two types of transients will be considered in sections 4.3 and 4.4, respectively.

4.3 ANS Reactor Transients with Extraneous Source

Two types of transients have been studied with an extraneous source. The first is the subcritical transient, and the second is the reactor startup. The variables in the two models have been normalized to their initial conditions. The extraneous source was normalized to 1 n/sec. Appendix A.2 shows the details of deriving the initial conditions and the normalized forms of the models.

4.3.1 Subcritical Transient: The reactor is assumed to be subcritical. A ramp reactivity insertion (Figure 4.1), that transformed the reactor from one subcritical state to another subcritical state has been applied. Six groups of delayed neutrons and nine groups of photoneutrons were used. The change in reactivity was induced by the regulating control rod, and thus the multiplication factors k_{c1} and k_{c2} represent the control variables; while the safety control rod was held in a fixed position that corresponded to $K_{rc} = 0.5251$. The initial value of k_{c1} is $k_{0c1}=0.56359$. These two values of K_{rc} and k_{0c1} correspond to an inital value of k_{eff} of 0.9368.

Figure 4.2(a) corresponds to the case in which the prompt-neutron lifetimes *l*'s were kept constant; i.e., the kinetics models were used in the forms 1P1G-A and 2P2G-A. These forms were used in connection with equation (4.23). The extraneous source was located in the core; i.e., S_r was set equal to zero. However, Figure 4.2(b) corresponds to the same conditions as Figure 4.2(a) except that the source was placed in the reflector; i.e., S_c was set equal to zero. Figure 4.3 corresponds to the case in which the generation times Λ's were kept constant; i.e., the kinetics models were used in the forms 1P1G-B and 2P2G-B; the other conditions were similar to those applied to Figure 4.2(a). All of the figures indicate that there is a difference among results of the 1P1G model and the 2P2G model.

A comparison between Figures 4.2(a) and 4.2(b) indicates that the location of the source has no impact on the results; and a

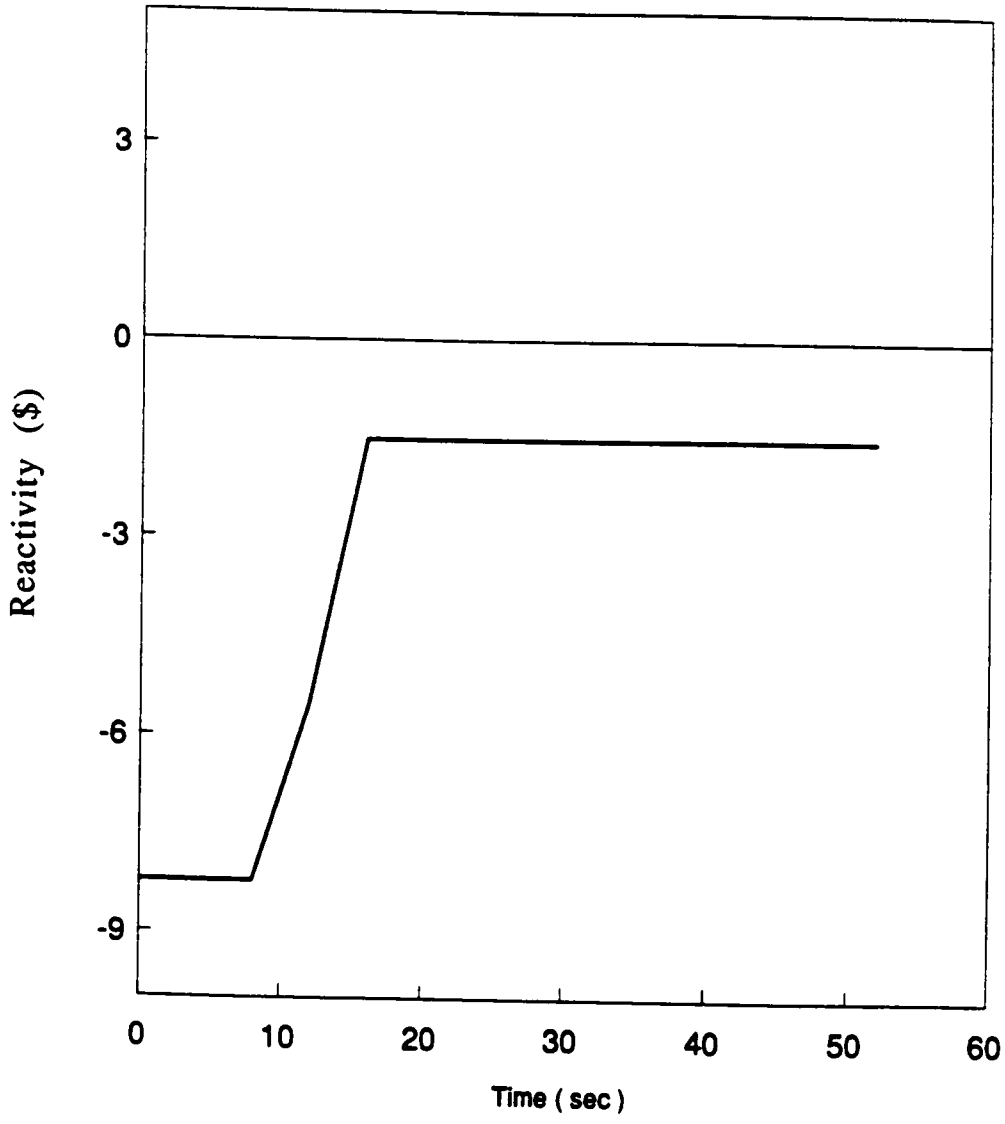

Fig.4.1 Reactivity insertion for the subcritical transient.

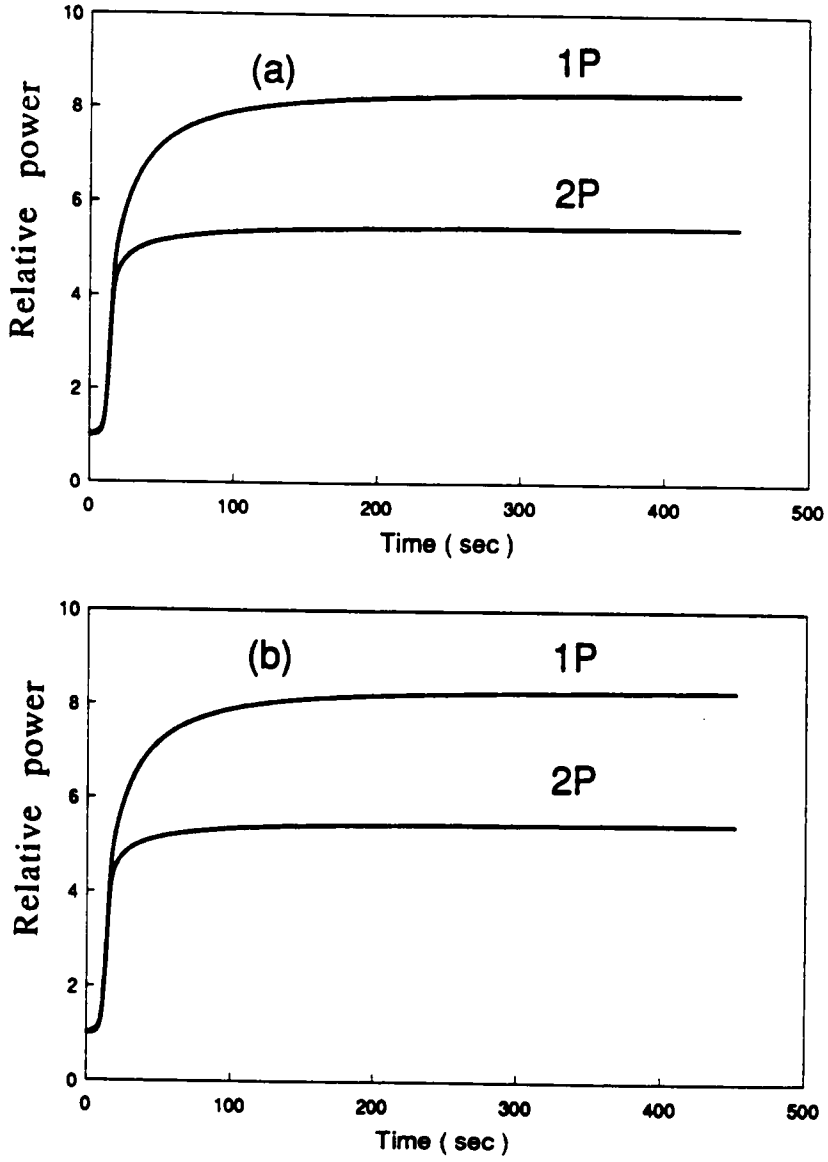

Fig.4.2 Power level for the subcritical transient with constant prompt neutron lifetime l (a) source in core (b) source in reflector.

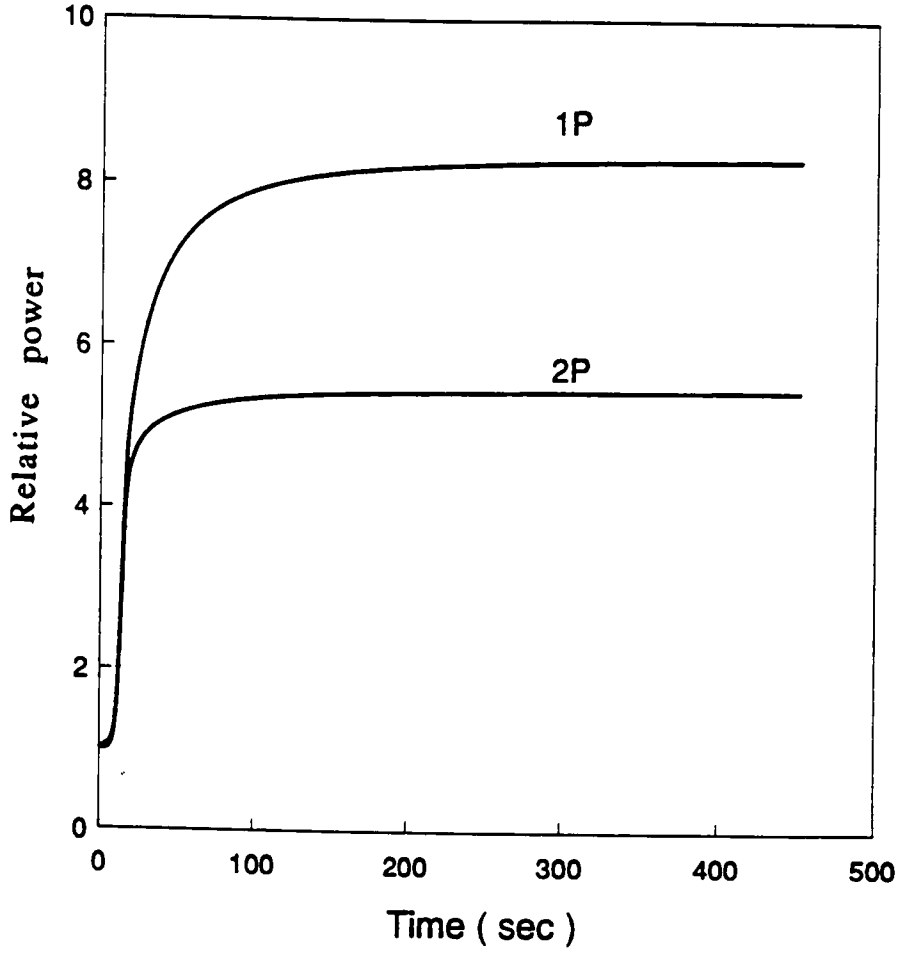

Fig.4.3 Power level for the subcritical transient with constant generation time, and with source in core

comparison between 4.2(a) and 4.3 indicates that there is no diffference in the results obtained by the first form of the models (i.e., the 1P1G-A and the 2P2G-A) and those obtained by the second form of the models (i.e., the 1P1G-B and the 2P2G-B).

4.3.2 Start-up of the Reactor: In this case the reactor was assumed to be initially in a subcritical state with an extraneous source in the core. Figure 4.4 shows the reactivity insertion required to render the reactor critical. In reference to Figure 4.4 , the final level of the power depends on the value of ρ_{max} and the time T_3. In addition, the source was removed at some time $T_4 \geq T_2$; the behavior of the power showed a significant dependence on the time of source removal T_4. In other words, the power level depends on ρ_{max} , T_3 , and T_4. Therefore, the times T_1, T_2, and T_3 have been fixed at values of 10, 15, and 25 seconds, respectively. Figures 4.5(a) through 4.5(c) correspond to the case in which the forms 1P1G-B and 2P2G-B of the kinetics models were used, the control variables were k_{c1} and k_{c2} and the value of ρ_{max} was \$0.2; the source removal times T_4 were 10, 50, and 100 seconds for Figures 4.5(a), 4.5(b), and 4.5(c), respectively. In figures 4.6(a) through 4.6(c) the value of ρ_{max} was \$0.4; and in figures 4.7(a) through 4.7(c) the value of ρ_{max} was \$0.8. These figures indicate clearly that the sensitivity of the power level to the source removal time T_4 decreases as the value of ρ_{max} increases. Also, it is evident that the sensitivity decreases for larger values of T_4. However, only ρ_{max} and T_4 have been varied,

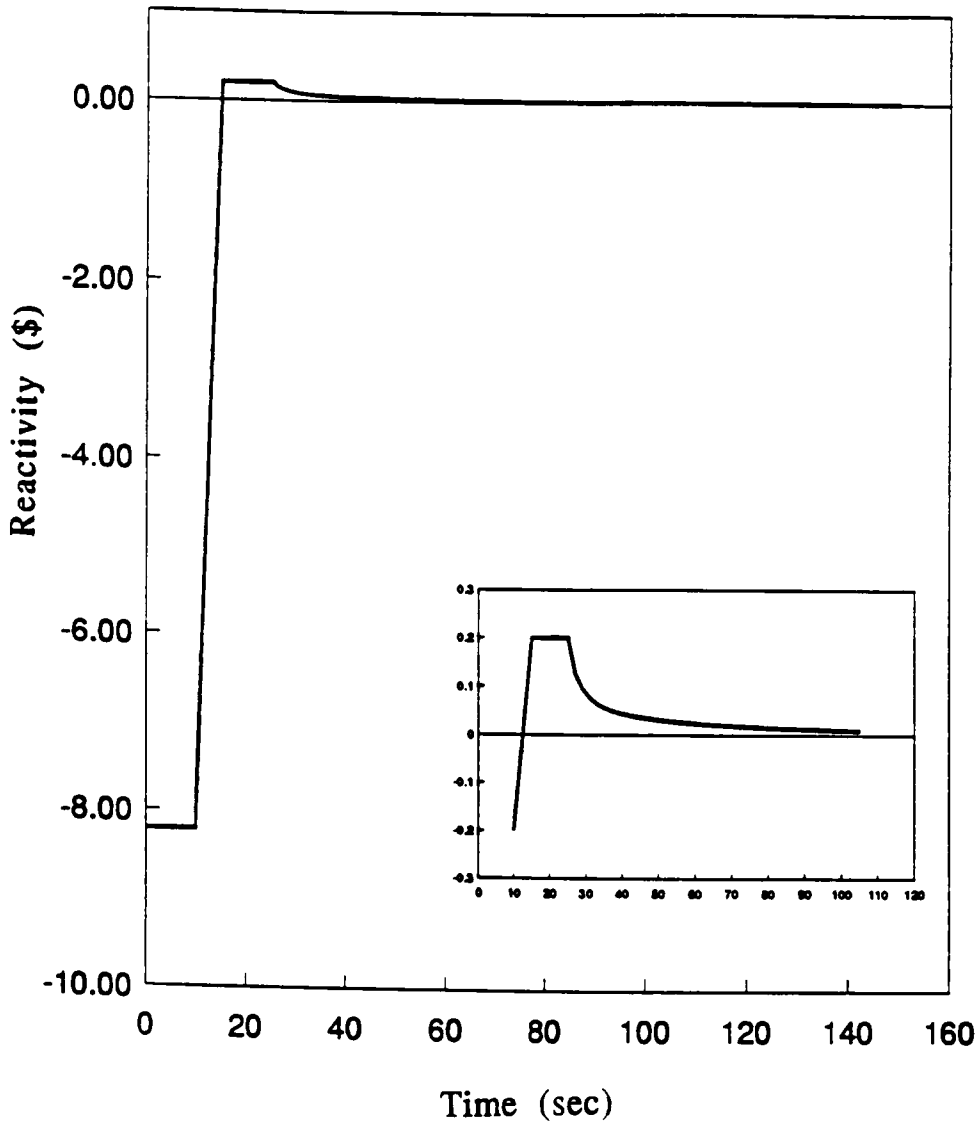

Fig.4.4 Reactivity insertion for the startup transient.

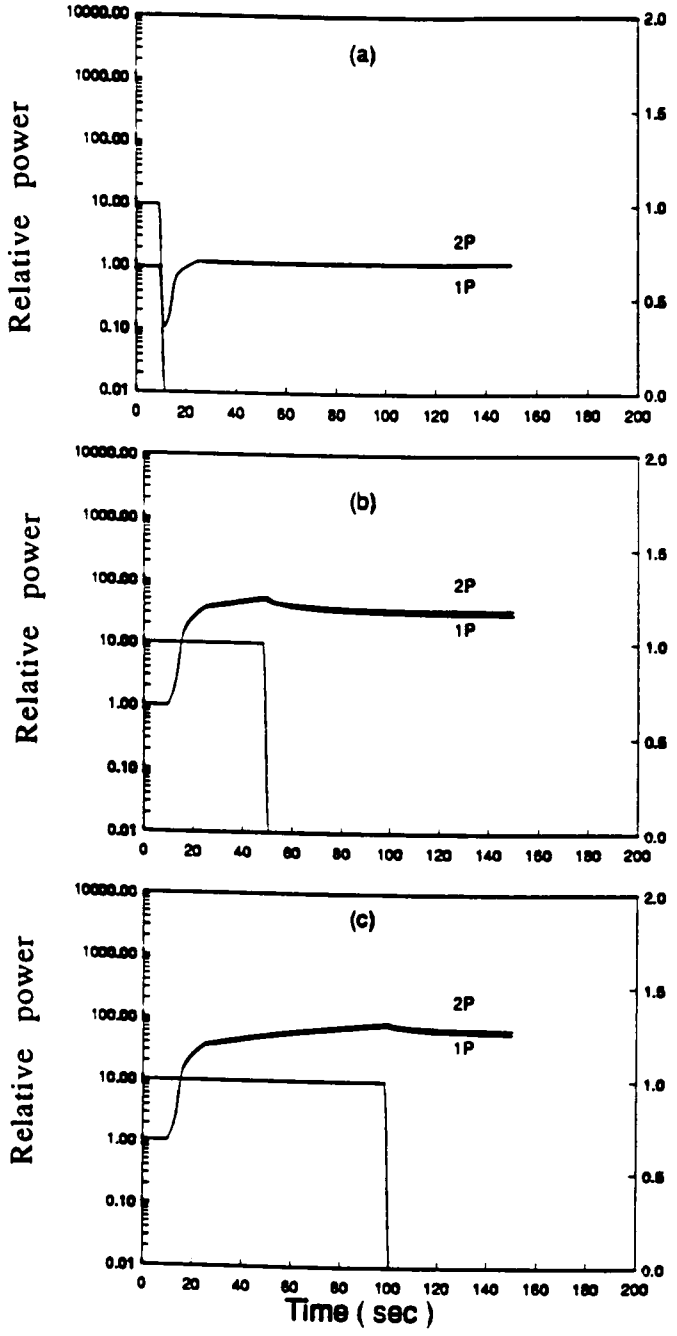

Fig.4.5 Power level after a positive reactivity insertion of \$0.2, with source removal times (a) 10 (b) 50 and (c) 100 sec.

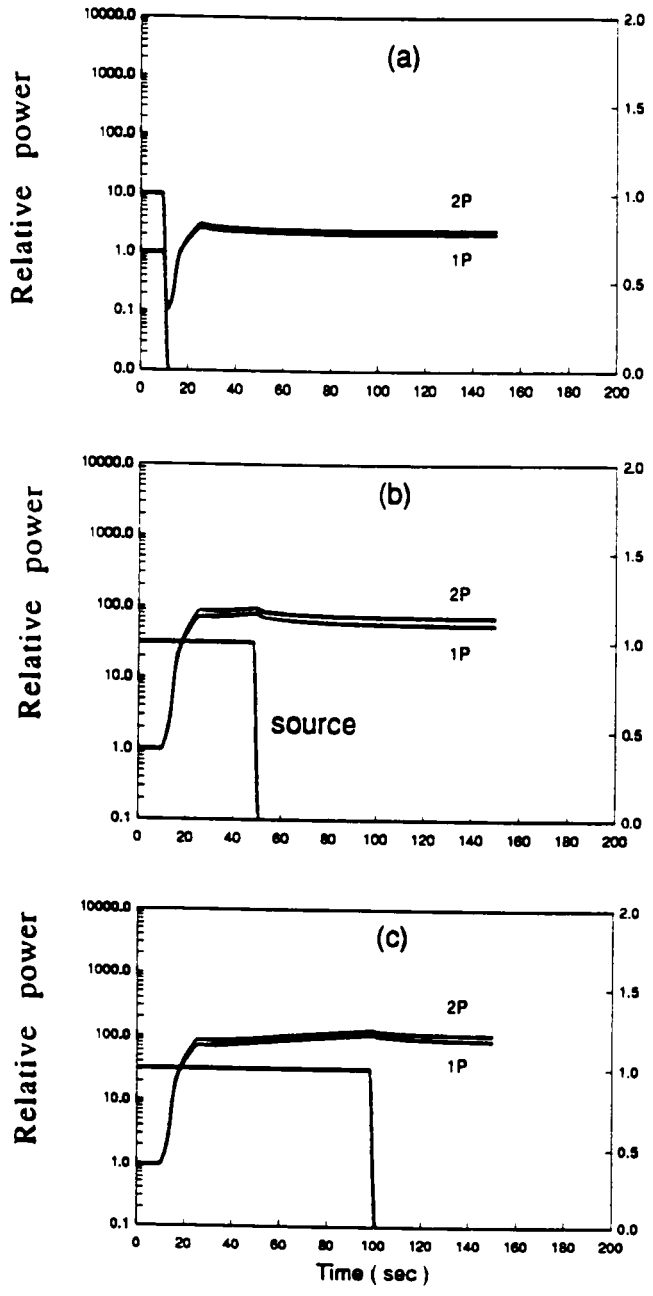

Fig.4.6 Power level after a positive reactivity insertion of \$0.4, with source removal times (a) 10 (b) 50 and (c) 100 sec.

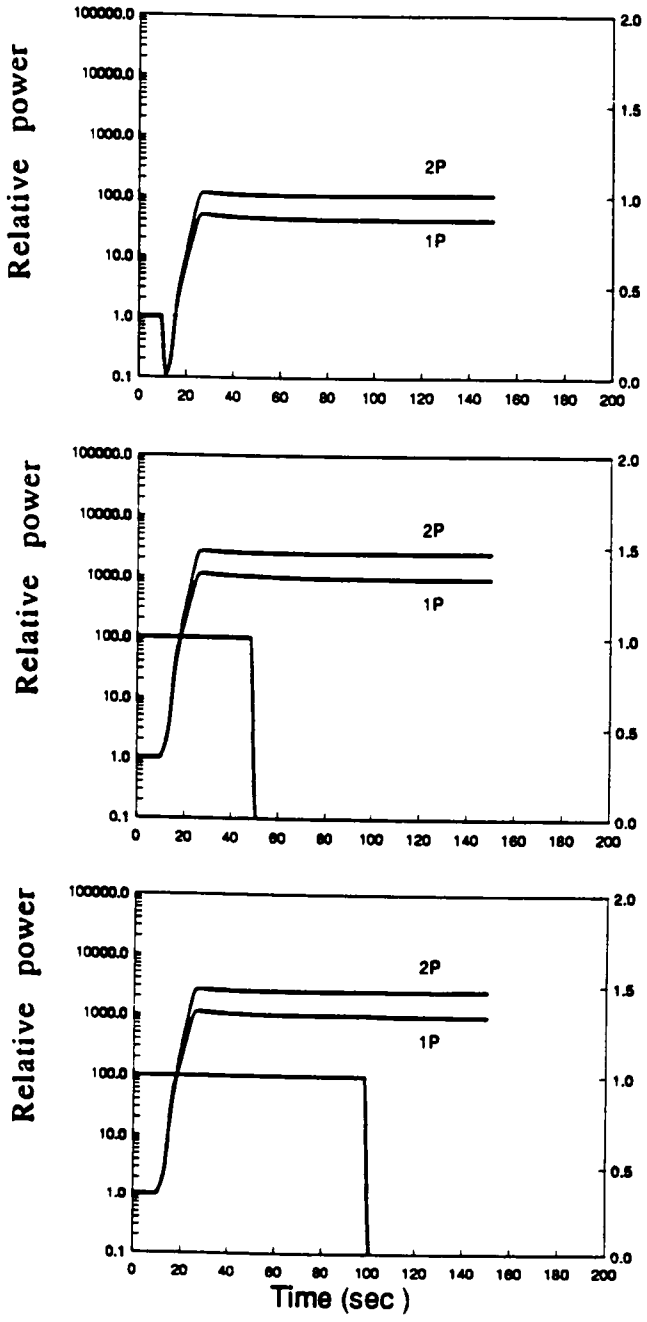

Fig.4.7 Power level after a positive reactivity insertion of \$0.8, with source removal times (a) 10 (b) 50 and (c) 100 sec.

in order to determine the minimum value of ρ_{max} that is the least sensitive to the source removal time T_4.

4.4 ANS Reactor Transients Without an Extraneous Source

Two important and practical transients with no extraneous sources have been studied. The first is the reactor shutdown and the second is the power change. The 1P1G-B and 2P2G-B forms of the kinetics models have been used.

4.4.1 ANS Reactor Shutdown: The reactor is assumed to have been initially in a critical state, then a ramp change in reactivity from $\rho=0$ to $\rho_{min}=$ -\$20 (in a period of one second) represents a sudden shutdown or "scram" of the reactor. Figure 4.8 shows the reactivity insertion required for the shutdown. However, Figure 4.9 corresponds to the case in which the reactor shutdown was achieved by the insertion of the safety control rods; i.e., the coupling coefficient k_{rc} was the control variable. Figure 4.10 corresponds to the case in which the shutdown was achieved by the insertion of the regulating rods; i.e., k_{c1} and k_{c2} were the control variables. Table 4.3 summarizes the change in the power level for the first 2 minutes after shutdown. The data in Table 4.3 indicate that the safety control rod is more effective for the shutdown than the regulating rod. The reason is that the safety rods shield the thermal neutrons coming from the reflector to the

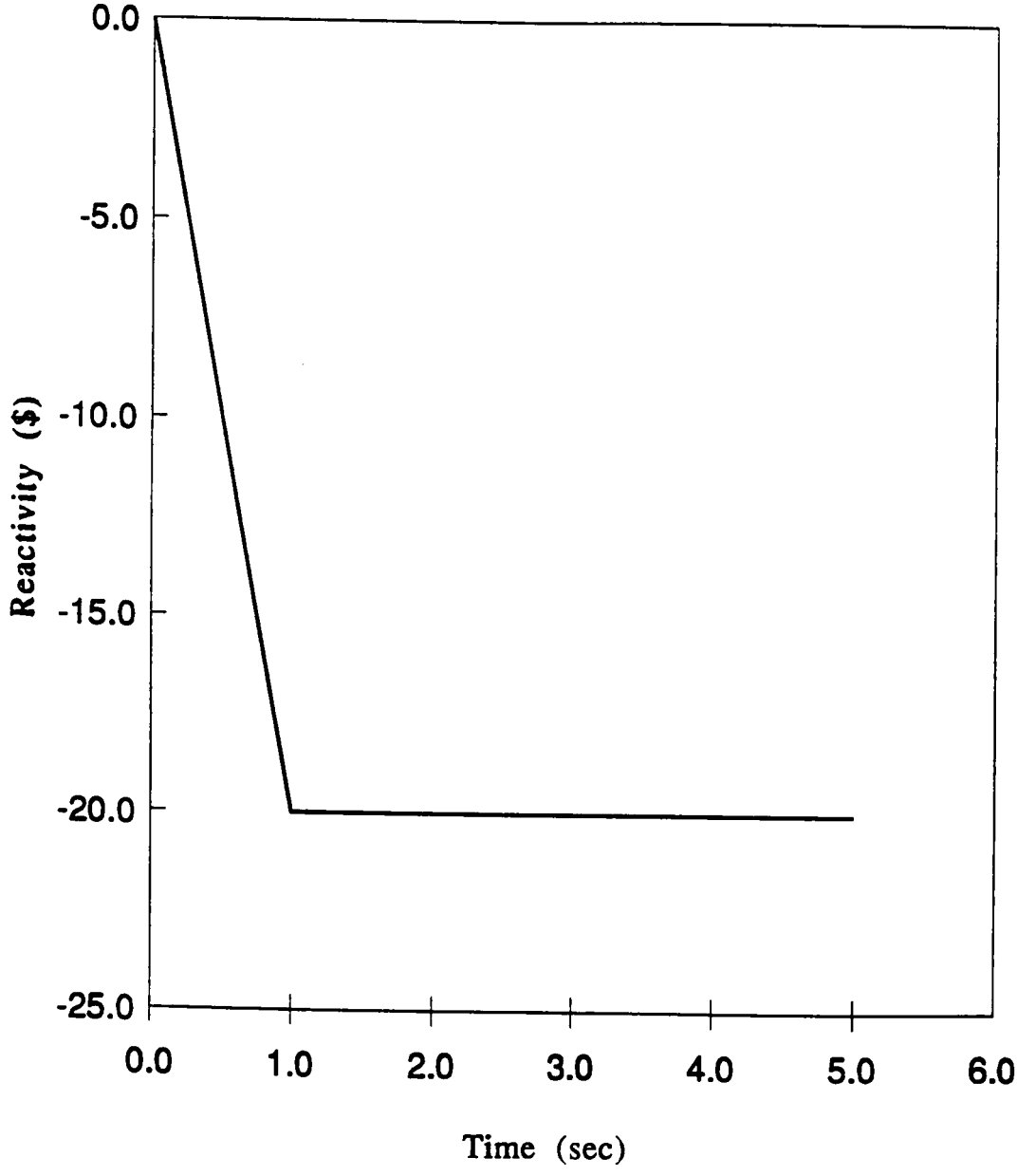

Fig.4.8 Reactivity insertion for the shutdown transient.

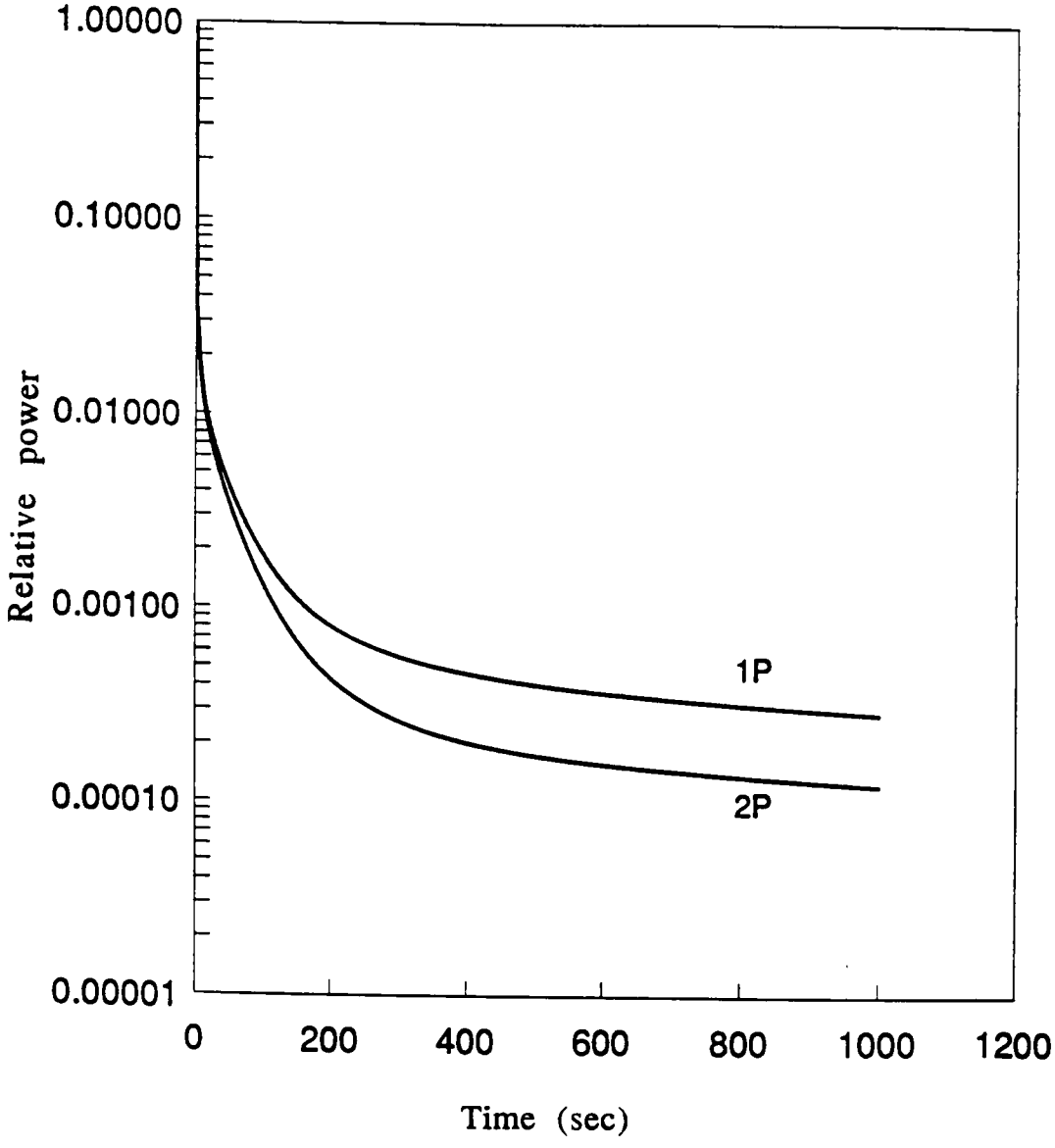

Fig.4.9 Power level for the shutdown transient with negative reactivity of - $ 20 induced by the safety rods.

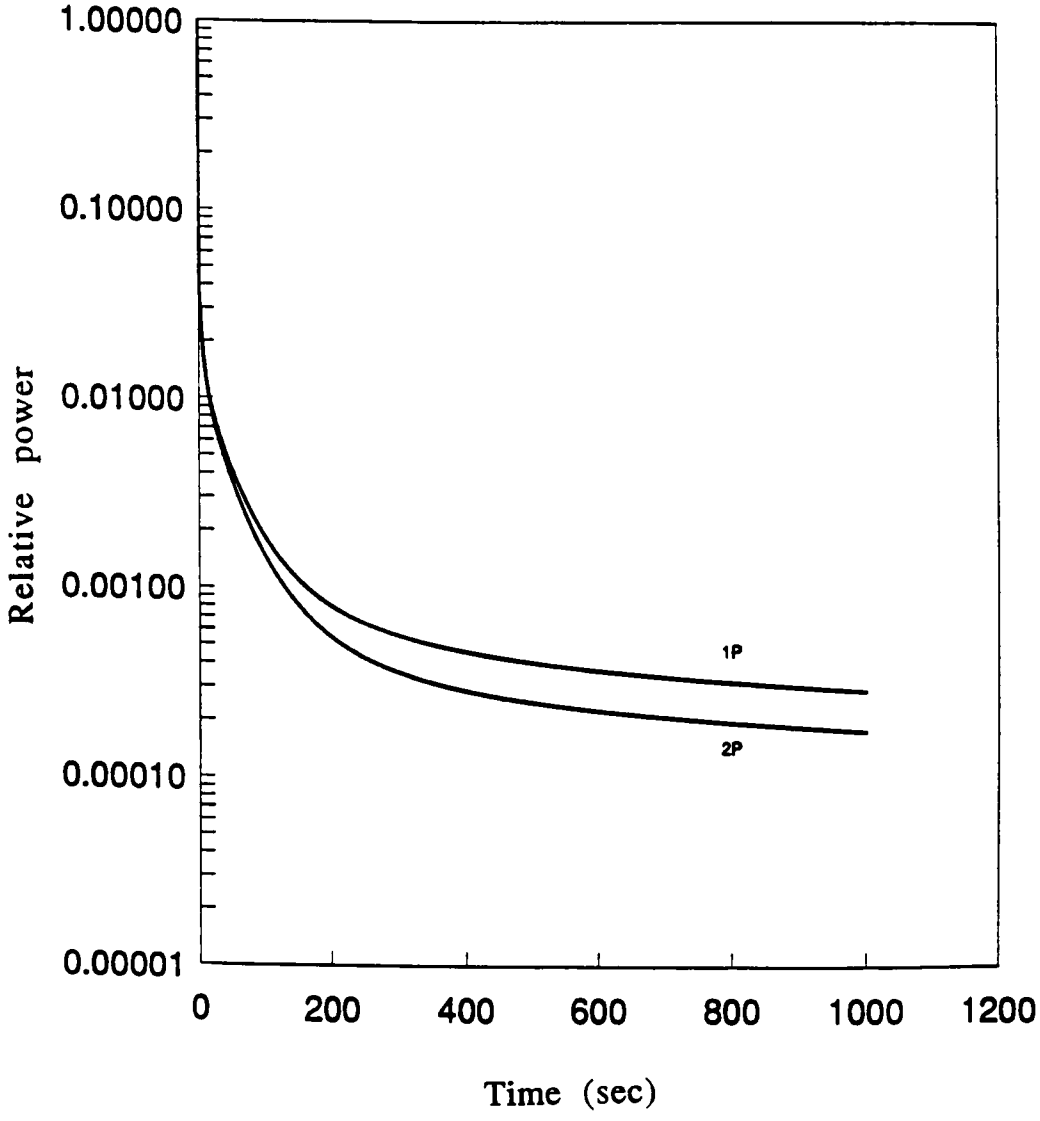

Fig.4.10 Power level for the shutdown transient with negative reactivity of - $ 20 induced by the regulating rods.

core; this in turn reduces the fission process in a fast and significant way.

Table 4.3 Power level after shutdown using different control mechanisms

Time (sec)	1P1G	2P2G	
	K_{rc} or K_{c1}	K_{rc}	K_{c1}
0.0	1.000	1.0000	1.0000
0.1	0.802	0.7849	0.7886
0.2	0.454	0.4507	0.4626
0.3	0.226	0.2274	0.2399
0.4	0.130	0.1276	0.1352
0.5	0.092	0.0875	0.0914
0.6	0.0727	0.0681	0.0704
0.7	0.0602	0.0560	0.0578
0.8	0.0512	0.0475	0.0490
0.9	0.0444	0.0410	0.0424
1.0	0.0390	0.0359	0.0372
1.1	0.0374	0.0345	0.0356
1.2	0.0366	0.0338	0.0348
1.3	0.0359	0.0331	0.0341
1.4	0.0352	0.0324	0.0334
1.5	0.0345	0.0318	0.0327
1.6	0.0338	0.0312	0.0321
1.7	0.0332	0.0306	0.0315
1.8	0.0327	0.0301	0.0310
1.9	0.0321	0.0295	0.0304
2.0	0.0316	0.0290	0.0299

4.4.2 Power Demand

In this case the reactor is assumed to have been operating in a critical state at some power level P_o. The regulating control rods were temporarily withdrawn (to increase K_{eff}), then they were reinserted in such a way to induce an exponential decay of K_{eff} or ρ, figure 4-11. This process has transformed the reactor to a new critical state with a new power level. In figures 4-12(a) and 4-12(b) six groups of delayed neutrons and nine groups of photoneutrons were used. In figures 4-13(a) and 4-13(b) only one delayed group averaged over 6 groups and one photo group averaged over nine groups were used. The amplitude of reactivity ρ_{max} for both figures was \$0.85. However, as in the case of reactor startup, the magnitude of ρ_{max} and the time T_2 (in reference to figure 4-11) are the factors that determine the value of the new power level. In figures 4-5(a) through 4-5(c) the effect of ρ_{max} was analyzed; therefore, in figures 4-12(a) and 4-12(b) the effect of T_2 is shown. In figures 4-12(a) and 4-13(a) the value of T_2 was 5 seconds, whereas in figures 4-12(b) and 4-13(b) T_2 was 15 seconds. Table 4.4 shows, quantitatively, the effect of T_2 on the final power level. The effect of the number of delayed and photoneutrons becomes more pronounced as the value of T2 increases, therefore the number of delayed and photo groups is indeed very crucial.

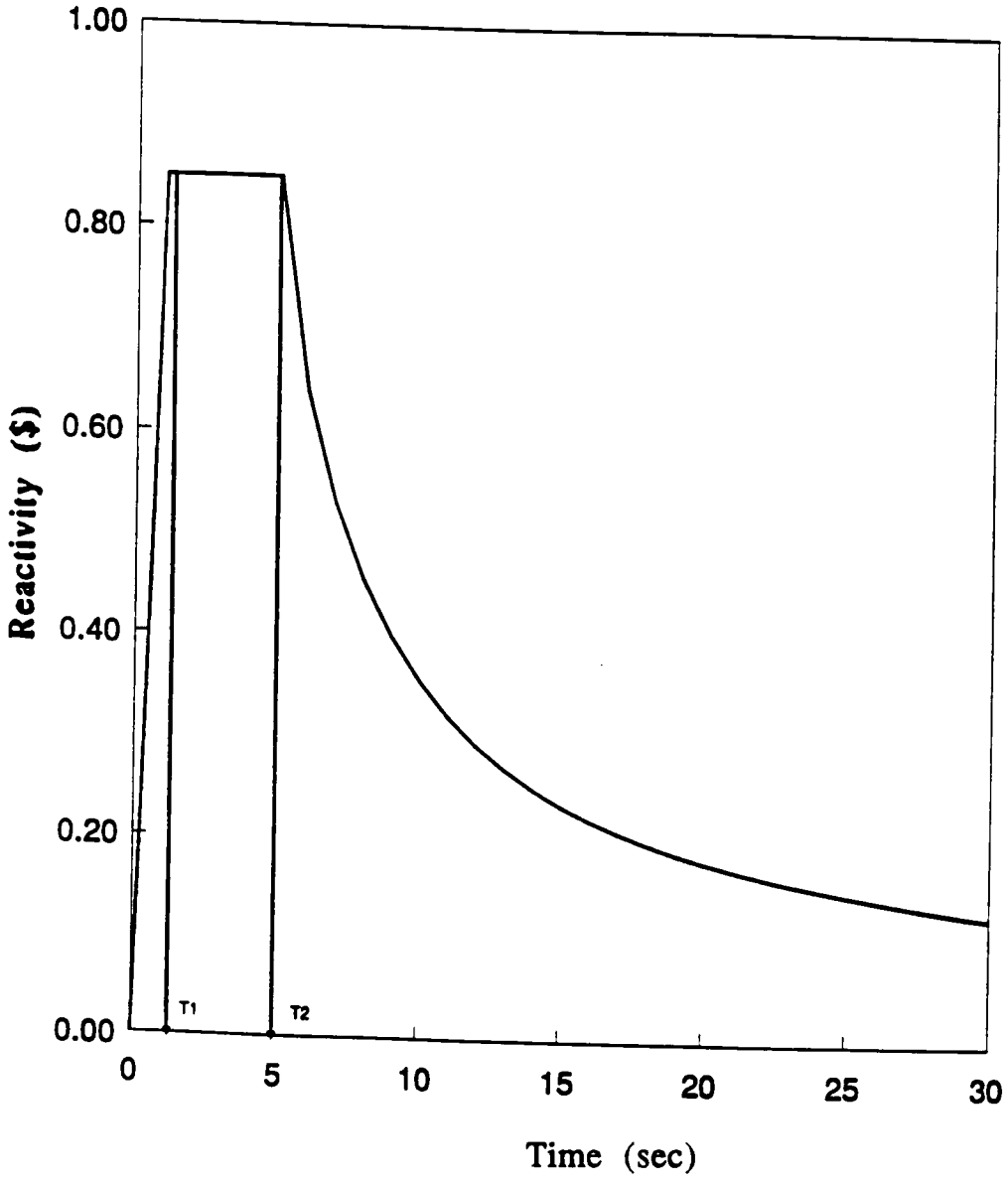

Fig.4.11 Reactivity insertion required to increase the power level.

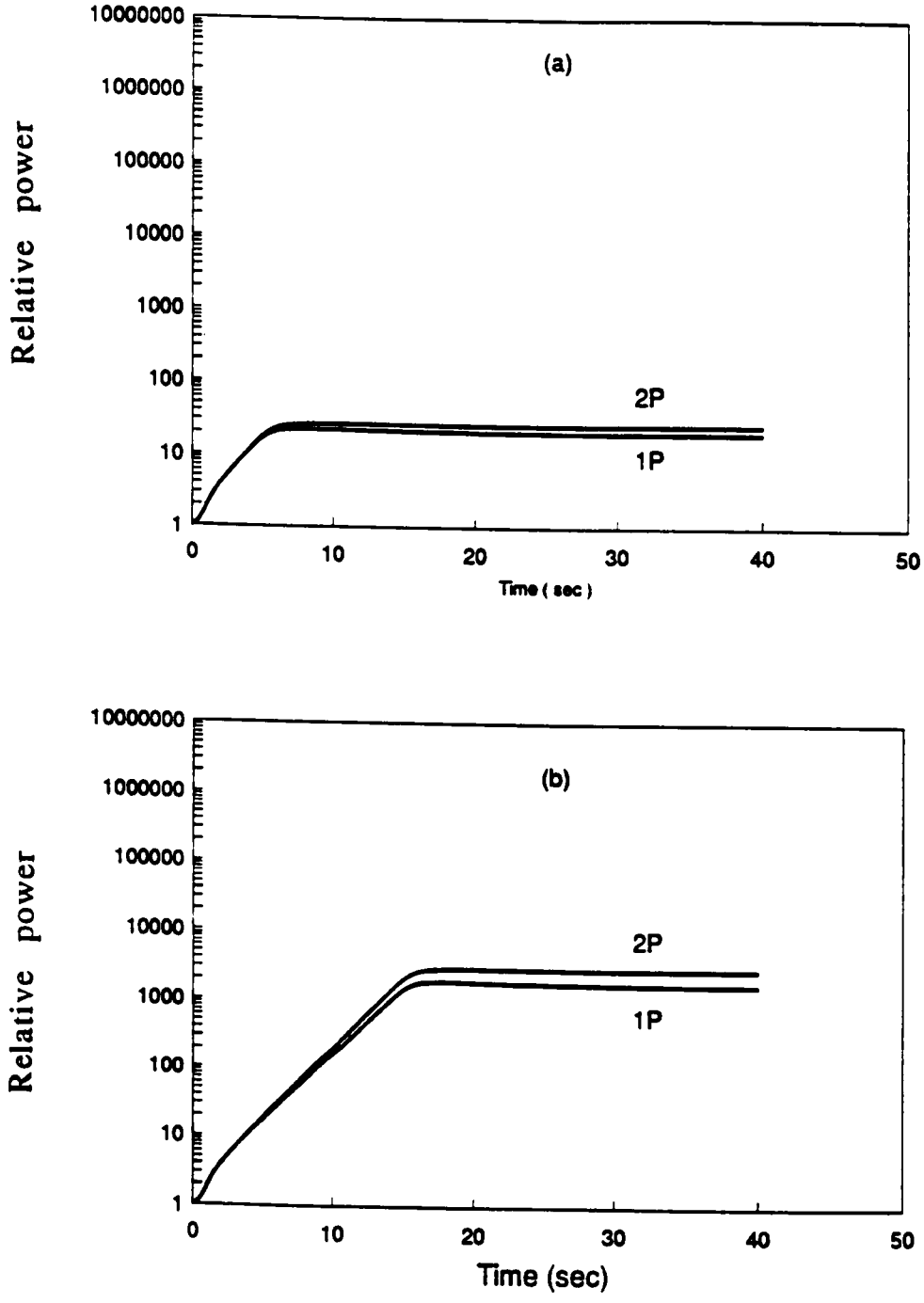

Fig.4.12 Power level using 6 groups of delayed and 9 groups of photoneutrons, (a) T2=5 sec. and (b) T2=15 sec.

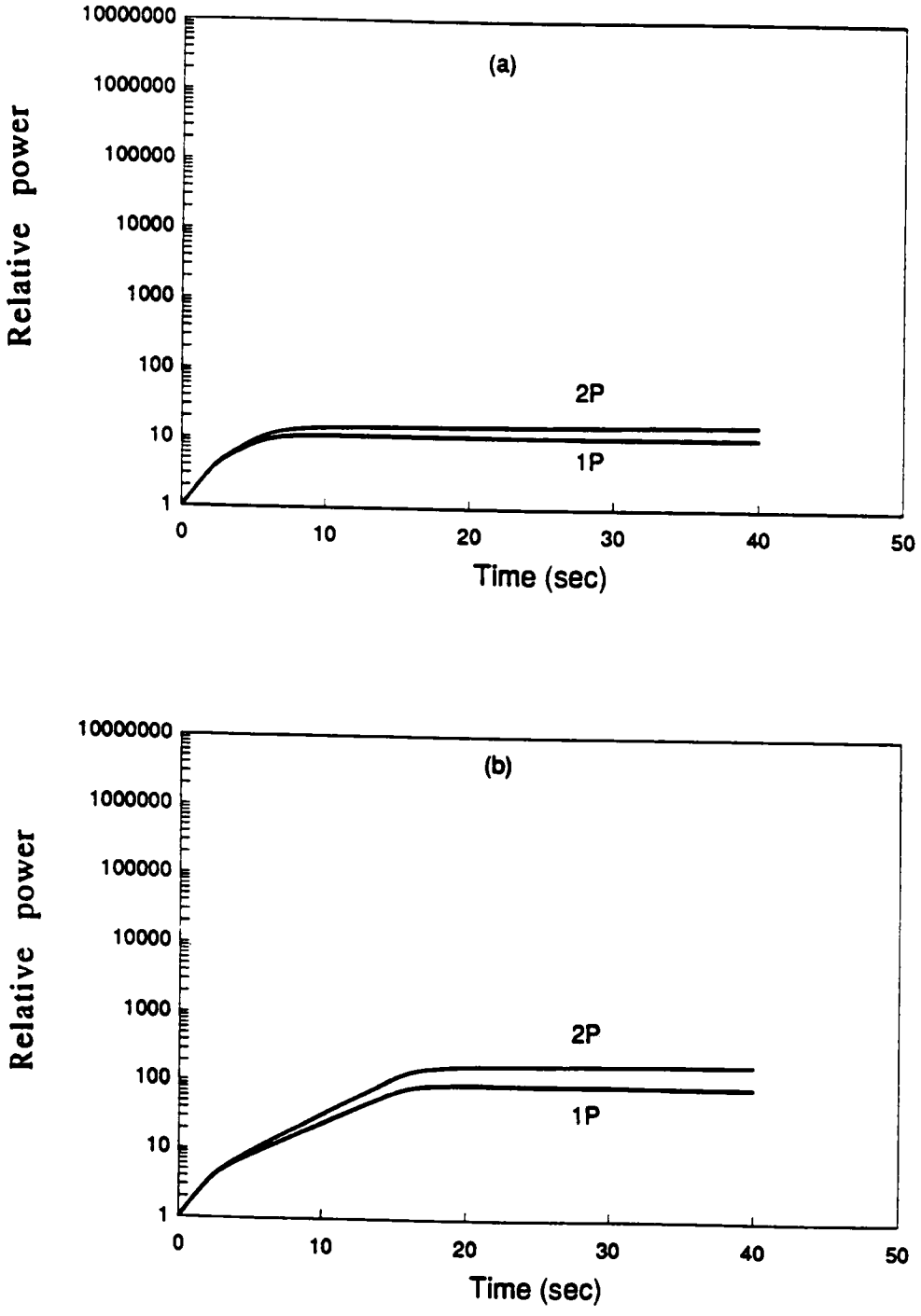

Fig.4.13 Power level using 1 group of delayed and 1 group of photoneutrons, (a) T2=5 sec. and (b) T2=15 sec.

Table 4.4 Power demand data for different numbers of delayed and photoneutron groups.

T2	1 delayed 1 photo groups		6 delayed 9 photo groups	
	1P1G	2P2G	1P1G	2P2G
5	37.7	74.3	76	108
10	234	588	1910	3191
15	1480	4687	48769	95208

4.5 Conclusions

Based on the results obtained, the conclusions for this chapter can be summarized as follows.

1. There is no difference in the results between the case in which the extraneous source was placed in the core, figure 4.2(a), and the case in which the source was placed in the reflector, figure 4.2(b).
2. There is no difference in the results when using the neutron lifetime as a constant, figure 4.2(a), and when using the generation time as a constant, figure 4.3.
3. The sensitivity of the power level to the source removal time decreases in the following cases:
   a. when the source removal time increases.
   b. when the amplitude of reactivity ρ_{max}, increases.

4. The safety control rods (located between the core and the reflector) are more effective in shutting down the reactor than the regulating control rods (located in the island region).
5. The effect of the number of groups of delayed neutrons is significant, especially for severe transients.
6. The difference in the results between the 1P1G and 2P2G models becomes more pronounced as the transients become more severe (Table 4.4). Therefore, a 1P1G model may not be sufficient to describe the kinetics behavior of the ANS reactor.

However, a question may arise, as to which model produced the correct results . The answer is : only experimental measurements can determine what the correct answer shoud be. Also, comparisons with other kinetics models may be useful.

Chapter V

Xenon Oscillations

Changes in core composition due to fuel burnup and isotope buildup usually occur over periods of days or months. It is extremely important to monitor the isotopic composition in the core during reactor operation, since changes in core composition can affect core multiplication as well as flux and power distributions. Certain fission products possess extremely large thermal neutron absorption cross sections. Of particular concern are Xe^{135} and Sm^{149}.

5.1 Xenon Fission Product Poisoning

Xe^{135} is the most significant fission product because of its large thermal neutron absorption cross section (2.7×10^6 b), and its relatively large fission yield (γ_{Xe}=0.3%). The existence of this fission product in the reactor introduces a number of potentially difficult control problems such as the need for large amounts of excess reactivity for startup and for operation at high flux levels. Such a fission product also introduces the possibility of flux instabilities of fairly long periods of time. The other reactivity feedback mechanisms present in the reactor, in addition to those associated with the flux absorption by Xe^{135}, are due to temperature effects. These feedback mechanisms are important factors which couple the

multiplicative properties of the reactor to its power level and thus render the kinetic equations non-linear.

In our analysis we have concerned ourselves with the stability of the flux (or power) in the ANS reactor in which the reactivity feedbacks due to xenon and temperature effects are simultaneously considered. A one point reactor kinetic model with reactivity feedbacks associated with variations in the xenon concentration, as well as fuel and coolant temperatures has been developed. The delayed neutron precursor concentration will also be included in the model. The non-linear phenomena associated with the xenon oscillations and temperature feedbacks have been studied; therefore, there has been no attempt to linearize the model equations.

As mentioned before, a gradation exists from a rather hard spectrum within the core to a thermal spectrum out in the reflector. In order to account for this gradation, some of the characteristics of the flux in the reflector will be introduced in the model equations. The definitions of the symbols used in the model are given in Table 5.1; other symbols are explained during the development of the model.

Table 5.1 A List of Symbols used in this chapter

Sym.	Description	Value
	State Variables:	
C	Total number of delayed neutron precursor atoms in the reactor.	
I_t	Total number of Iodine atoms in the reactor.	
P	Total reactor power.	
T_b	Average coolant temperature, °C.	
T_p	Average fuel plate temperature, °C.	
X_t	Total number of xenon atoms in the reactor.	
	Note: The superscript star "*" refers to the relative values of the state variables (i.e., the state variables normalized to their initial conditions.) The subscript zero "$_0$" refers to the initial conditions (or steady state values) of the variables.	
	Constants and Parameters:	
A_H	Total heat transfer area of the fuel plates, cm^2	2.755×10^5
σ_a^{xe}	Microscopic absorption cross-section of xenon cm^2	1.62×10^{-18}
β	Effective delayed neutron fraction for the delayed and the photoneutrons	0.00821
C_c	Specific heat of the coolant, $\frac{J}{g \cdot °C}$	4.184
C_p	Specific heat of the fuel plates, $\frac{J}{g \cdot °C}$	0.565
ε	Ratio of the peak thermal flux in the reflector to the production rate (cm^{-2}).	4.0×10^{-4}
Σ_f	macroscopic fission cross-section of U^{235}, cm^{-1}	0.3547
h_p	Overall heat transfer coefficient between the fuel plates and the coolant, $\frac{J}{cm^2 \cdot sec \cdot °C}$	13.55

Table 5.1 (continued)

λ	Decay constant averaged over the delayed and photoneutrons, sec^{-1}.	0.0685
λ_I	Decay constant of iodine, sec^{-1}.	2.875×10^{-5}
λ_X	Decay constant of xenon, sec^{-1}.	2.092×10^{-5}
Λ	Neutron generation time, sec.	0.0034
M_p	Total mass of the fuel plates, g.	9.678×10^4
M_c	Total mass of the coolant, g.	1.917×10^4
q	Heat flux, $\frac{J}{cm^2 \cdot sec \cdot}$.	
ν	Average number of neutrons produced per fission.	2.43
S	Ratio of the average thermal flux in the core to the peak thermal flux in the reflector, dimensionless.	0.0506
T_{in}	Inlet temperature of the coolant, °C.	49
T_s	surface temperature of the plates, °C.	
V_{core}	Total volume of the core, cm^3.	3.5×10^4
w	Total amount of energy produced per fission, J.	3.236×10^{-11}
W	Mass flow rate of the coolant, g/sec.	1.4×10^6
γ_I	Fission yield of iodine.	0.056
γ_X	Fission yield of xenon.	0.003

The equations for the xenon and its parent iodine will first be considered in their usual form as space-time dependent quantities:

$$\frac{\partial I}{\partial t} = \gamma_I \Sigma_f \phi_{core} - \lambda_I I \tag{5-1}$$

$$\frac{\partial X}{\partial t} = \lambda_I I + \gamma_x \Sigma_f \phi_{core} - \lambda_x X - \sigma_a^{xe} \phi_{core} X \tag{5-2}$$

where:

$I = I(r,t)$ = space-time dependent iodine concentration

$X = X(r,t)$ = space-time dependent xenon concentration

Dividing by the core volume and integrating over the core volume will yield the average values, and the above equations become

$$\frac{\partial \bar{I}}{\partial t} = \gamma_I \Sigma_f \bar{\phi}_{core} - \lambda_I \bar{I} \tag{5-3}$$

$$\frac{\partial \bar{X}}{\partial t} = \lambda_I \bar{I} + \gamma_x \Sigma_f \bar{\phi}_{core} - \lambda_x \bar{X} - \frac{1}{V_{core}} \int \sigma_a^{xe} \phi_{core} X \, dv \tag{5-4}$$

where

$\bar{X}$ = number of xenon atoms per cm^3 averaged over the core volume

$\bar{I}$ = number of iodine atoms per cm^3 averaged over the core volume

$\bar{\phi}_{core}$ = thermal flux in the core averaged over the core volume

Due to the strong spatial dependence of ϕ_{core} and X, the integral in equation (5-4) will be assumed to yield the average values of ϕ_{core} and X multiplied by some correction factor f_1, the evaluation of which will be given in appendix B.1. Hence

$$\frac{1}{V_{core}} \int \sigma_a^{xe} \phi_{core} X \, dv = \sigma_a^{xe} \bar{\phi}_{core} \bar{X} f_1 \qquad (5\text{-}5)$$

Substituting equation (5-5) into (5-4) and multiplying equations (5-3) and (5-4) by the core volume yields

$$\frac{\partial I_t}{\partial t} = \gamma_I V_{core} \Sigma_f \bar{\phi}_{core} - \lambda_I I_t \qquad (5\text{-}6)$$

$$\frac{\partial X_t}{\partial t} = \lambda_I I_t + \gamma_x V_{core} \Sigma_f \bar{\phi}_{core} - \lambda_x X_t - \sigma_a^{xe} \bar{\phi}_{core} X_t f_1 \qquad (5\text{-}7)$$

where

X_t = total number of xenon atoms in the whole reactor,

I_t = total number of iodine atoms in the whole reactor.

In order to introduce some of the characteristics of the ANS reactor into the above equations, the following quantities will be defined:

Production Rate = P.R. = total number of neutrons produced in the reactor per sec.

$$P.R. = \nu \, \Sigma_f \, \bar{\phi}_{core} \, V_{core} \tag{5-8}$$

$$\bar{P} = w \, \Sigma_f \, \bar{\phi}_{core} = \frac{P}{V_{core}} \tag{5-9}$$

where

P = total reactor power

$\bar{P}$ = power density averaged over the core volume

$$\bar{\phi}_{core} = \frac{\bar{P}}{w \Sigma_f} \tag{5-10}$$

$$P.R. = \nu \frac{P}{w} \tag{5-11}$$

Equating (5-8) and (5-11), yields

$$\Sigma_f \, \bar{\phi}_{core} \, V_{core} = \frac{P}{w} = \text{fission rate} \tag{5-12}$$

define

$$\varepsilon = \frac{\phi_{ref.}^{peak}}{P.R.} \tag{5-13}$$

$$S = \frac{\bar{\phi}_{core}}{\phi_{ref.}^{peak}} \qquad \text{and hence} \qquad \bar{\phi}_{core} = S\,\phi_{ref.}^{peak} \tag{5-14}$$

Where: $\phi_{ref.}^{peak}$ = Peak thermal flux in the reflector

substituting the above definitions into equations (5-6) and (5-7) will yield:

$$\frac{dI_t}{dt} = \gamma_I \frac{P}{w} - \lambda_I I_t \tag{5-15}$$

$$\frac{dX_t}{dt} = \lambda_I I_t + \gamma_x \frac{P}{w} - \lambda_x X_t - A_1 P X_t \tag{5-16}$$

Where:

$$A_1 = \sigma_a^{xe} S \varepsilon \nu \frac{f_1}{w} \tag{5-17}$$

The equations for the reactor power and the delayed neutron precursors will be used in their usual forms:

$$\frac{dP}{dt} = \frac{(\rho-1)\beta}{\Lambda} P + \lambda C \tag{5-18}$$

$$\frac{dC}{dt} = \frac{\beta}{\Lambda} P - \lambda C \tag{5-19}$$

In the above two equations only one group of delayed neutrons has been considered. The reactivity ρ is in units of dollars.

The other two variables to be considered in the model are the fuel plate temperature T_p, and the bulk coolant temperature T_b. The energy balance equations for the fuel plates and the coolant will be derived.

1) Fuel Plate

Assume that

$$T_b = \frac{T_{out} + T_{in}}{2} \tag{5-20}$$

Then

$$C_p\, M_p \frac{dT_p}{dt} = P - A_H\, h_p (T_p - T_b) \tag{5-21}$$

$$\frac{dT_p}{dt} = \frac{1}{C_p\, M_p} P - \frac{A_H\, h_p}{C_p\, M_p} (T_p - T_b) \tag{5-22}$$

$$\text{define} \quad \tau_p = \frac{C_p\, M_p}{A_H\, h_p} = \frac{1}{\lambda_p} \tag{5-23}$$

$$\frac{dT_p}{dt} = \frac{1}{C_p\, M_p} P - \frac{1}{\tau_p} (T_p - T_b) \tag{5-24}$$

2) Coolant

$$C_c\, M_c \frac{dT_b}{dt} = h_p\, A_H (T_p - T_b) - W\, C_c\, (T_{out} - T_{in}) \tag{5-25}$$

$$\frac{dT_b}{dt} = \frac{h_p\, A_H}{C_c\, M_c} (T_p - T_b) - \frac{W}{M_c} (2T_b - T_{in} - T_{in}) \tag{5-26}$$

$$\frac{dT_b}{dt} = \frac{1}{\tau_c}(T_p - T_b) - \frac{1}{\tau_r}(T_b - T_{in}) \qquad (5\text{-}27)$$

where:

$$\lambda_c = \frac{1}{\tau_c} = \frac{h_p A_H}{C_c M_c} \quad , \quad \lambda_r = \frac{1}{\tau_r} = \frac{2W}{M_c} \quad , \quad \lambda_p = \frac{1}{\tau_p} = \frac{A_H h_p}{C_p M_p} \qquad (5\text{-}28)$$

Equations (5-15), (5-16),(5-18), (5-19), (5-24), and (5-27) constitute the basic equations for the model. However, each state variable in the model will be normalized to its initial value. In Appendix B.2 the initial conditions for all of the state variables of the model will be derived. The reactivity term ρ in equation (5-18) represents the feedback effects of the xenon and temperature. Therefore, a detailed analysis of this term will be given presently. The total reactivity is given as

$$\rho = \rho_{xe} + \rho_{temp.} + \rho_{ext.} \qquad (5\text{-}29)$$

where

ρ_{xe} = reactivity feedback of the xenon

$\rho_{temp.}$ = temperature feedback

$\rho_{ext.}$ = external reactivity from sources such as control rods, etc.

The xenon feedback reactivity is given by the usual first-order approximation:

$$\rho_{xe} = \frac{-\sigma_a^{xe}}{\xi \Sigma_f V_{core} \beta} \quad (X\text{-}X_0) \qquad (5\text{-}30)$$

The constant ξ is given by a very complicated expression in reference number [19] (p. 213). However, if the macroscopic absorption cross-sections of xenon and the fuel, as well as the flux are all space-independent then

$\xi = \nu = 2.43$

Because of the strong spacial dependence of the cross-sections and the flux, the constant ξ is assumed to be equal to ν multiplied by a correction factor f_2. The evaluation of this factor is given in Appendix B.3.

The temperature feedback reactivity is composed of the coolant temperature feedback and the fuel plate temperature feeback. The coolant temperature feedback is composed of the portion of the coolant inside the core (to be referred to as the active core coolant) and the portion of the coolant on top of the core (to be referred to as the axial coolant). Table 5.2 shows the reactivity coefficients of the coolant in the active core as well as the axial reflector regions.

Table 5.2 Void Reactivity Coefficients for the Coolant

Region	Cents/(%)
active core	-6.35
axial reflector	-9.79

In the above table % refers to the percent change in the coolant number density. It should be mentioned also that 1% change in the coolant number density is equivalent to 26.6 °C change in the coolant temperature. Based on these data the temperature feedback reactivity is given by

$$\rho_{temp} = \rho_{active} + \rho_{ref.} \tag{5-31}$$

$$\rho_{active} = \frac{-6.35}{(26.6)(100)} (T_b - T_{bo}) \tag{5-32}$$

and

$$\rho_{ref.} = \frac{-9.79}{(2)(26.6)(100)} (T_{(out)} - T_{(out)_o}) \tag{5-33}$$

The fuel plate temperature feedback is given by

$$\rho_{plate} = \alpha_p (T_p - T_{p_o}) \tag{5-34}$$

where α_p is the plate temperature reactivity coefficient. Since no experimental data were available for α_p, its value was assumed to

be of the same order of magnitude as that of the coolant.

The heat transfer coefficient h_p is not a constant quantity; it depends on the thickness δ of the oxide layer that builds on the surface of the fuel plate. The following formula[24] gives the relation between h_p and δ:

$$h_p = \frac{1}{0.0649 + 44.44\ \delta} \tag{5-35}$$

The oxide thickness δ is a function of time t and also a function of the plate surface temperature T_s. The relationship between these quantities is given by the following empirical formula[25]:

$$\delta = \delta_o + 9.4093 \times 10^{-4}\ (t)^{0.778}\ e^{-(4600/273+T_s)} \tag{5-36}$$

where δ_o = 0.0002 cm is the oxide thickness at the beginning of the core lifetime. This builds up within the first few hours after operation.

The plate surface temperature is given by the following formula

$$T_s = T_b + \frac{q}{h_w} \tag{5-37}$$

$$q = \frac{p}{A_H} \tag{5-38}$$

The normalized state variables are

$$X^* = \frac{X}{X_0}, \quad I^* = \frac{I}{I_0}, \quad P^* = \frac{P}{P_0}, \quad C^* = \frac{C}{C_0}, \quad T_p^* = \frac{T_p}{T_{p0}}, \text{ and } \quad T_b^* = \frac{T_b}{T_{b0}}$$

The normalized equations of the dynamics model are

$$\frac{dX^*}{dt} = \left(\frac{\lambda_x + A1\ P_0}{\gamma_I + \gamma_x}\right)\left[\ \gamma_I I^* + \frac{\gamma_x}{w} P^*\ \right] - \lambda_x X^* - A1\ P_0 P^* X^* \tag{5-39}$$

$$\frac{dI^*}{dt} = \lambda_I (P^* - I^*) \tag{5-40}$$

$$\frac{dP^*}{dt} = \frac{(\rho^* - 1)\beta}{\Lambda} P^* + \frac{\beta}{\Lambda} C^* \tag{5-41}$$

$$\frac{dC^*}{dt} = \lambda\ (P^* - C^*) \tag{5-42}$$

$$\frac{dT_p^*}{dt} = \frac{P_0}{C_p M_p T_{P0}} P^* - \lambda_p \left[\ T_p^* - T_b^* \left(\frac{T_{b0}}{T_{p0}}\right)\ \right] \tag{5-43}$$

$$\frac{dT_b^*}{dt} = \lambda_c \left[\ \left(\frac{T_{p0}}{T_{b0}}\right) T_p^* - T_b^*\ \right] - \lambda_r \left[T_b^* - \frac{T_{in}}{T_{b0}}\ \right] \tag{5-44}$$

where ρ^* is the reactivity in dollars expressed in terms of the normalized state variables. This system of six first-order

equations was integrated with a stiffly-stable integrator[30] with very stringent error controls.

Our motivation for examining space-independent xenon oscillations was to search for the nonlinear behavior of the equations induced by external perturbations such as oscillating control rods.

It was found that the interaction of xenon and other reactivity effects (e.g., thermal) can result in nonlinear oscillations (stable limit cycles). The controlling dynamic processes are extremely slow. The half-lives for the fission products I^{135} and Xe^{135} are about 7 hours and 9 hours respectively. Control is therefore relatively easy, although space-dependent xenon effects in large reactors, which are not considered here, can present a difficult control problem.

Figures 5-1(a) through 5-1(d) show the periodic oscillations of the reactivity ρ, the relative power P*, the relative concentration of xenon X*, and the relative concentration of iodine I*, respectively. Figure 5-2 is the xenon-iodine plane in state space showing a stable limit cycle around the equilibrium point (1,1).

It was also found that the peak values of the limit cycle of the power decrease as the value of ρ_{ext} decreases . This is shown in figures 5-3(a) and 5-3(b) for which ρ_{ext} was -\$1.0 and -\$2.0, respectively. Figure 5-4 is a plot of the peak value of the power vs. ρ_{ext}, this curve was useful in determining the stability of the reactor against the excitation of the higher modes of the neutron flux. The BOLD VENTURE computation code was used to calculate the eigenvalue of the first harmonic. It was found that the most

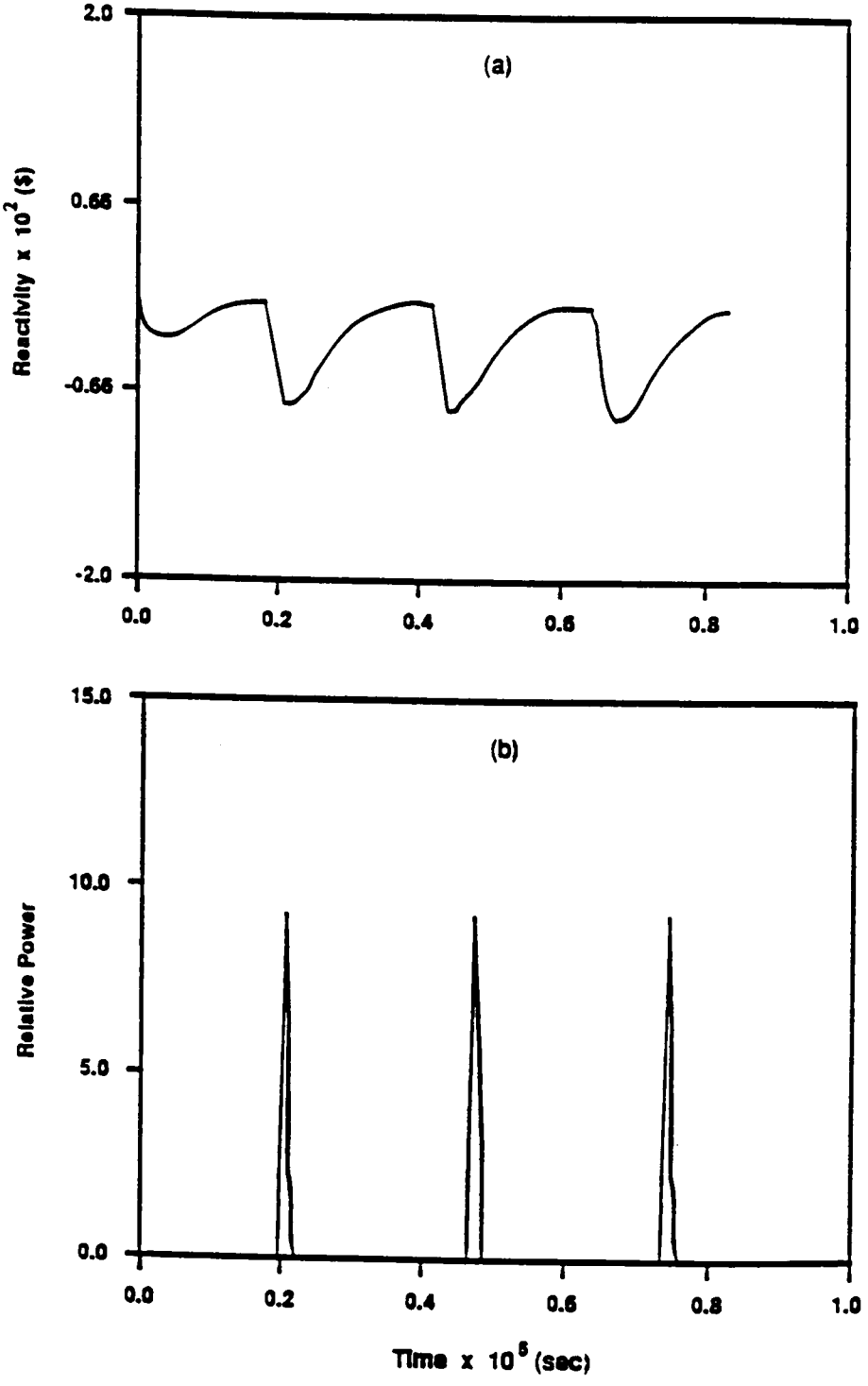

relative power (c) relative xenon concentration and (d) relative iodine concentration

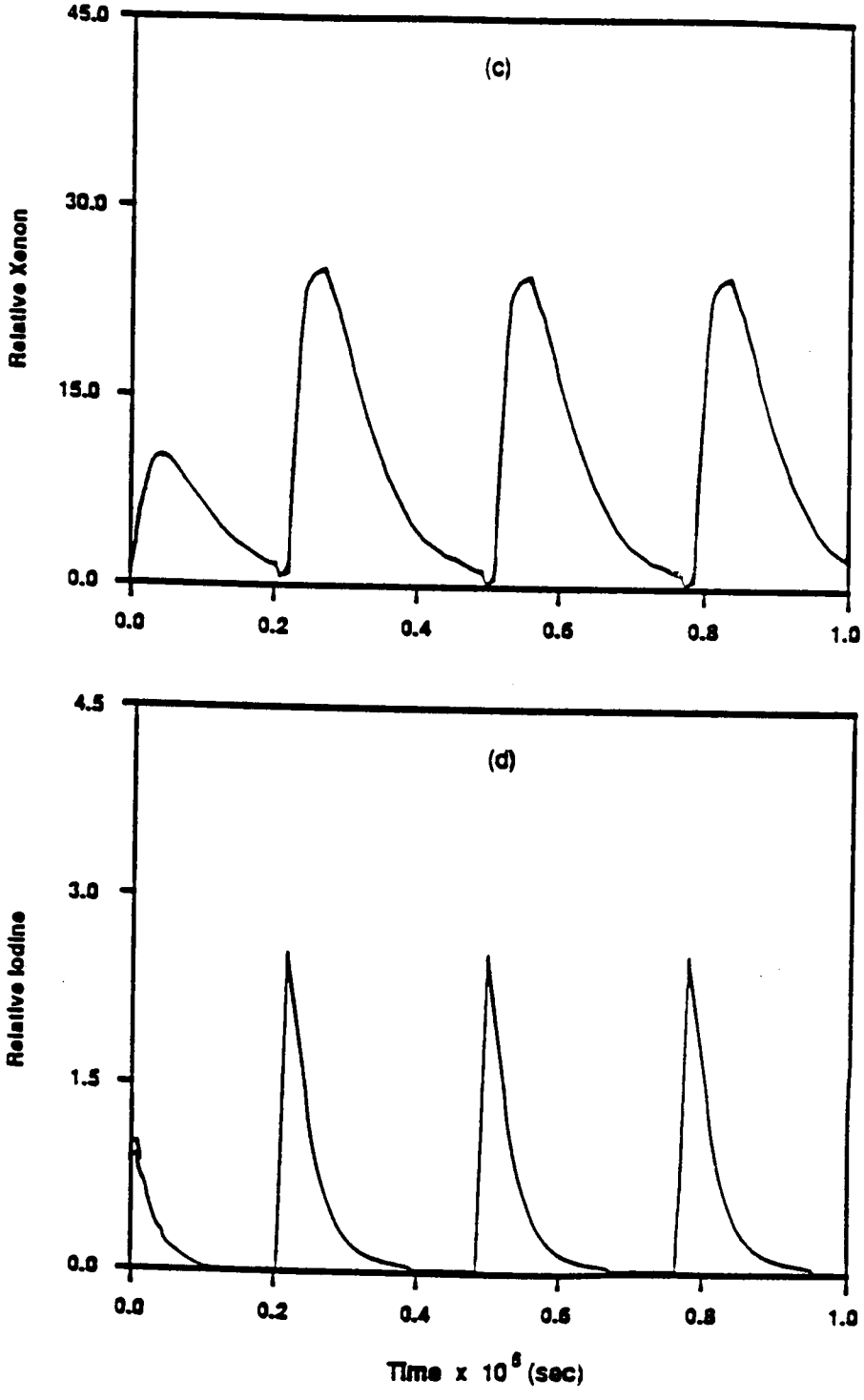

Figure 5.1 (continued)

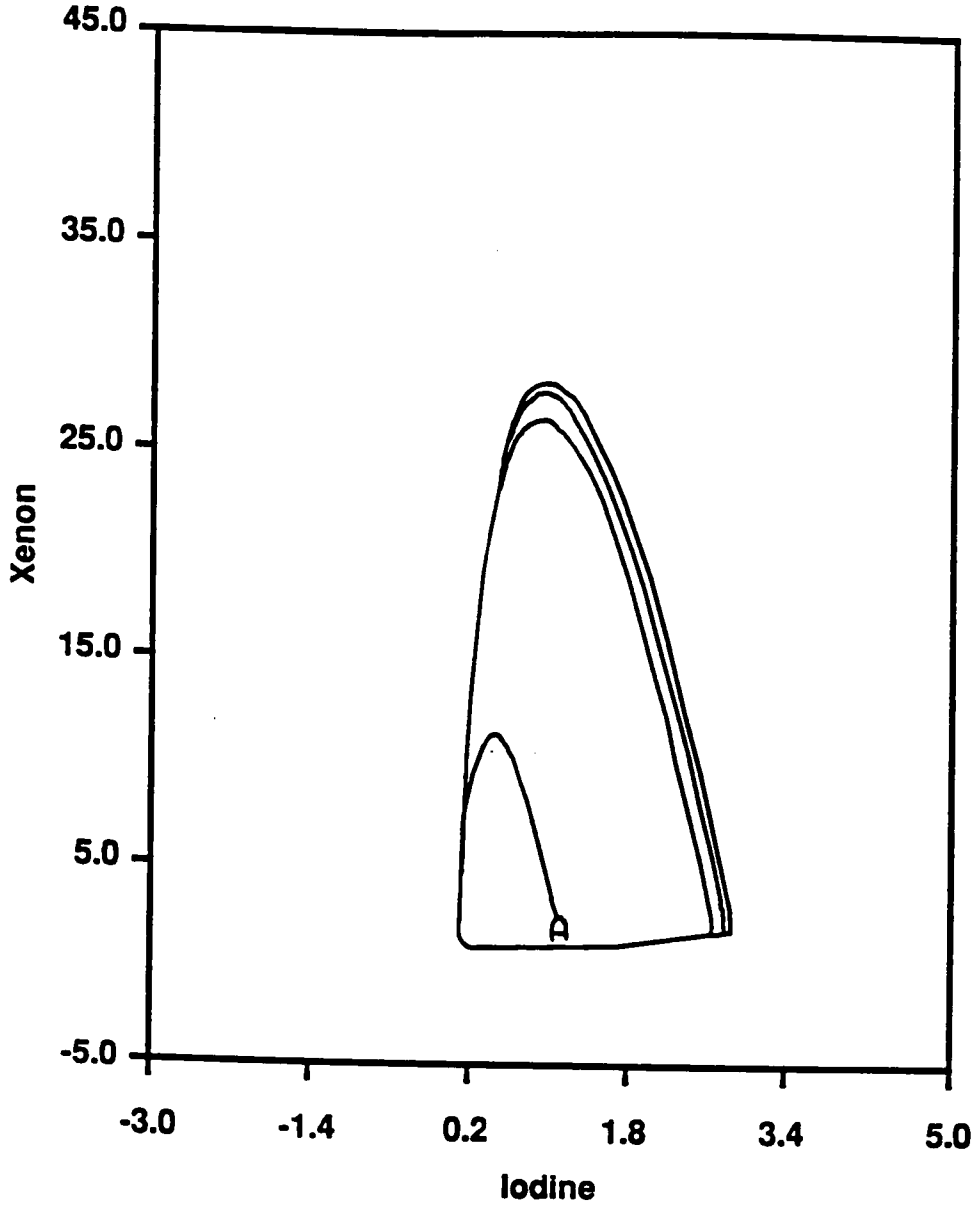

Figure 5.2 Xenon-Iodine plane in state space showing a stable limit cycle.

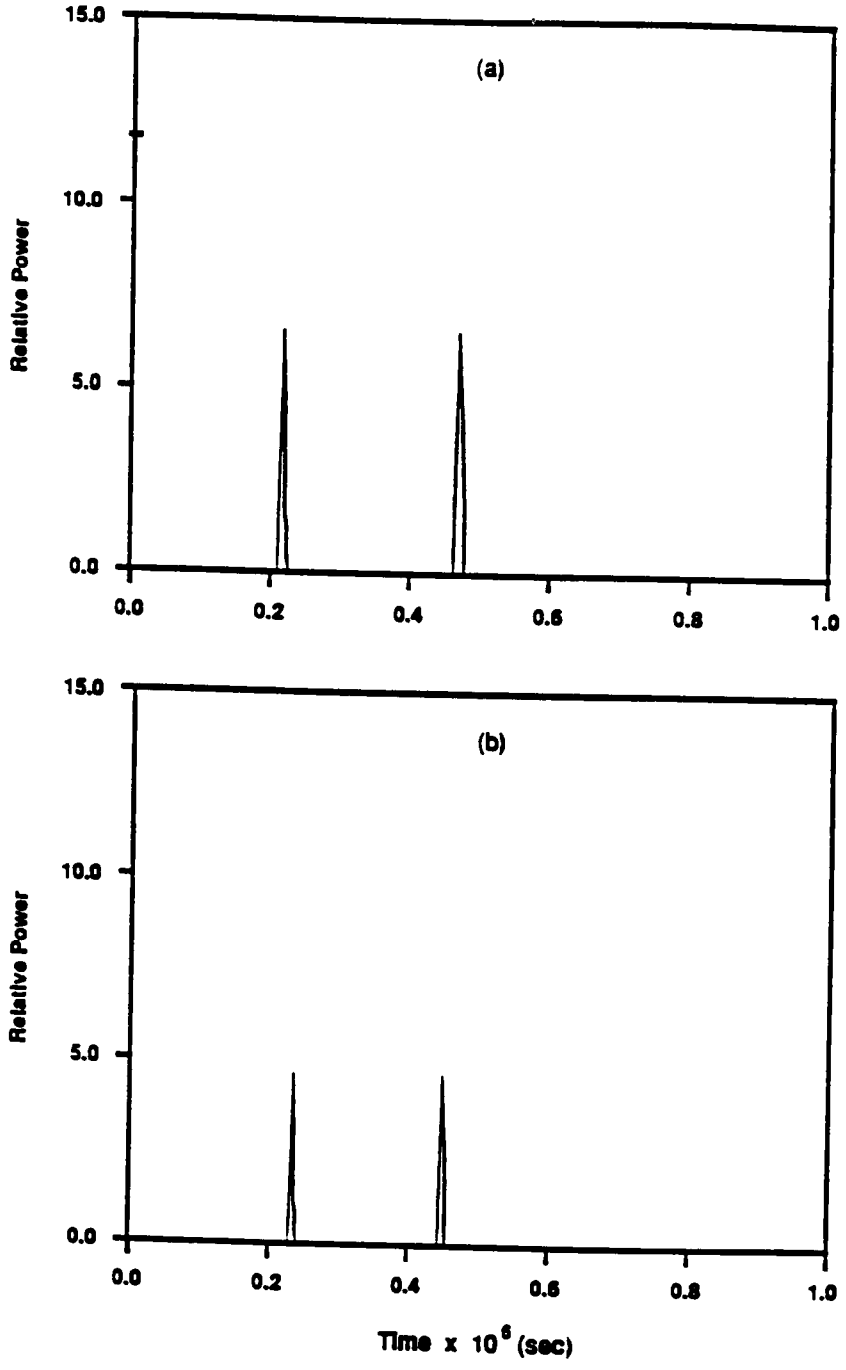

Figure 5.3 The limit cycle of relative power with two different values of ρ_{ext} (a) ρ_{ext} = -\$1.0 and (b) ρ_{ext} =-\$2.0.

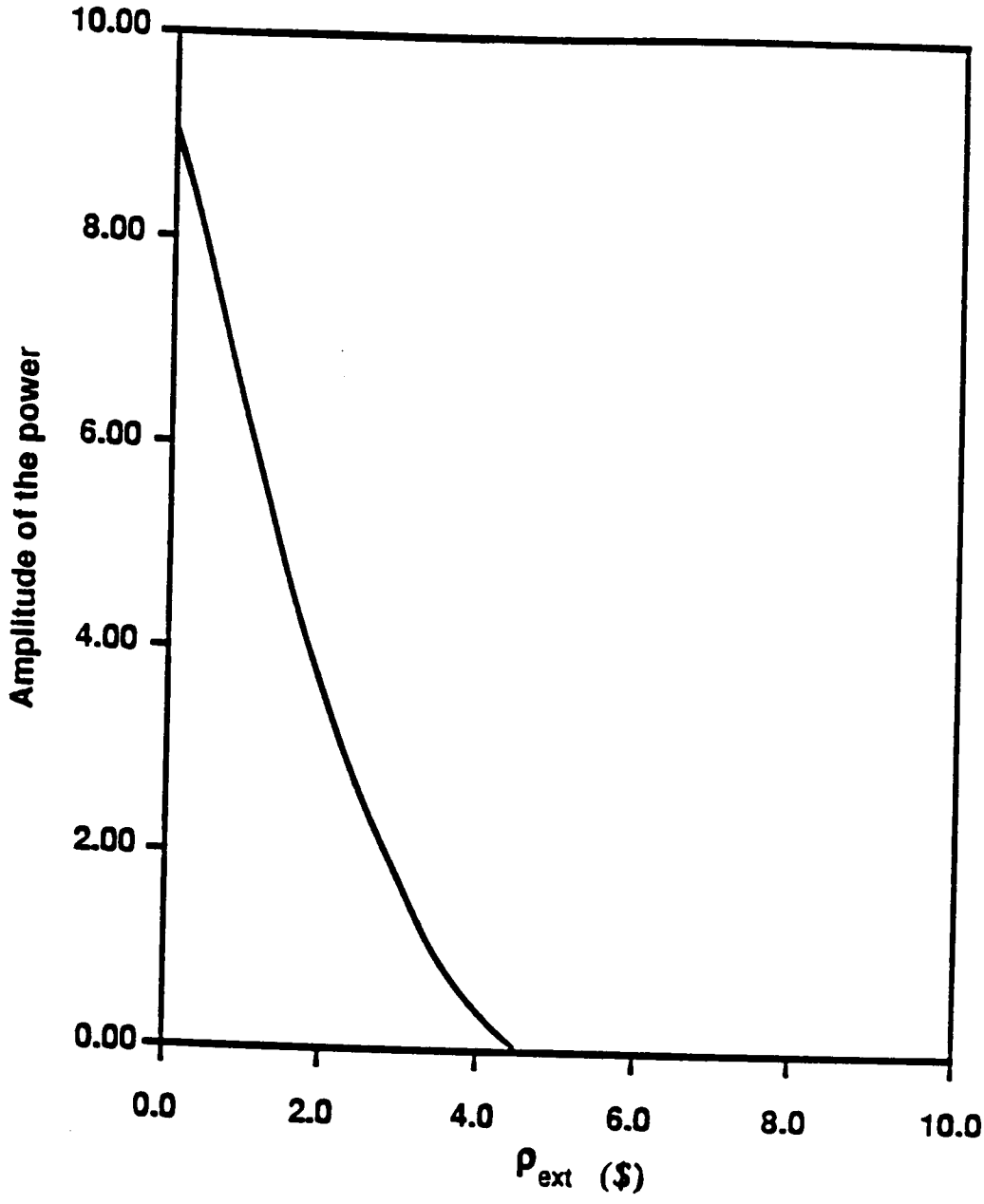

Figure 5.4 Peak values of the relative power vs. ρ_{ext}.

dominant first harmonic was in the axial direction with eigenvalue equivalent to -$24. According to figure 5-4, the excitations of the higher harmonics do not induce any power oscillations, since a negative reactivity of -$4.5 was enough to prevent the oscillations. Accordingly, the one-point kinetics equations (which are based on the fundamental mode of the neutron flux) have been used to study the xenon oscillations.

5.2 Samarium Fission Product Poisoning

A very similar analysis can be given for Sm^{149}, which is also characterized by very large fission yield and absorption cross section (43,504 b). The differential equations that describe the behavior of samarium and its parent promethium will be added to the previous model. The effect of this isotope on the dynamic behavior of the reactor will be analyzed. The equations for samarium and its parent promethium are

$$\frac{dSm}{dt} = \lambda_{pm} P_m - A2\ Sm\ P \tag{5-45}$$

$$\frac{dP_m}{dt} = \gamma_{pm} \frac{P}{w} - \lambda_{pm} P_m \tag{5-46}$$

where:

$$A2 = \sigma_a^{Sm} S \varepsilon \nu / w \tag{5-47}$$

The introduction of these equations into the above model has changed the dynamic behavior of the equations. Instead of periodic oscillations with a constant amplitude , a damped oscillatory behavior was observed which eliminated the presence of the limit cycles. Figure 5-5 shows the damped oscillations of the reactor power. Figures 5-6 and 5-7 show the oscillatory behavior of xenon and samarium respectively. Figure 5-8 shows the negative growth of reactivity due to the samarium buildup, while figure 5-9 is the xenon-iodine plane in phase space showing the convergence of the solution towards a stable point. Accordingly, it was concluded that samarium has a stabilizing effect on the system.

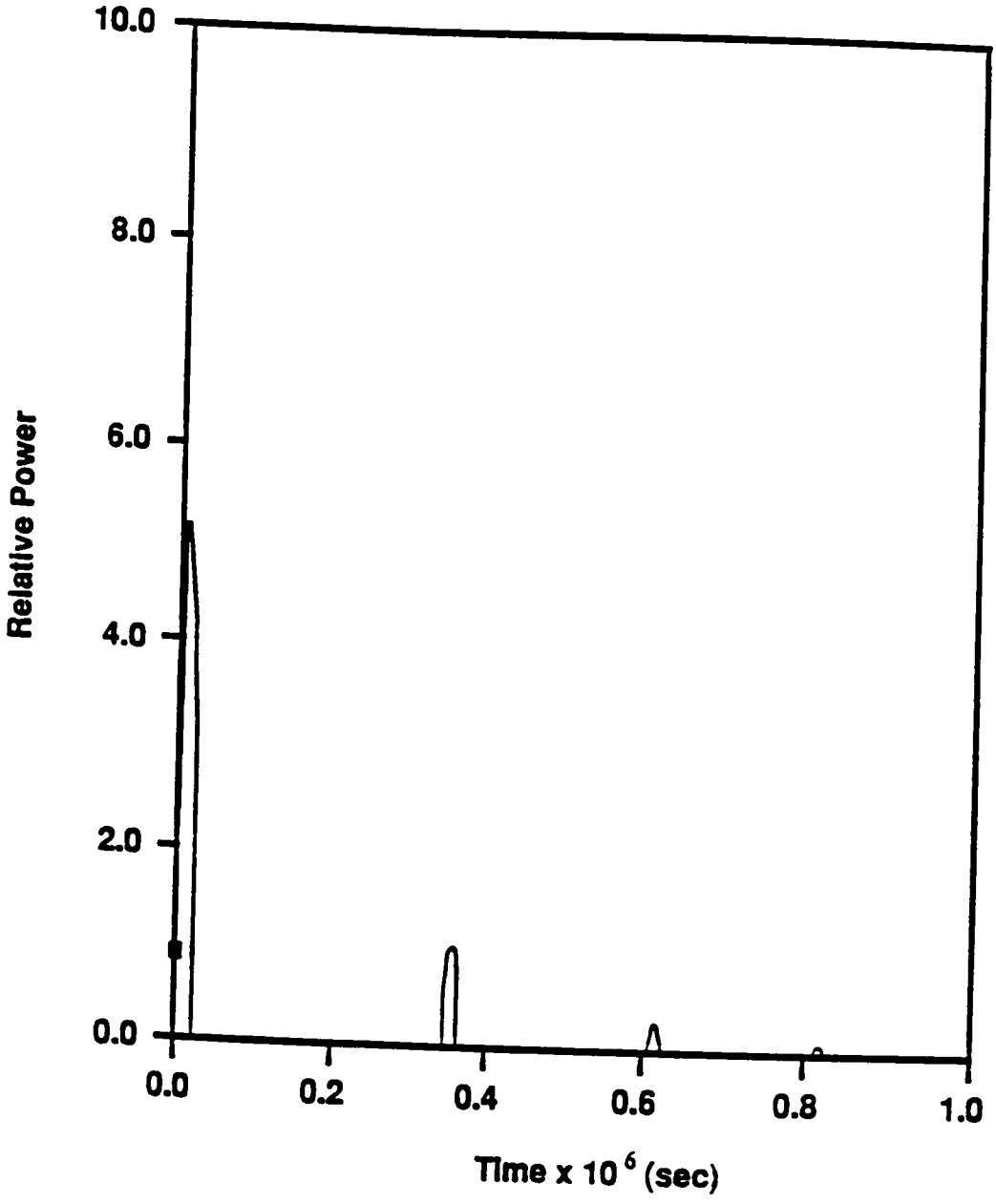

Figure 5.5 Damped oscillations of the relative power in the presence of samarium.

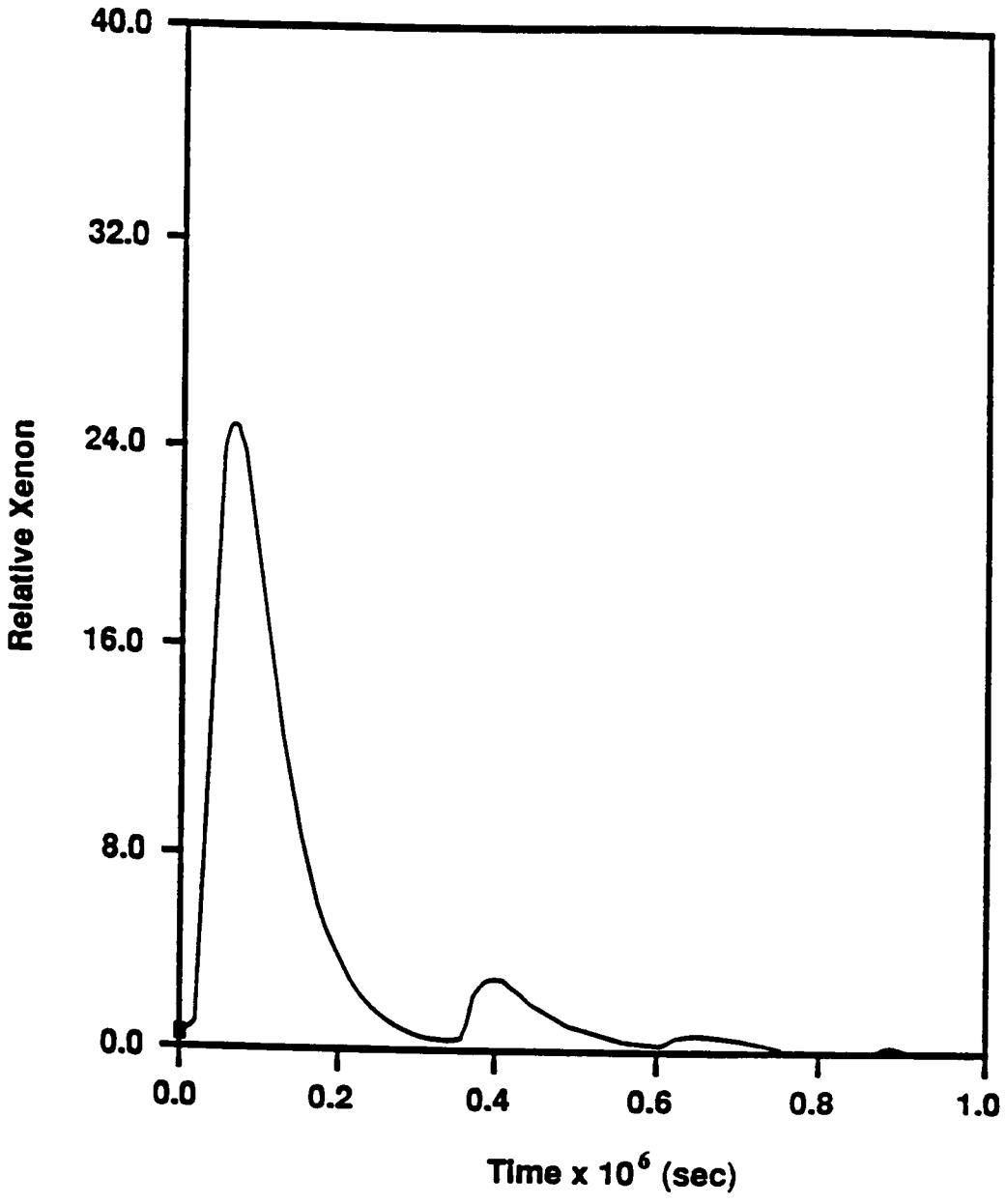

Figure 5.6 Oscillatory behavior of xenon in the presence of samarium.

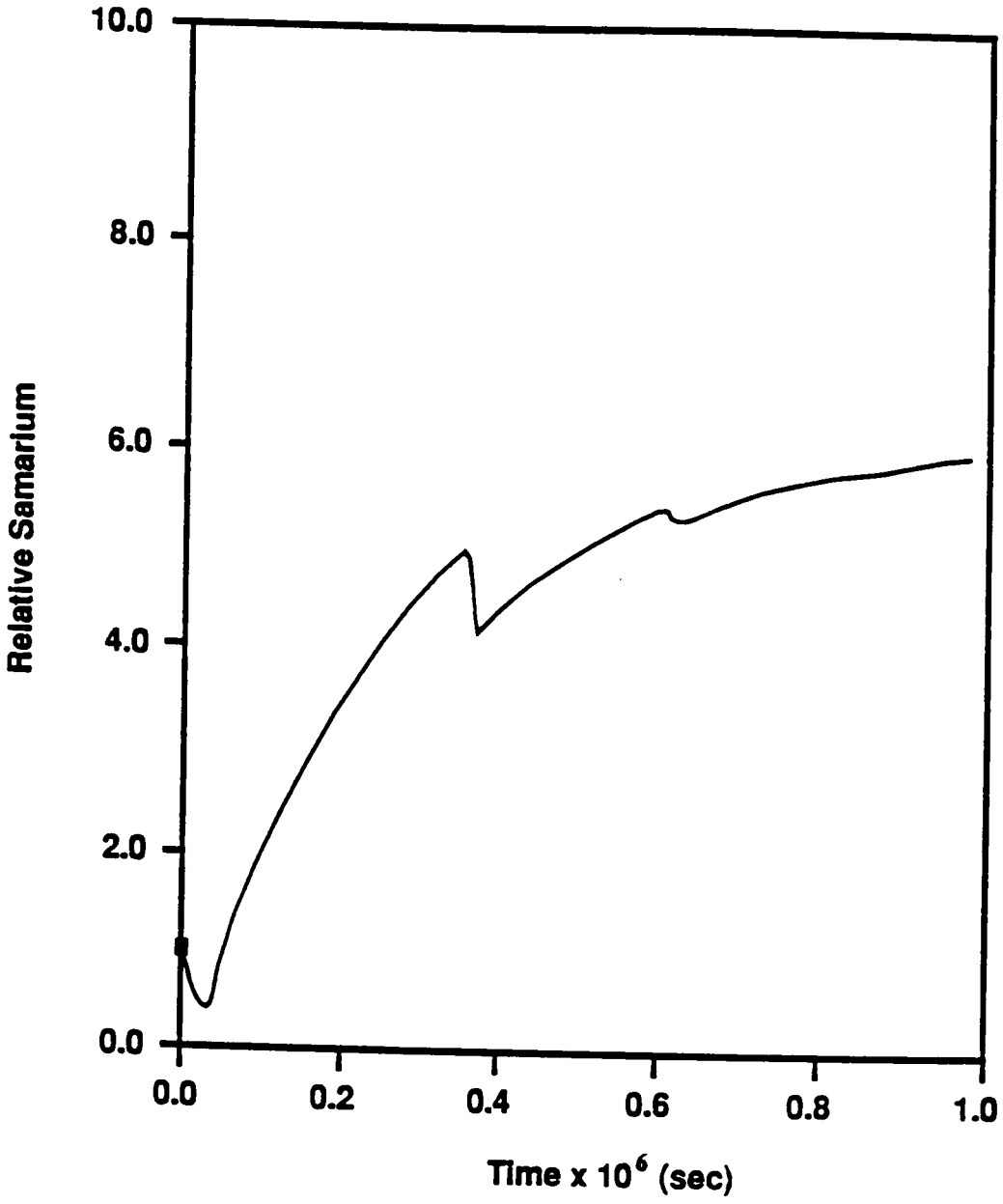

Figure 5.7 Oscillatory behavior of samarium.

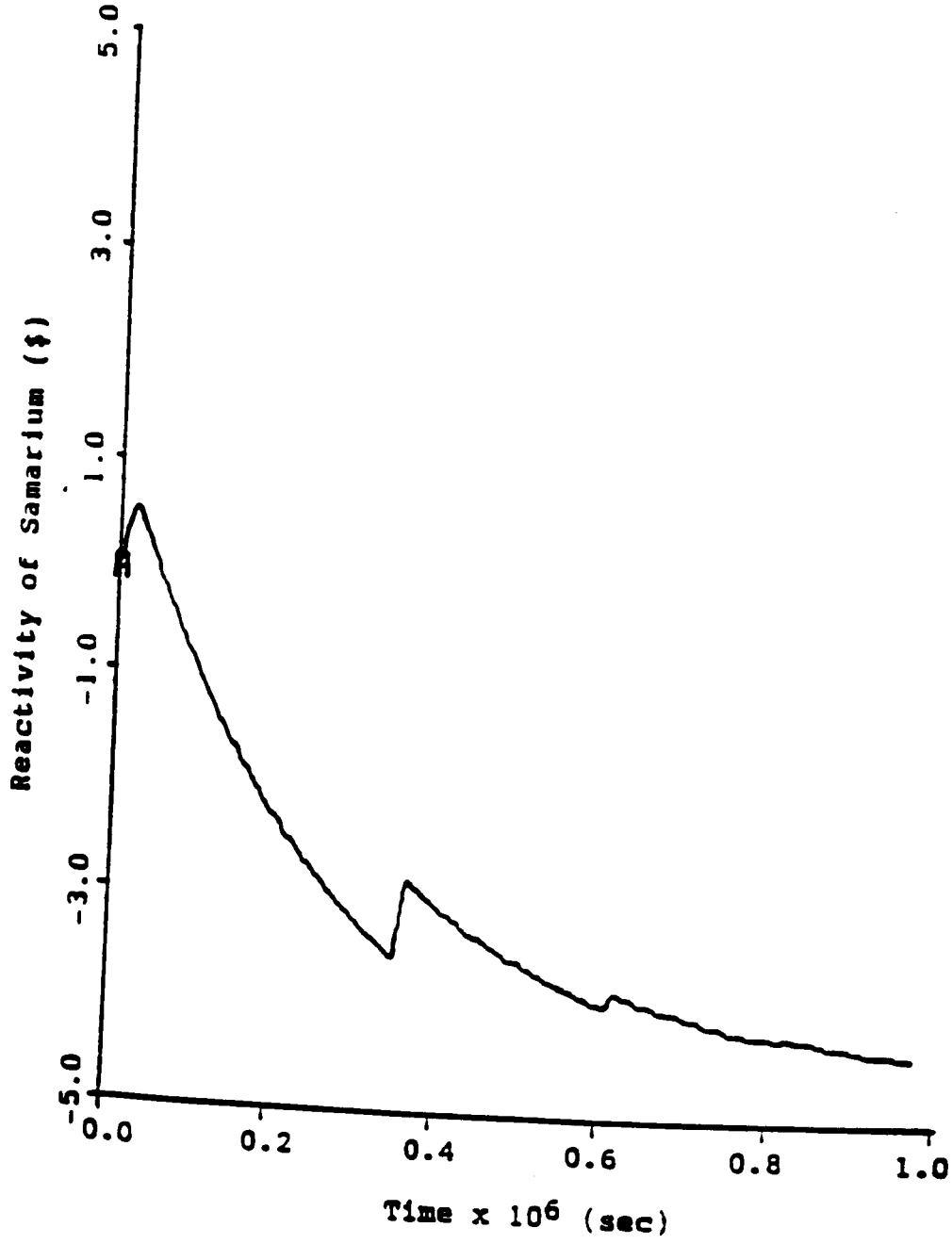

Figure 5.8 Negative reactivity due to the samarium buildup.

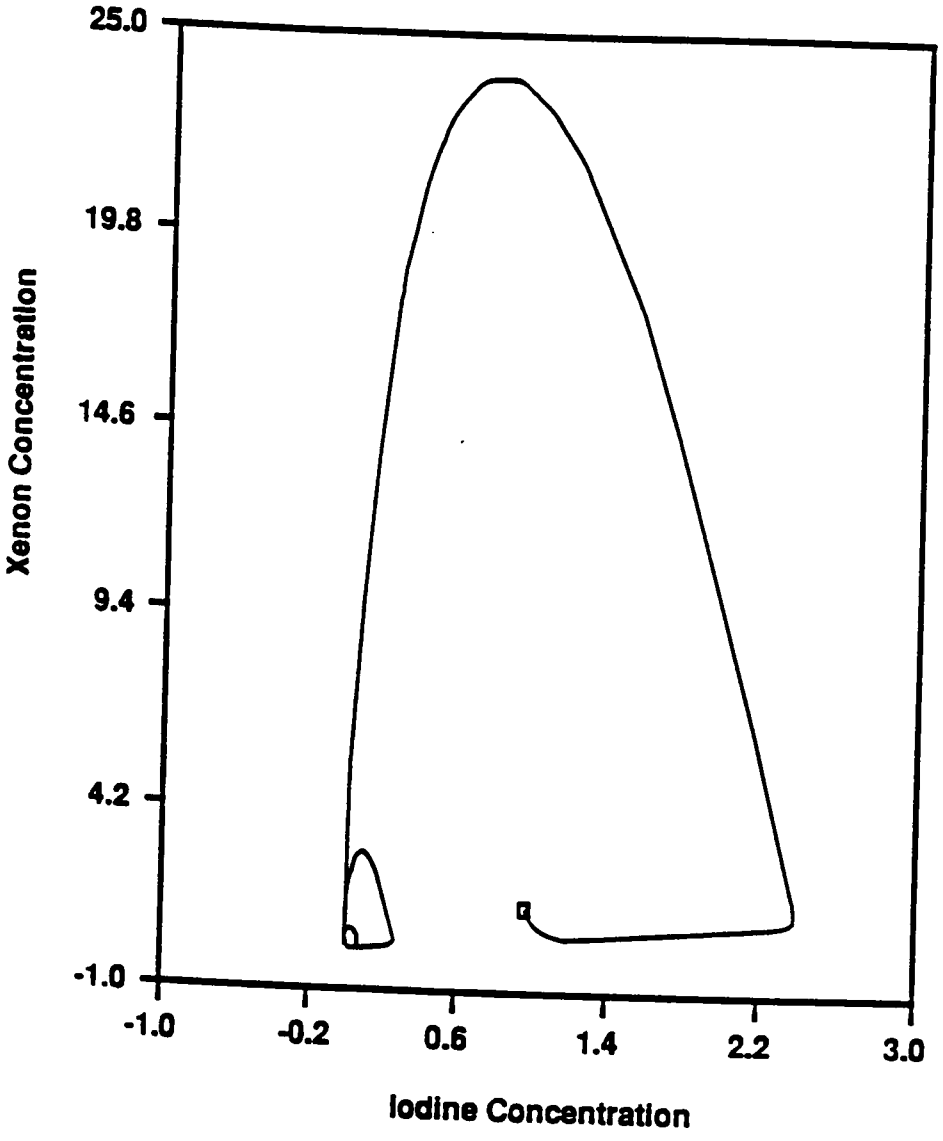

Figure 5.9 Xenon-Iodine plane in state space showing the propagation towards a stable point.

5.3 Xenon After Shutdown

Because of the buildup of X_e^{135} after a shutdown, if a high flux thermal neutron reactor is shut off, it immediately starts to lose reactivity.

The maximum reactivity loss after a shutdown depends on the power level at which the reactor operated before the shutdown; and this maximum loss occurs at about 12 hours after shutdown. In order for the reactor to be re-started it has to have extra reactivity built into it for post-shutdown X_e^{135} override.

Figure 5-10 shows the reactivity loss due to xenon buildup for three different power levels, 300 MW, 325 MW, and 355 MW. Figure 5-10 is the result of the one point kinetics model; whereas figure 5-11 shows the result of the BOLD VENTURE calculations for a power level of 355 MW . According to figure 5-10, for the case of 355 MW power, if the ANS reactor possesses \$10 ($\rho = 0.0821$) worth of excess reactivity in its control rods, then the reactor can be re-started within the first 16 minutes after shutdown or after 43 hours. The peak value for the 355 MW case is 0.41 (equivalent to \$50). According to figure 5-11 the reactor can be re-started within the first 21 minutes after the shutdown or after 56 hours. Also the peak value for figure 5-11 is 0.50 (equivalent to \$60). The reasons for these differences in the results can be summarized as follows:

1. In the one point kinetics model the reactivity loss was due to

xenon and samarium only; whereas in the BOLD VENTURE calculations, the reactivity loss was due to xenon, samarium, and 17 other fission products.

2. The one point kinetics model did not take into account the spatial effects of the xenon distribution. These effects were taken into considerations in the BOLD VENTURE calculations .
3. The point kinetics model did not take in to account the effect of B^{10} burnable poison; this was accounted for in the BOLD VENTURE calculations. Therefore, the peak value and the re-starting times for the BOLD VENTURE calculations were higher.

Accordingly, correction factors based on the BOLD VENTURE calculations must be introduced into the model, in order to improve the point kinetics results.

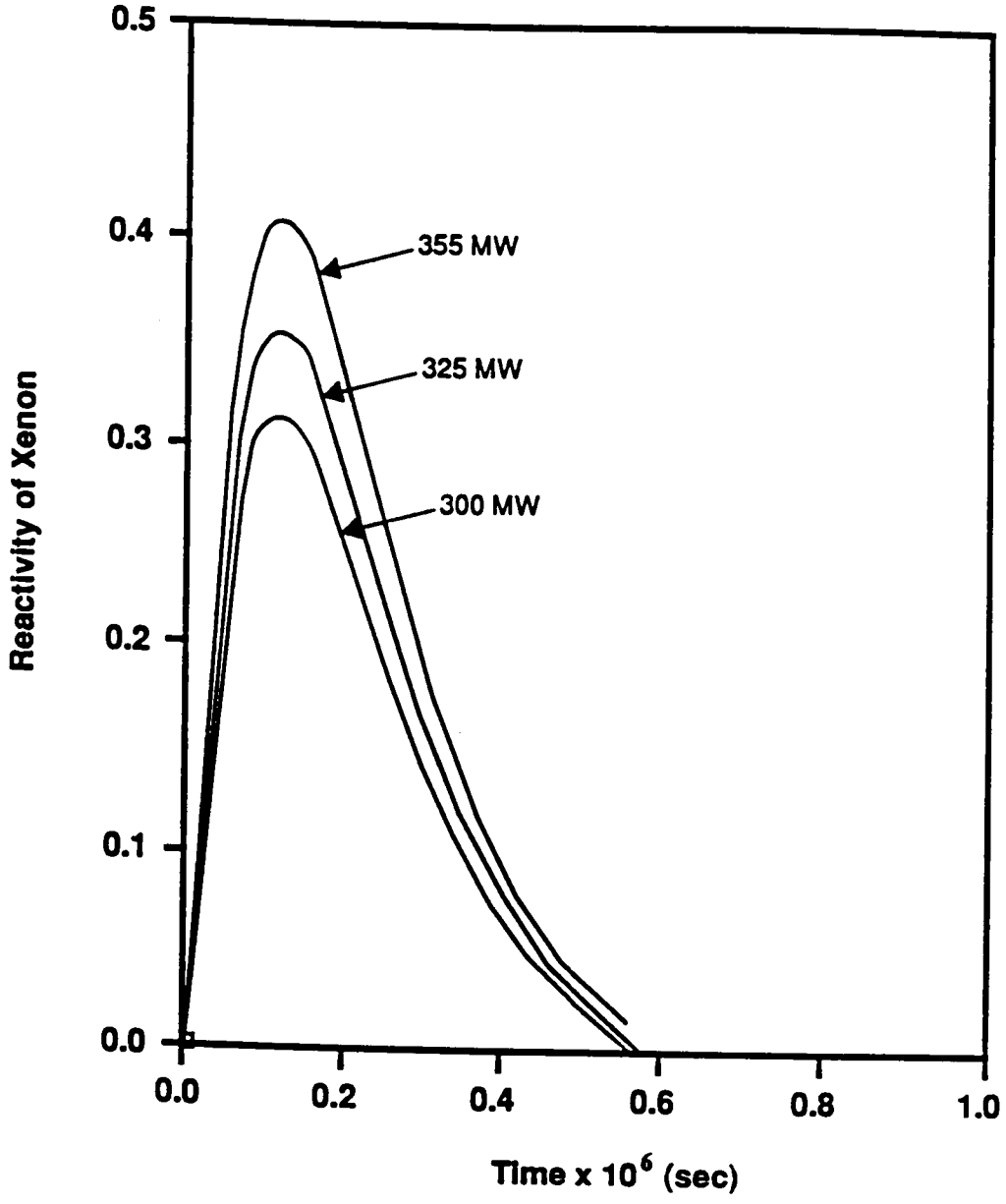

Figure 5.10 Negative reactivity of xenon after shutdown for three different power levels as a result of the one-point kinetics model.

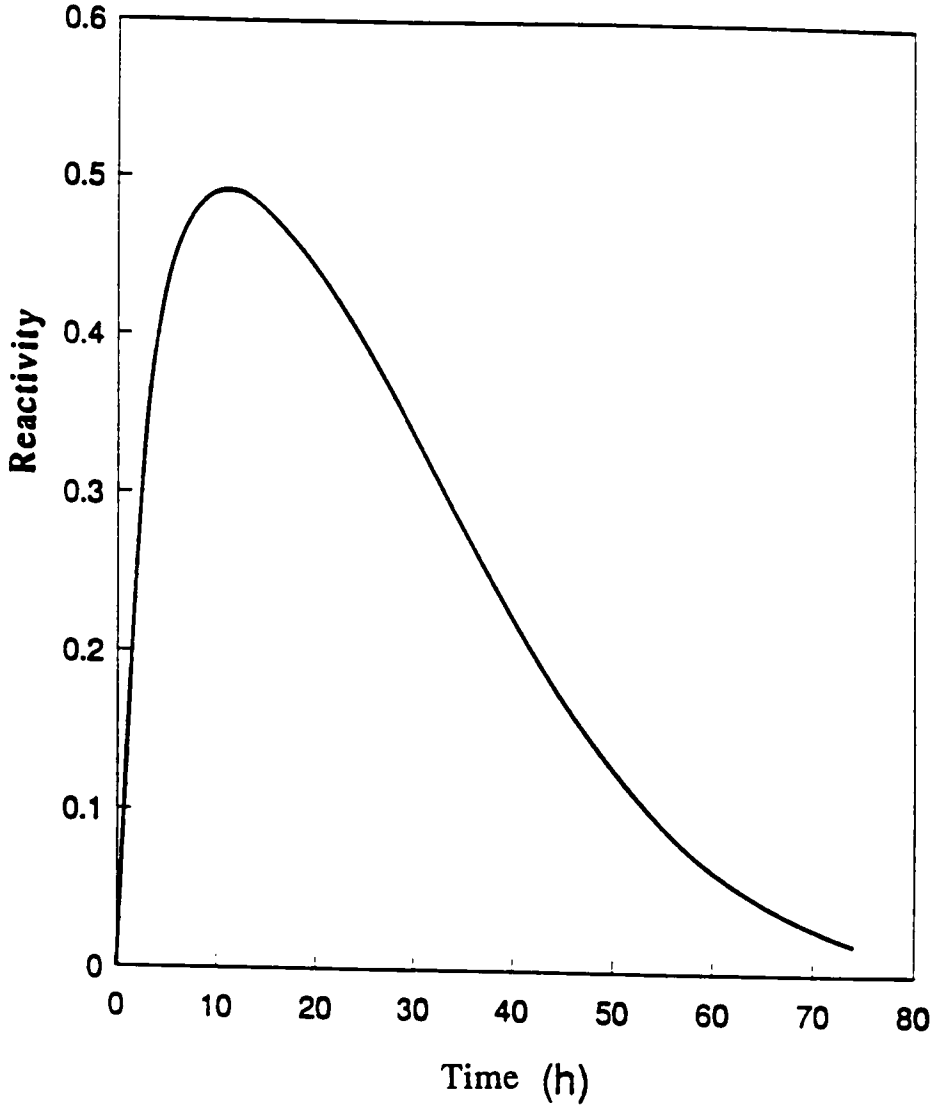

Figure 5.11 Negative reactivity of xenon after shutdown for an initial power level of 355 MW as a result of the BOLD VENTURE calculations.

Chapter VI

Reactor Diagnostics Algorithm

The discussion in this chapter contains the development of diagnostics tools for the ANS reactor. Specifically it addresses four main problems:

(i) Estimation of the average oxide thickness that deposits on the fuel plates.

(ii) Estimation of the average fuel plate temperature.

(iii) Development of a reactivity meter.

(iv) Development of a flow meter.

The mathematical tools for this chapter are an extension of previous work[29] in optimal control theory at the University of Tennessee Department of Nuclear Engineering.

6.1 General Theory

The idea of a diagnostics algorithm is to estimate parameters, uncertain parts of the plant dynamics and/or state variables which are not accessible by measurement.

Let X_i be a set of state variables, $(i = 1,...,I_0)$, of which the subset X_l of state variables is measureable, $(l = 1,...,l_0 \leq I_0)$.

The plant is simulated by the set of nonlinear coupled equations:

$$\dot{X}_i = Y_i (X_i, X_j) \qquad (i, j = 1,...,I_0) \tag{6-1}$$

However, only an incomplete model of the above information is available to the system's analyst. This incomplete (uncertain) model is given by:

$$\dot{m}_i = U_i \; F_i (m_i, m_j) + A_i \; (m_i, m_j) + g_i = Z_i \qquad (i, j = 1,...,I_0) \tag{6-2}$$

with the initial conditions

$$m_i (0) = m_{i0} \tag{6-3}$$

where

U_i (t) = uncertain time-varying parameters

g_i (t) = uncertain part of the system's dynamics

A_i (m_i, m_j), F_i (m_i, m_j) = known terms of the systems dynamics.

The objective is: given a set X_l of plant signals, estimate the uncertain terms of the system's dynamics. We set up the following Lagrangian function:

$$L = -\frac{1}{2}\sum_{l=0}^{l_0}(m_l - X_l)^2 - \frac{1}{2}\sum_i\left[R_i(U_i - U_{iF})^2 + K_i(g_i - g_{iF})^2\right] + \sum_i w_i(\dot{m}_i - Z_i) \qquad (6\text{-}4)$$

where R_i and K_i are positive constants and,

w_i = Lagrange multipliers (the set of adjoint state variables),

U_{iF} , g_{iF} = equilibrium values of the uncertain terms.

The Euler-Lagrange equations corresponding to the system are

$$\frac{\partial L}{\partial w_i} - \frac{d}{dt}\left(\frac{\partial L}{\partial \dot{w}_i}\right) = 0 \qquad (6\text{-}5)$$

$$\frac{\partial L}{\partial m_i} - \frac{d}{dt}\left(\frac{\partial L}{\partial \dot{m}_i}\right) = 0 \qquad (6\text{-}6)$$

$$\frac{\partial L}{\partial U_i} - \frac{d}{dt}\left(\frac{\partial L}{\partial \dot{U}_i}\right) = 0 \qquad (6\text{-}7)$$

$$\frac{\partial L}{\partial g_i} - \frac{d}{dt}\left(\frac{\partial L}{\partial \dot{g}_i}\right) = 0 \qquad (6\text{-}8)$$

which in view of equation (6-4) for the Lagrangian function yield

$$\dot{m}_i = Z_i \tag{6-9}$$

$$\dot{w}_i = \sum_{l=0}^{l_0} (m_l - X_l)\,\delta_{il} - \sum_{j=1}^{I_0} w_j \frac{\partial Z_j}{\partial m_i} \tag{6-10}$$

$$U_i = U_{iF} - \sum_j \frac{w_j}{R_i} \frac{\partial Z_j}{\partial U_i} \tag{6-11}$$

$$g_i = g_{iF} - \sum_j \frac{w_j}{R_i} \delta_{ij} \tag{6-12}$$

The simultaneous solution of equations (6-9) - (6-12) yields the uncertain terms and plant signal estimates.

6.2 A simplified model of the ANS

In the previous chapter, we developed a model that consisted of six equations, (5-39) - (5-44), which described the long-term transients of the ANS reactor. Since the dynamics considered in this chapter are of short term, the equations for the xenon and iodine would be eliminated and only equations (5-41) through 5-44 are considered for the current study. These equations are slightly modified for convenience. The following definitions are introduced :

$$\Lambda^* = \frac{\Lambda}{\beta}, \quad \rho^* = \rho_c - \rho_b$$

where

ρ_c = control rod reactivity in dollars.

$\rho_b = \alpha_b (T_b - T_{b0})$

= feedback reactivity of the bulk coolant temperature and α_b is the feedback reactivity coefficient.

The coolant and fuel plate temperatures will be normalized to the inlet temperature T_{in}, instead of their initial conditions. Considering the above definitions and the new normalization of T_p and T_b, equations (5-41) through (5-44) become

$$\frac{dP^*}{dt} = \frac{(\rho^* - 1)}{\Lambda^*} P^* + \frac{1}{\Lambda^*} C^* = \frac{dX_1}{dt} \qquad (6\text{-}13)$$

$$\frac{dC^*}{dt} = \lambda (P^* - C^*) = \frac{dX_2}{dt} \qquad (6\text{-}14)$$

$$\frac{dT_p^*}{dt} = \frac{P_0}{C_p M_p T_{in}} P^* - \lambda_p \left[T_p^* - T_b^* \right] = \frac{dX_3}{dt} \qquad (6\text{-}15)$$

$$\frac{dT_b^*}{dt} = \lambda_c \left[T_p^* - T_b^* \right] - \lambda_r \left[T_b^* - 1 \right] = \frac{dX_4}{dt} \qquad (6\text{-}16)$$

Where the state variables P*, C*, T_p*, and T_b^* will be referred to as X_1, X_2, X_3, and X_4 respectively.

6.2.1 Estimation of the thickness of the oxide layer

The problem addressed here is to obtain an on-line estimate of the plate-bulk coolant overall heat transfer coefficient h_p, thus determining the oxide thickness by use of the correlation given by equation (5-35) and repeated below as

$$h_p = \frac{1}{0.0649 + 44.44\ \delta} \tag{6-17}$$

To this end the model equations are written in the form

$$\dot{m}_1 = [\ \alpha_c - \alpha_b\ (m_4 - m_{04})]m_1 + \frac{m_2}{\Lambda^*} \quad = F_1 \tag{6-18}$$

$$\dot{m}_2 = \lambda\ (m_1 - m_2\ ) \qquad = F_2 \tag{6-19}$$

$$\dot{m}_3 = \lambda_{p1}\, m_1 - \ K_0U(m_3 - m_4) \qquad = F_3 \tag{6-20}$$

$$\dot{m}_4 = \ K_1U(m_3 - m_4) - \ \lambda_r(m_4 - 1) \qquad = F_4 \tag{6-21}$$

where in the above model the heat transfer coefficient h_p has been replaced by the unknown parameter U, and

$$K_0 = \frac{A_H}{C_p M_p} \ , \ K_1 = \frac{A_H}{C_c M_c} \tag{6-22}$$

The Lagrangian function (6-4) becomes

$$L = -\frac{1}{2} Q_1(m_1 - X_1)^2 - \frac{1}{2} Q_4(m_4 - X_4)^2 - \frac{1}{2} R(U - U_0)^2 + \sum_i w_i(\dot{m}_i - F_i) \tag{6-23}$$

The associated Euler-Lagrange equations yield the following expressions for the unknown term U, and the adjoint set w_i

$$U = U_0 + \frac{1}{R} \left[(m_3 - m_4) (K_0 w_3 - K_1 w_4) \right] \tag{6-24}$$

$$- \dot{w}_1 = Q_1(m_1 - X_1) + \rho^* w_1 + \lambda w_2 + \lambda_{p1} w_3 \tag{6-25}$$

$$- \dot{w}_2 = \frac{w_1}{\Lambda^*} - \lambda w_2 \tag{6-26}$$

$$- \dot{w}_3 = - K_0 U w_3 + K_1 U w_4 \tag{6-27}$$

$$- \dot{w}_4 = Q_4(m_4 - X_4) + K_0 U w_3 - (\lambda_r + K_1 U) w_4 - \alpha_b m_1 w_1 \tag{6-28}$$

where

$$\rho^* = \alpha_c - \alpha_b (m_4 - m_{04}) \tag{6-29}$$

and

$$\alpha_c = \frac{\rho_c - 1}{\Lambda^*} \tag{6-30}$$

To determine the unknown parameter U, the reacitivity ρ_c was ramped for 3 seconds up to a value of 10 cents, kept constant for 2 seconds and then ramped down to zero. Notice that since the value of the heat transfer coefficient is not available, the equilibium value U_0 has to be guessed. Figure 6-1 shows the result of using a guess which is 26% smaller than the actual value h_{p0} = 13.6, while figure 6-2 shows the result of using a guess which is 269% larger than the actual value. The algorithm quickly finds the right answer and then oscillates around it after the reactivity transient has been completed. The overall heat transfer coefficient h_{p0} can also be obtained by a simple heat balance at equilibrium, this is given by

$$h_{p0} = \left(\frac{2WC_c}{A_H}\right) \left(\frac{T_{b0} - 1}{T_{in}}\right) \tag{6-31}$$

where T_{b0} and T_{in} are measurable parameters of the plant.

The advantage of the proposed dynamical method is its capability of estimating the average fuel plate temperature during a reactor transient. Alternatively, one could use equation (6-31) to determine the overall heat transfer coefficient, and use the present technique to measure other parameters of the system.

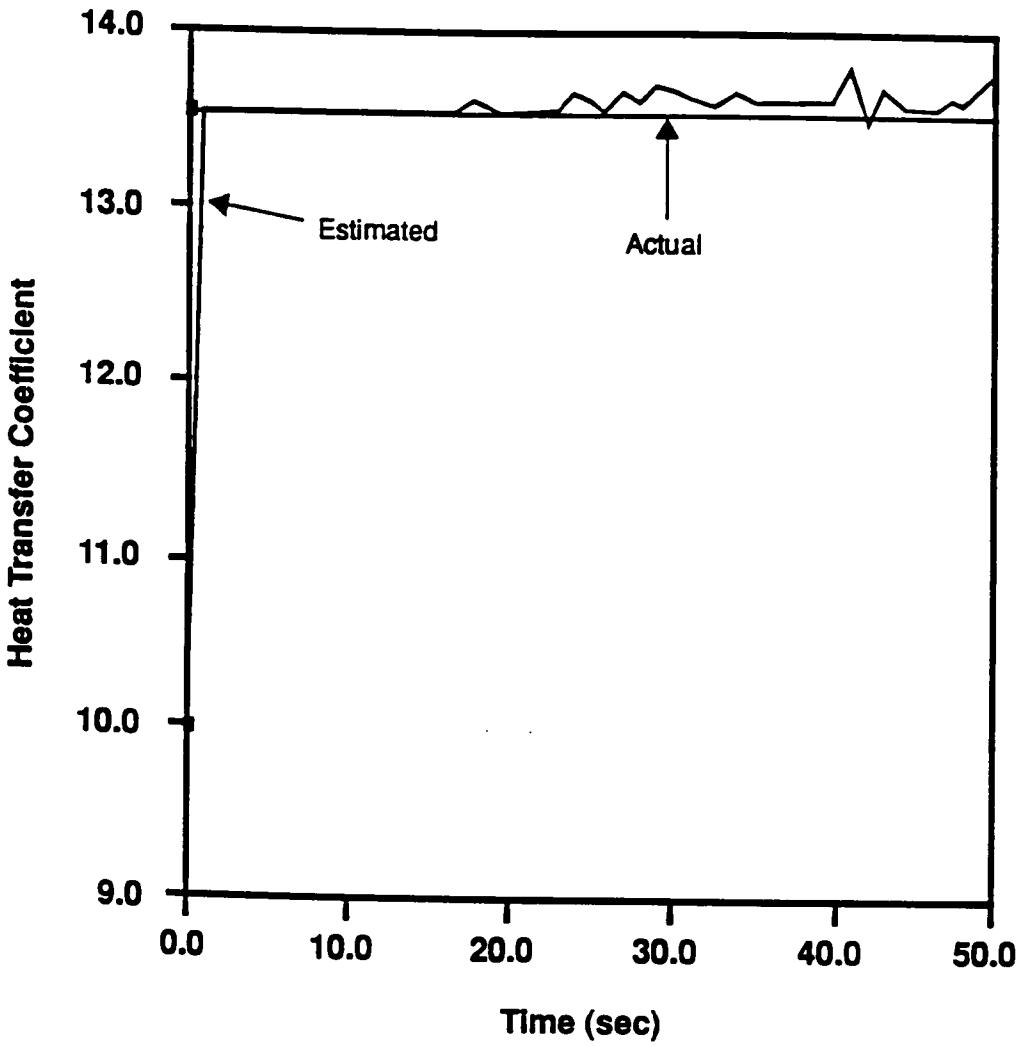

Fig. 6.1 Actual and estimated heat transfer coefficient for a guess of 26% smaller than the actual value.

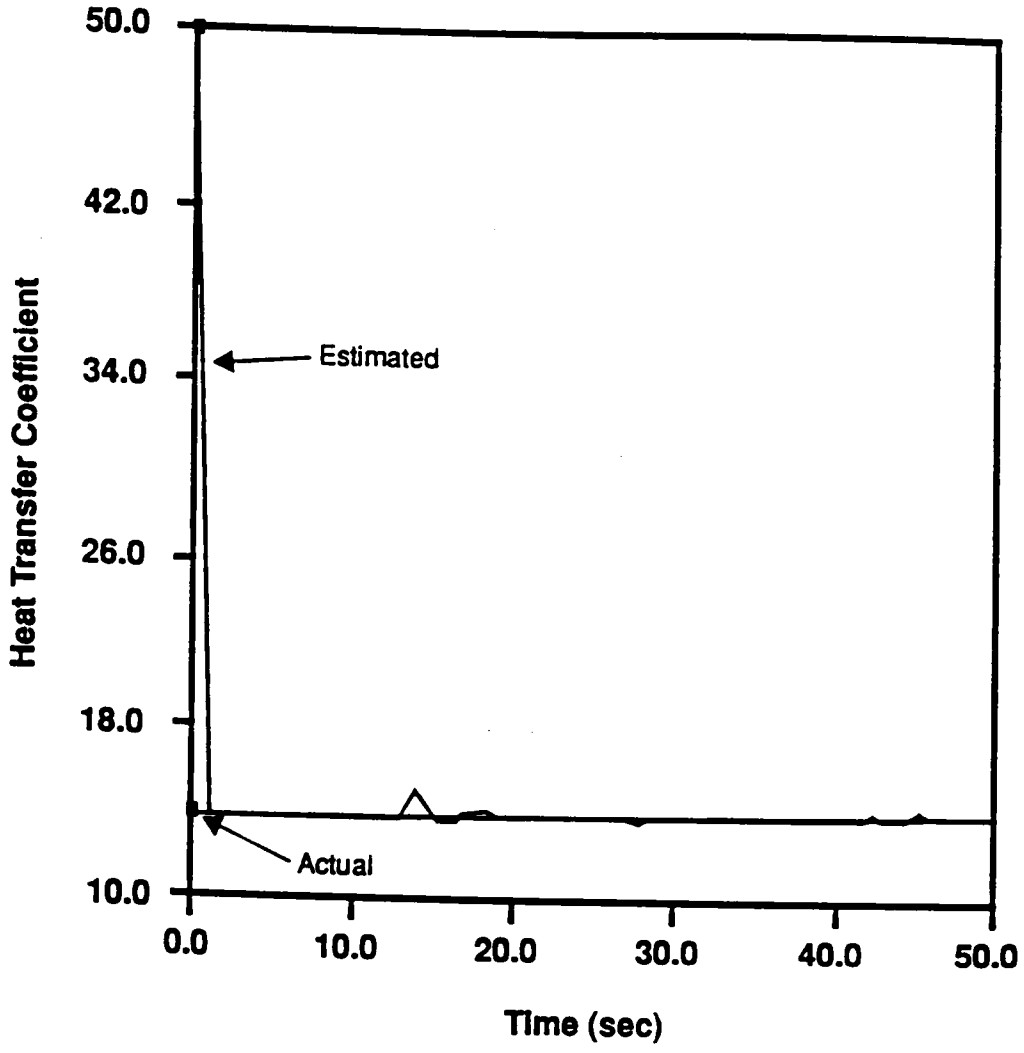

Fig. 6.2 Actual and estimated heat transfer coefficient for a guess of 269% larger than the actual value.

6.2.2. Reactivity and Average Plate Temperature Estimators

The problem of checking compliance in the reactivity inserting procedure and apparatus (i.e., the uncertain term is now the reactivity as a function of time) is addressed here. It is also assumed that the flow meter is not working, thus the coolant mass flow rate W is unknown, and therefore the system parameter λ_r cannot be calculated. The average plate temperature will also be estimated. The model equations will be modified in such a way that the reactivity term ρ_c becomes unknown and that the term containing λ_r becomes an unknown term. Therefore we assume that

$$g_4 = \lambda_r (X_4 - 1)$$

The model equations are

$$\dot{m}_1 = \rho_u m_1 + \frac{m_2}{\Lambda^*} = F_1 \qquad (6\text{-}32)$$

$$\dot{m}_2 = \lambda (m_1 - m_2) = F_2 \qquad (6\text{-}33)$$

$$\dot{m}_3 = \lambda_{p1} m_1 - \lambda_{p2}(m_3 - m_4) = F_3 \qquad (6\text{-}34)$$

$$\dot{m}_4 = \lambda_c(m_3 - m_4) - g_4 = F_4 \qquad (6\text{-}35)$$

$$\rho_u = \alpha_c - \alpha_b(m_4 - m_{04}) \tag{6-36}$$

The Lagrangian for this problem is

$$L = -\frac{1}{2} Q_1(m_1 - X_1)^2 - \frac{1}{2} Q_4(m_4 - X_4)^2 - \frac{1}{2} R_1(\alpha_c - \alpha_{0c})^2 - \frac{1}{2} R_2(g_4 - g_{04})^2 + \sum_i w_i(\dot{m}_i - F_i) \tag{6-37}$$

where Q_1, Q_4, R_1, R_2 are positive constants, α_{oc} and g_{o4} are the equilibrium initial values for the reactivity α_c and the uncertain term g_4, respectively. The adjoint state variables and uncertain terms are given by

$$-\dot{w}_1 = Q_1(m_1 - X_1) + \rho_u w_1 + \lambda w_2 + \lambda_{p1} w_3 \tag{6-38}$$

$$-\dot{w}_2 = \frac{w_1}{\Lambda^*} - \lambda w_2 \tag{6-39}$$

$$-\dot{w}_3 = -\lambda_{p2} w_3 + \lambda_c w_2 \tag{6-40}$$

$$-\dot{w}_4 = Q_4(m_4 - X_4) - \alpha_b m_1 w_1 - \lambda_c w_4 \tag{6-41}$$

$$\alpha_c = \alpha_{0c} - \frac{m_1 w_1}{R_1} \tag{6-42}$$

$$g_4 = g_{04} - \frac{w_4}{R_2} \qquad (6\text{-}43)$$

To obtain the value of g_{04}, consider equation (6-35). Setting $\dot{m}_4 = 0$, results in the following : $g_{04} = \lambda_c(m_{04} - m_{03})$. Substituting this value in equation (6-42) yields

$$g_4 = \lambda_c(m_{04} - m_{03}) - \frac{w_4}{R_2} \qquad (6\text{-}44)$$

The transient begins by ramping the reactivity for 3 seconds up to 10 cents, keeping it constant for 2 seconds, then ramping it down to zero. Then it was assumed that the mass flow rate has changed by 10% in the form of a unit impulse at some time after the reactivity transient has been completed. Figure 6-3 shows the actual and the estimated reactivity transient. Figure 6-4 shows the actual and estimated mass flow rates; and figure 6-5 shows the actual and estimated values of the fuel plate temperatures. It is evident that the algorithm provides accurate estimates of the unkown parameters; since the actual and estimated values followed the exact same trajectories in all cases. The accuracy of the algorithm is also demonstrated by observing the effect of the reactivity transient and the change in the mass flow rate on the other state variables; figures 6-6 and 6-7 show the effects of these changes on the coolant temperature and reactor power, respectively. It is interesting to notice that the coolant temperature decreased while the power increased when

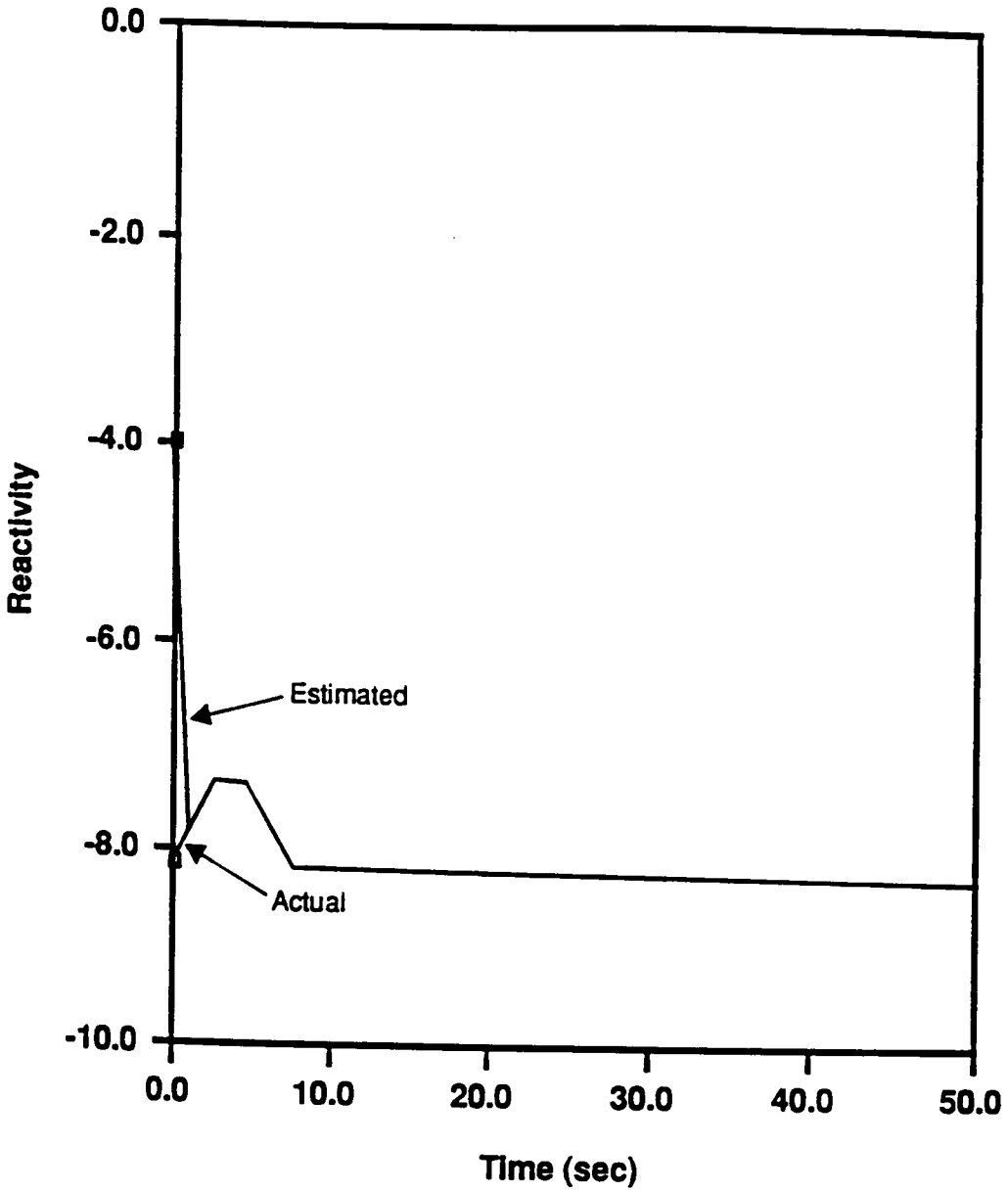

Fig. 6.3 Actual and estimated reactivity transient.

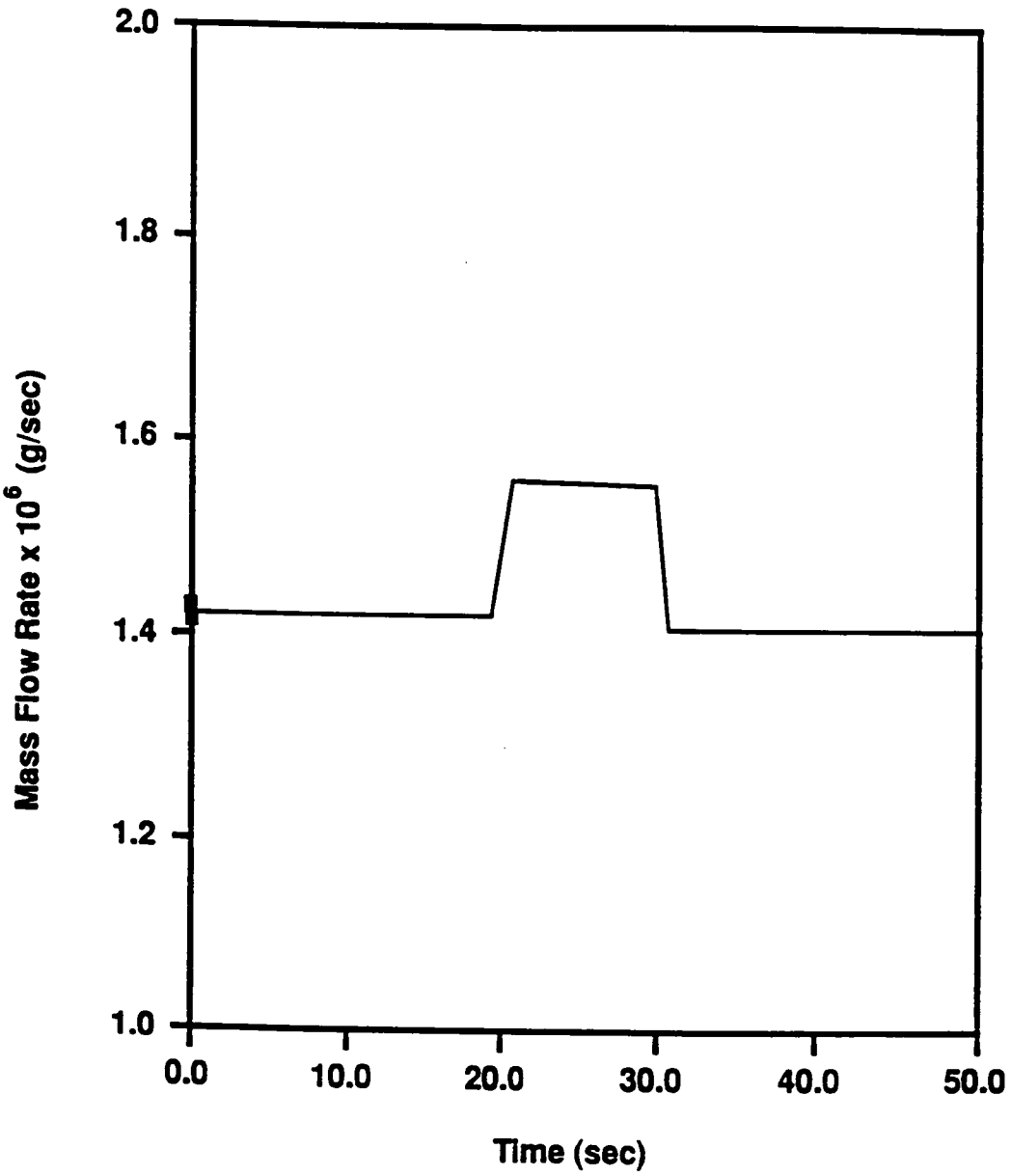

Fig. 6.4 Actual and estimated mass flow rates.

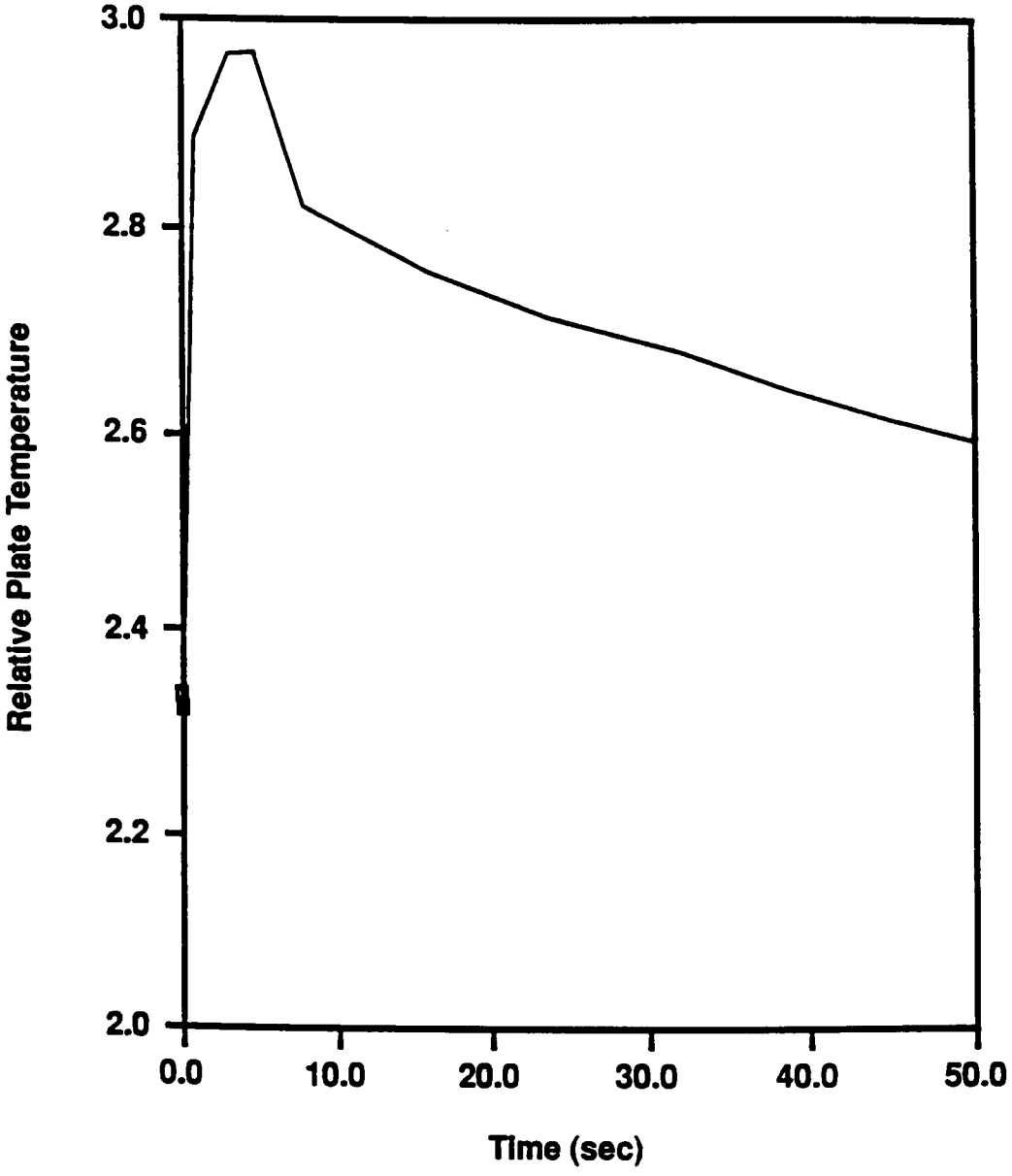

Fig. 6.5 Actual and estimated fuel plate temperature.

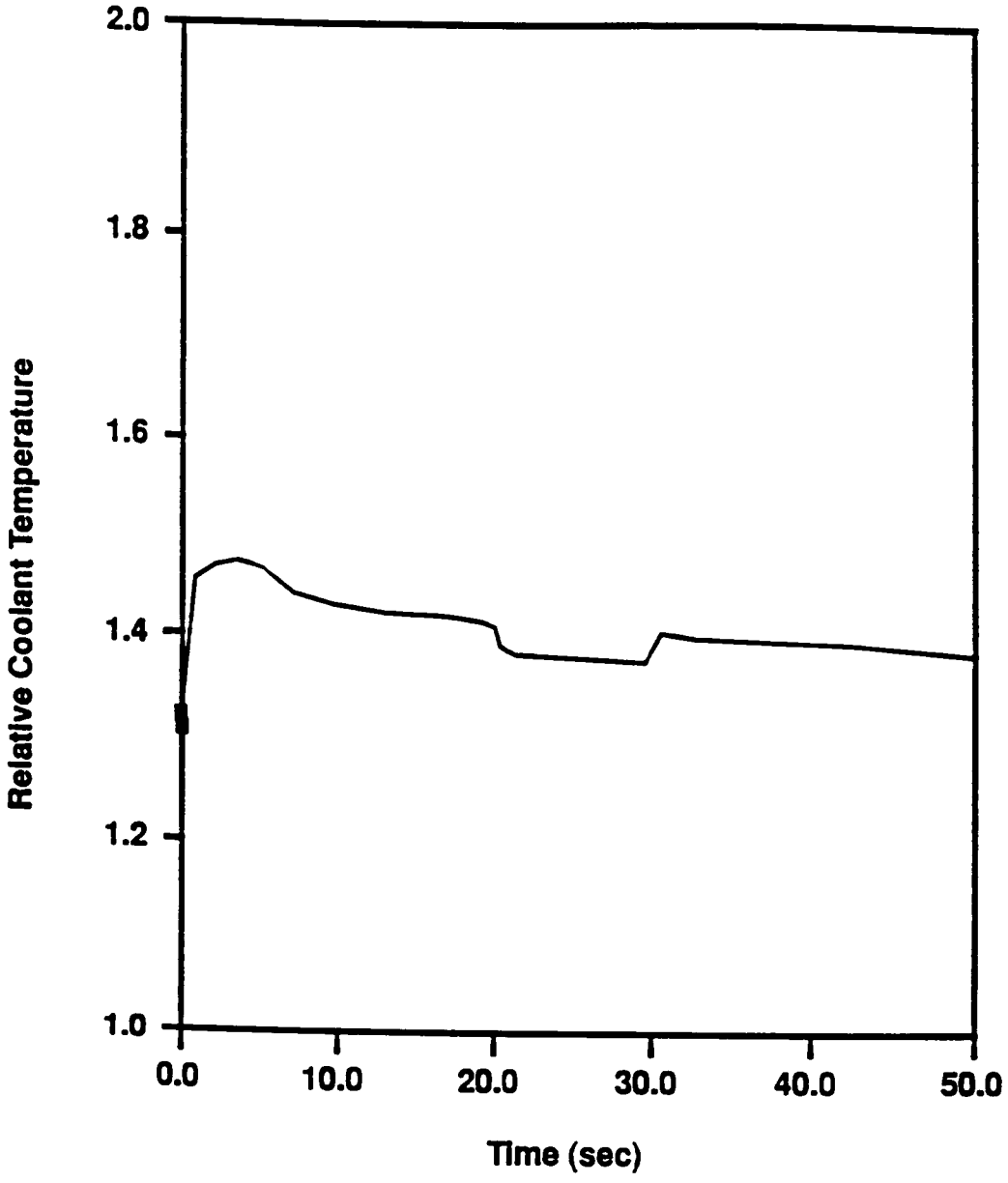

Fig. 6.6 Effect of the transient on the coolant temperature.

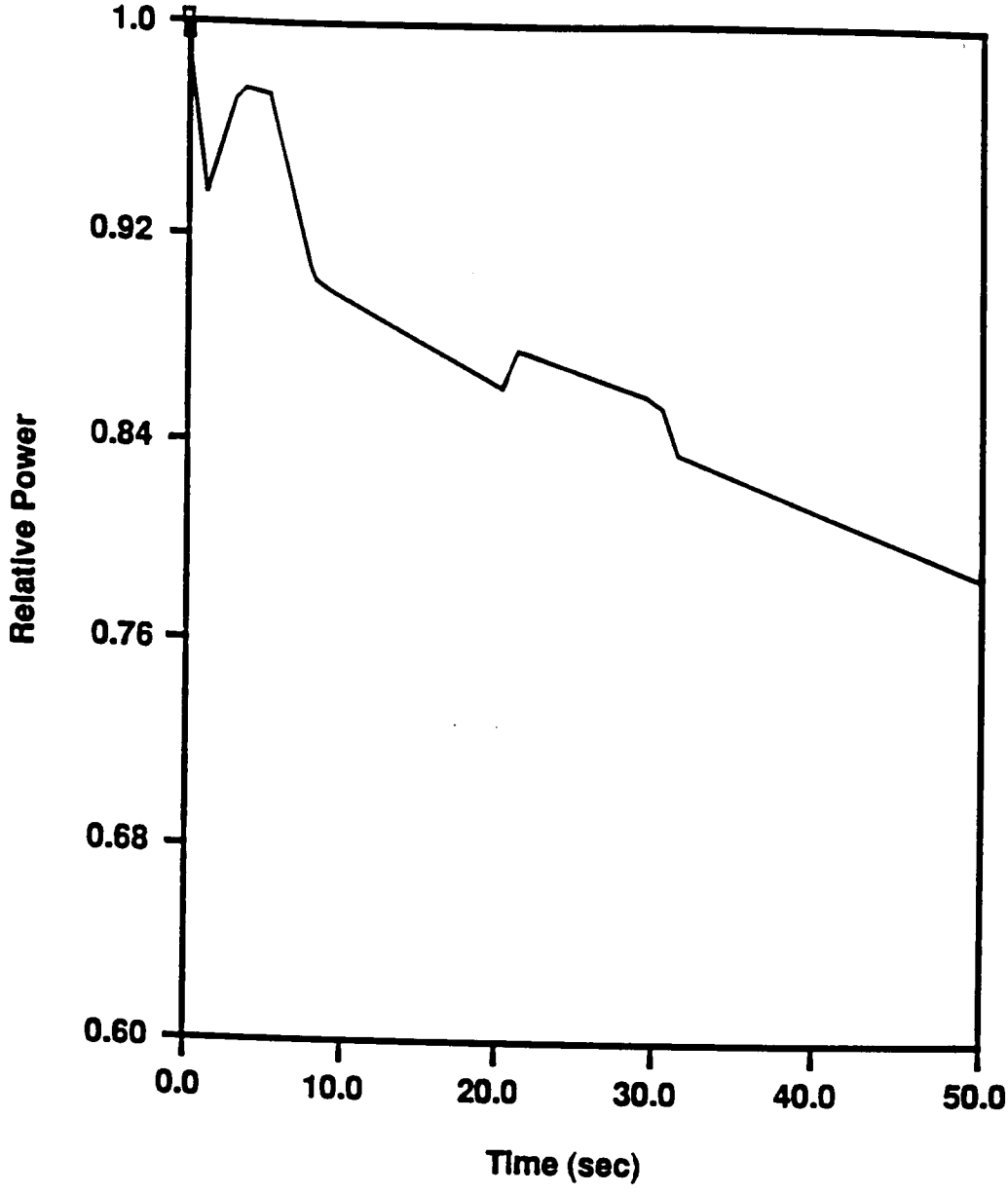

Fig. 6.7 Effect of the transient on the reactor power.

the mass flow rate increased. This can be explained by the fact that an increased mass flow rate means a shorter residence time of the coolant inside the core, which results in a drop in the coolant temperature. A lower coolant temperature, however, means a smaller negative coolant reactivity feedback, which in turn entails an increase in the reactor power.

Chapter VII

Conclusions

The one-dimensional statics calculations have shown the importance of the dimensions of the different reactor components in optimizing the core lifetime. It was shown in chapter II that the thicknesses of D_2O inside the island region and outside in the reflector played important roles in optimizing the core lifetime. It is recommended that other factors which may largely contribute to the optimization of the core lifetime be investigated, these factors include the fuel enrichment and fuel loading.

The two-dimensional calculations have been used to determine the amount of B^{10} as a burnable poison required to control the initial reactivity present in the ANS reactor. Calculations have shown that hafnium is the most suitable material for reactor control. Also the two-dimensional BOLD VENTURE computation system was used to calculate the ANS kinetic parameters; i.e., neutron lifetime and effective delayed neutron fraction. It is highly recommended that these kinetic parameters be calculated using kinetic methods and compare the results to those obtained from the static calculations.

The Two-Point-Two-Group kinetic model developed to study the kinetic behavior of the ANS reactor was compared to a One-Point-One-Group model. The results have shown a dramatic difference between the two models, especially for severe transients.

In spite of the fact that the 1P1G model was questionable due to the strong spatial dependence of the neutron flux, the results of the 2P2G model cannot be easily justified; only experimental measurements can prove the validity of the results. A more detailed calculation based on the space-time dependent diffusion calculations may be helpful in determining the validity of either one of the two models which were based on point kinetics approach.

The fission product xenon has always concerned the designers of nuclear reactors; especially large reactors and/or reactors operating at very high neutron fluxes. The study of this fission product poisoning has shown some very interesting results of the nonlinear phenomena (i.e., the presence of limit cycles) associated with the xenon and temperature feedback effects. A comparison between figure 5.3(a) and 5.3(b) shows that not only does the peak of the limit cycle decreases as the external reactivity becomes more negative, but also the period of oscillation decreases as well. It is recommended that extensive theoretical study be made in order to explain this result. The introduction of samarium to the model equations has eliminated the periodic constant-amplitude oscillations (i.e., limit cycles) of the state variables, and forced the solution towards a stable point.

Finally, the diagnostics algorithm based on the optimum control theory has successfully estimated the presumably unknown parameters and state variables of the system. Since the

methodology worked for the simplified model, it can be applied to more complicated models. Improvement over our model may include the estimation of the time-dependent heat transfer coefficient instead of the time-independent parameter presented in this study.

REFERENCES

References

1. F. C. Difilippo, W. R. Gambil, R. M. Moon, R. T. Primm, C.D. West, "A Preliminary Reactor Design for the Center for Neutron Research," Nuclear Instruments and Methods in Physics Research, pp 58-65 (1986).

2. F.C. Difilippo, W.R. Gambil, R.M. Moon, R.T. Primm, C. D.West, "An Intense Steady State Neutron Source," The CNR Reactor Proceedings of the Topical Meeting on Reactor Physics and Safety, September 17-19, 1986 Vol. 2, pp 1-18

3. J. Ryskamp, C. Oh, J. Lake, W. Lussie, R. Wadkins, "Comparison of Single and Split Core Concepts for the Advanced Neutron Source," [Proceedings of the International Reactor Physics Conference, American Nuclear Society], September, 1988, Vol. 2, pp 173-182

4. F. Difilippo, M. Abu-Shehadeh, R. Perez "Reactor Physics Calculations for the Control of the Advanced Neutron Source Reactor," [Proceedings of the International Reactor Physics Conference, American Nuclear Society], September, 1988, Vol. 2, pp 195-201.

5. F. Difilippo, M. Abu-Shehadeh, R. Perez
"Two-Point and Two-Energy Group Kinetics Model of the ANS Reactor," Transactions of the American Nuclear Society, June, 1989, Vol. 59, pp. 347-348.

6. T. Noh, S. Oh, S. Kim, D. Kim
Two-Point Reactor Kinetics for Large D_2O Reflected Systems, Nuclear Science and Engineering, American Nuclear Society, July 1987, manuscript no. 77-88.

7. "Post-Irradiation Analysis of Experimental Uranium Silicide Dispersion Fuel Plates," Proceedings of the 1984 International meeting on Reduced Enrichment for Research and Test Reactors, Argonne, IL, October 15-18, 1984, ANL/PERTR/TM-6 (July, 1985).

8. J.March- Leuba, D. Cacuci, R. Perez
"Nonlinear Dynamics and Stability of Boiling Water Reactors: Part 1- Qualitative Analysis," Nuclear Science and Engineering: Vol. 93, pp 111-123 (1986).

9. G.C. Baldwin
Kinetics of a Reactor Composed of Two Loosely Coupled Cores, Nuclear Science and Engineering: Vol. 6, pp 320-327 (1952).

10. J. Chernick, G. Lellouche, and W. Wollman,
"The Effect of Temperature on Xenon Instability," Nuclear Science and Engineering: Vol. 10, pp 120-131 (1961).

11. Y. Asahi, A. Akcasu
"An Investigation of Nonlinear Xenon Oscillation By Method of Averaging," Journal of Nuclear Energy, Vol. 27, pp. 839-855 (1973).

12. S. Kaplan, J. Yasinsky
"Natural Modes of the Xenon Problem with Flow Feedback," Nuclear Science and Engineering: Vol. 25, pp 430-438 (1966).

13. J. Chernick
"The Dynamics of a Xenon-Controlled Reactor"
Nuclear Science and Engineering: Vol. 8, pp 233-243 (1960).

14. David L. Hetrick
"Nonlinear Xenon Oscillations," Department of Nuclear and Energy Engineering, University of Arizona, Tucson, Arizona 85721, U.S.A.

15. Lynn E. Weaver
"Reactor Dynamics and Control," American Elsevier Publishing Company, New York, 1968.

16. W. Kermit Anderson and J.S. Theilacker,
"Neutron Absorber Materials for Reactor Control," Naval Reactors, Division of Reactor Development United States Atomic Energy Commission, 1962.

17. G. Robert Keepin
"Physics of Nuclear Kinetics," Addison-Wesley Publishing Company, 1965.

18. S. Glasstone
"Principles of Nuclear Reactor Engineering" D. Van Nostrand Company, 1955

19. Z. Akcasu, G. Lellouche, L. Shotkin,
"Mathematical Methods in Nuclear Reactor Dynamics," Academic Press, New York, 1971.

20. A.F. Henry
"Nuclear Reactor Analysis," The MIT Press, 1982.

21. J.R. Lamarsh
"Introduction to Nuclear Reactor Theory," Addison- Wesley Publishing Company, 1972.

22. J. Duderstadt, L. Hamilton,
"Nuclear Reactor Analysis," John Wiley and Sons, 1976.

23. A. Weinberg, E. Wigner,
"The Physical Theory of Neutron Chain Reactors," The University of Chicago Press, 1958.

24. F. Difilippo, Private communications, ORNL, EP&MD, MS 6363 Oak Ridge, Tennessee, 1987-1989

25. W.R.Gambill
"Recommended Correlations for Thermal Design for HFIR Core Composed of PLate-Type Element Without Spacers," memo to J. R. McWherter, ORNL, March 1, 1960.

26. J . C. Griess et al.,
"Effect of Heat Flux on the Corrosion of Aluminum by Water, Part I. Experimental Equipment and Preliminary Test Results," ORNL-2939, 1961.

27. D. E. Eastman and F. Seitz,
Cochairman Major Material Facilities Committee, National Research Council, National Academy Press, Washington, D.C., 1984.

28 D. R. Vondy, T. B. Fowler, G. W. Cunningham,
"The BOLD VENTURE Computation System for Nuclear Reactor Core Analysis, Version III," ORNL-5711 (1981)

29 C. March-Leuba
"Study and Development of Advanced Control Techniques for Nuclear Reactors and Robots," Dissertation presented for the Doctor of Philosophy Degree, The University of Tennessee, Knoxville, 1989

30 Advanced Continuous Simulation Language (ACSL), This language is designed for modelling and evaluating the performance of continuous systems described by time dependent, nonlinear differential equations.
Mitchel and Gauther Associates, edition 4.1, Concord, Mass. 01742

APPENDICES

Appendix A

A.1 Calculations of the global K_{eff} for the 2P2G model

Consider equations (4-9) to (4-14), set the extraneous sources S_c and S_r equal to zero, then set the time derivatives equal to zero as follows:

$$0 = \frac{k_{c1}(1-\beta^n)-1}{l_{c1}} N_{c1} + \frac{k_{c2}(1-\beta^n)}{l_{c2}} N_{c2} + \Sigma \lambda_i^n c_i^n \qquad (A\text{-}1)$$

$$0 = -\lambda_i^n c_i^n + \beta_i^n \left[\frac{k_{c1}}{l_{c1}} N_{c1} + \frac{k_{c2}}{l_{c2}} N_{c2} \right] \qquad (A\text{-}2)$$

$$0 = -\frac{N_{c2}}{l_{c2}} + \frac{N_{c1}}{l_{csl}} + k_{rc} \frac{N_{r2}}{l_{r2}} \qquad (A\text{-}3)$$

$$0 = -\frac{N_{r1}}{l_{r1}} + k_{cr} \frac{N_{c1}}{l_{c1}} + \Sigma \lambda_j^\gamma c_j^\gamma \qquad (A\text{-}4)$$

$$0 = -\lambda_j^\gamma c_j^\gamma + \beta_j^\gamma \left[\frac{k_{c1}}{l_{c1}} N_{c1} + \frac{k_{c2}}{l_{c2}} N_{c2} \right] \qquad (A\text{-}5)$$

$$0 = -\frac{N_{r2}}{l_{r2}} + \frac{N_{r1}}{l_{rsl}} \qquad (A\text{-}6)$$

using A-2, take summation over 'i' and solve for $\Sigma \lambda_i^n C_i^n$, this yields

$$\Sigma \lambda_i^n C_i^n = \frac{\beta^n}{l_{c1}} K_{c1} N_{c1} + \frac{\beta^n}{l_{c2}} K_{c2} N_{c2} \qquad (A\text{-}7)$$

Substitute A-7 in A-1, rearrange to obtain

$$0 = \frac{K_{c1}-1}{l_{c1}} N_{c1} + \frac{K_{c2}}{l_{c2}} N_{c2} \qquad \text{(A-8)}$$

Similarly, consider equation A-5, take summation over 'j' and solve for $\Sigma \lambda_j^{\gamma} C_j^{\gamma}$, this yields

$$\Sigma \lambda_j^{\gamma} C_j^{\gamma} = \frac{\beta^{\gamma}}{l_{c1}} K_{c1} N_{c1} + \frac{\beta^{\gamma}}{l_{c2}} K_{c2} N_{c2} \qquad \text{(A-9)}$$

substitute A-9 into A-4 and rearrange to obtain

$$0 = \frac{K_{cr} + \beta^{\gamma} K_{c1}}{l_{c1}} N_{c1} + \frac{\beta^{\gamma} K_{c2}}{l_{c2}} N_{c2} + \frac{-1}{l_{r1}} N_{r1} \qquad \text{(A-10)}$$

Now consider equations (A-3), (A-6), (A-8), and (A-10). Divide each production term by K_{eff}, i.e., divide each term containing K_{c1} or K_{c2} by K_{eff}. Then arrange in matrix form:

$$\mathbf{Ax} = \mathbf{0} \qquad \text{(A-11)}$$

where the vector **x** is given by

$$\mathbf{x} = \begin{bmatrix} N_{c1} \\ N_{c2} \\ N_{r1} \\ N_{r2} \end{bmatrix}$$

and the coefficient matrix A is given by

$$A = \begin{bmatrix} \frac{(K_{c1}/K_{eff})-1}{l_{c1}} & \frac{K_{c2}}{K_{eff} l_{c2}} & 0 & 0 \\ \frac{1}{l_{c1}} & \frac{1}{l_{c2}} & 0 & \frac{K_{rc}}{l_{r2}} \\ \frac{K_{rc}+\beta^{\gamma}(K_{c1}/K_{eff})}{l_{c1}} & \frac{\beta^{\gamma} K_{c2}}{l_{c2} K_{eff}} & \frac{-1}{l_{r1}} & 0 \\ 0 & 0 & \frac{-1}{l_{rsl}} & \frac{-1}{l_{r2}} \end{bmatrix}$$

Obtain the determinant of A, rearrange, and solve for K_{eff} to obtain

$$K_{eff} = K_{c1} + K_{c2} \left[\frac{l_{c1}}{l_{csl}} + K_{rc} K_{cr} \frac{l_{r1}}{l_{rsl}} \right] + \beta^{K} K_{c2} K_{rc} \frac{l_{r1}}{l_{rsl}} \qquad \text{(A-12)}$$

A.2 Calculations of the Initial Conditions for the 2P2G model

Consider equations (4-9) through (4-14), set the time derivatives equal to zero; obtain

$$0 = \frac{K_{0c1}(1-\beta^n)-1}{l_{c1}} N_{0c1} + \frac{K_{0c2}(1-\beta^n)}{l_{c2}} N_{0c2} + \sum \lambda_i^n c_{0i}^n + S_c \qquad \text{(A-13)}$$

$$0 = -\lambda_i^n c_{0i}^n + \beta_i^n \left[\frac{K_{0c1}}{l_{c1}} N_{0c1} + \frac{K_{0c2}}{l_{c2}} N_{0c2} \right] \qquad \text{(A-14)}$$

$$0 = -\frac{N_{0c2}}{l_{c2}} + \frac{N_{0c1}}{l_{csl}} + k_{0rc} \frac{N_{0r2}}{l_{r2}} \qquad \text{(A-15)}$$

$$0 = -\frac{N_{0r1}}{l_{r1}} + K_{0cr} \frac{N_{0c1}}{l_{c1}} + \sum \lambda_j^\gamma c_{0i}^\gamma + S_r \qquad \text{(A-16)}$$

$$0 = -\lambda_j^\gamma c_{0j}^\gamma + \beta_j^\gamma \left[\frac{K_{0c1}}{l_{c1}} N_{0c1} + \frac{K_{0c2}}{l_{c2}} N_{0c2} \right] \qquad \text{(A-17)}$$

$$0 = -\frac{N_{0r2}}{l_{r2}} + \frac{N_{0r1}}{l_{rsl}} \qquad \text{(A-18)}$$

Where the subscript "$_0$" refers to the initial values of the variables.

Solve equation (A-18) for N_{0r1}, this yields

$$N_{0r1} = \frac{l_{rsl}}{l_{r2}} N_{0r2} \qquad \text{(A-19)}$$

Consider equation (A-14), take summation over 'i' and solve for $\sum \lambda_i^n C_{0i}^n$, this yields

$$\sum \lambda_i^n C_{0i}^n = \frac{\beta^n}{l_{c1}} K_{0c1} N_{0c1} + \frac{\beta^n}{l_{c2}} K_{0c2} N_{0c2} \qquad \text{(A-20)}$$

Substitute (A-20) into (A-13) and solve for N_{0c2}, obtain

$$N_{0c2} = \frac{l_{c2}}{K_{0c2}}\left[\frac{1-K_{0c1}}{l_{c1}} N_{0c1} - S_c \right] \qquad \text{(A-21)}$$

Substitute (A-21) into (A-15), rearrange to obtain

$$X_1 Sc = X_2 N_{0c1} - X_3 N_{0r2} \qquad \text{(A-22)}$$

Where

$$X_1 = \frac{1}{K_{0c2}}, \quad X_2 = \frac{1-K_{0c1}}{K_{0c2} l_{c1}} - \frac{1}{l_{csl}}, \text{ and } \quad X_3 = \frac{K_{0rc}}{l_{r2}}$$

Now, simillarily consider equation (A-17), take summation over 'j' and solve for $\Sigma \lambda_j^n C_{0j}^n$, then substitute in (A-16), rearrange to obtain

$$Y_1 Sc = Y_2 N_{0c1} - Y_3 N_{0r2} + S_r \qquad \text{(A-23)}$$

where

$$Y_1 = \beta^{\gamma}, \quad Y_2 = \frac{k_{0cr} + \beta^{\gamma}}{l_{c1}}, \quad Y_3 = \frac{-l_{rsl}}{l_{r1} l_{r2}}$$

Consider (A-22) and (A-23), multiply (A-22) by Y_3, multiply (A-23) by X_3 and then add the two equations, this yields

$$(X_1 Y_3 + X_3 Y_1) Sc = (X_2 Y_3 + X_3 Y_2) N_{0c1} + X_3 S_r \qquad \text{(A-24)}$$

Solve for N_{0c1} to obtain

$$N_{0c1} = Z_1 Sc - Z_2 Sr \qquad \text{(A-25)}$$

where

$$Z_1 = \frac{(X_1 Y_3 + X_3 Y_1)}{(X_2 Y_3 + X_3 Y_2)} \quad , \quad Z_2 = \frac{X_3}{(X_2 Y_3 + X_3 Y_2)}$$

Now that N_{0c1} has been defined by equation (A-25), the other initial conditions can be defined in terms of N_{0c1}. Therefore, equations (A-19) and (A-21) are valid definitions for N_{0r1} and N_{0c2}, respectively. To calculate the initial conditions for N_{0r2}, we solve equation (A-22) for N_{0r2}, this yields

$$N_{0r2} = \frac{X_2}{X_3} N_{0c1} - \frac{X_1}{X_3} S_c \qquad \text{(A-26)}$$

The initial conditions for C^n_{0i} is obtained by solving equation (A-14) for C^n_{0i}, this yields

$$C^n_{0i} = \frac{\beta^n_i}{\lambda^n_i} \left[\frac{K_{0c1}}{l_{c1}} N_{0c1} + \frac{K_{0c2}}{l_{c2}} N_{0c2} \right] \qquad \text{(A-27)}$$

and the initial conditions for C^γ_{0i} is obtained by solving equation (A-17) for C^γ_{0i} as follows

$$C_{0i}^{\gamma} = \frac{\beta_i^{\gamma}}{\lambda_i^{\gamma}} \left[\frac{K_{0c1}}{l_{c1}} N_{0c1} + \frac{K_{0c2}}{l_{c2}} N_{0c2} \right] \qquad \text{(A-28)}$$

Thus, we have calculated the initial conditions for all of the state variables. In order to normalize the state variables to their initial conditions, we have to divide each state variable (equations (4-9) to (4-14)) by its initial condition.

Appendix B

B.1 Calculations of the Correction factor f_1

The amount of equilibrium xenon is given by the following formula (which will be derived in the next section)

$$X_0 = \frac{(\gamma_x + \gamma_I)\, P_0}{w(\lambda_x + A_1 P_0)} \qquad \text{(B-1)}$$

where P_0 is the initial power level. The BOLD VENTURE code was used to calculate the amount of equilibrium xenon X_0 for a power level P_0 = 280 MW. The other parameters in equation B-1 are all constants given in table 5.1 (except A_1).

Therefore, the value of A_1 can be calculated from equation B-1, the result is

$$A_1 = 2.40558 \times 10^{-12}$$

But A_1 is given by equation (5-17), solving this equation for f_1 yields

$$f_1 = \frac{A_1 w}{\sigma_a^{Xe} S \varepsilon \nu} \qquad \text{(B-2)}$$

Using table 5.1 and the value of A_1 above, the value of f_1 can be calculated. The result is

$$f_1 = 0.9626$$

B.2 Calculations of the Initial Conditions of the State Variables

Consider equations (5-15), (5-16), (5-18) (5-19), (5-24), (5-27), (5-45), and (5-46). Set the time derivatives equal to zero. The subscript "$_0$" will be added to each state-variable symbol to refer to the initial conditions:

$$0 = \lambda_I I_0 + \gamma_x \frac{P_0}{w} - \lambda_x X_0 - A_1 P_0 X_0 \qquad \text{(B-3)}$$

$$0 = \gamma_I \frac{P_0}{w} - \lambda_I I_0 \qquad \text{(B-4)}$$

$$0 = \frac{(\rho-1)\beta}{\Lambda} P_0 - \lambda C_0 \qquad \text{(B-5)}$$

$$0 = \frac{\beta}{\Lambda} P_0 - \lambda C_0 \qquad \text{(B-6)}$$

$$0 = \frac{1}{C_p M_p} P_0 - \frac{1}{\tau_{p0}} (T_{p0} - T_{b0}) \qquad \text{(B-7)}$$

$$0 = \frac{1}{\tau_{c0}} (T_{p0} - T_{b0}) - \frac{1}{\tau_r} (T_{b0} - T_{in}) \qquad \text{(B-8)}$$

$$0 = \lambda_{pm} P_{m0} - A2\ Sm_0 P_{m0} \qquad \text{(B-9)}$$

$$0 = \gamma_{pm} \frac{P_0}{w} - \lambda_{pm} P_{m0} \qquad \text{(B-10)}$$

Solve equation (B-4) for I_0 to obtain the initial conditions for iodine, the result is

$$I_0 = \frac{\gamma_I}{w\lambda_i} P_0 \qquad \text{(B-11)}$$

Substitute (B-11) into (B-3) and solve for X_0 to obtain the initial conditions for xenon

$$X_0 = \frac{(\gamma_x + \gamma_I) P_0}{w(\lambda_x + A_1 P_0)} \qquad \text{(B-12)}$$

Solve equation (B-5) for C_0 to obtain the initial conditions for the delayed neutron precursor(notice that $\rho=0$ at steady state), the result is

$$C_0 = \frac{\beta}{\Lambda\lambda} P_0 \qquad \text{(B-13)}$$

Solving equation (B-13) for Pm0 gives the initial conditions for Promethium

$$Pm_0 = \frac{\gamma_{Pm}}{w\lambda_{Pm}} P_0 \qquad \text{(B-14)}$$

Substitute equation (B-14) into equation (B-9) and solve for Sm_0 to obtain the initial conditions for samarium

$$Sm_0 = \frac{\gamma_{Sm}}{S\varepsilon v \sigma_a^{Sm}} P_0 \qquad \text{(B-15)}$$

To obtain the initial conditions for the average temperatures of the bulk and fuel plates, consider equations (B-7) and (B-8). Solve equatin (B-7) for $(T_{p0}-T_{b0})$, this yields

$$(T_{p0}-T_{b0}) = \frac{1}{C_p\ M_p\ \lambda_{P0}} P_0 \qquad \text{(B-16)}$$

Also solve equation B-8 for $(T_{p0}-T_{b0})$, this yields

$$(T_{p0}-T_{b0}) = \frac{\lambda_r}{\lambda_{c0}} (T_{b0} - T_{in}) \qquad \text{(B-17)}$$

Equating the right- hand sides of equations (B-16) and (B-17) yields

$$\frac{\lambda_r}{\lambda_{c0}} (T_{b0} - T_{in}) = \frac{1}{C_p\ M_p\ \lambda_{P0}} P_0 \qquad \text{(B-18)}$$

Solve B-18 for T_{b0} to obtain the initial conditions for the average bulk coolant temperature

$$T_{b0} = \frac{\lambda_{c0}}{C_p\ M_p\ \lambda_{P0}\ \lambda_r} P_0 + T_{in} \qquad \text{(B-19)}$$

Solving equation B-16 for T_{p0} gives the initial conditions for the average plate temperature

$$T_{p0} = \frac{1}{C_p\ M_p\ \lambda_{P0}} P_0 + T_{b0} \qquad \text{(B-20)}$$

The normalized form of the model equations is obtained by dividing each state variable by its initial condition.

B.3 Calculations of the Correction Factor f_2

The reactivity loss due to equilibrium xenon is given by

$$\rho_{xe_0} = \frac{\sigma_a^{xe}}{\xi \Sigma_f V_{core} \beta} X_0$$

The parameter ξ is given in reference 19 ,(p.213), by a very complicated expression. However, if the flux, macroscopic fission x-section of the fuel, and the xenon concentration are all uniform throughout the reactor core then

$$\xi = \nu = 2.43$$

But since these quantities have strong spatial dependence, then ξ has been assumed to be equal to ν multiplied by some fudge factor f_2. Solving the above equation for ξ yields

$$\xi = \frac{\sigma_a^{xe}}{\beta \rho_{xe_0} \Sigma_f V_{core}} X_0$$

But since $\xi = \nu f_2$ then

$$f2 = \frac{\sigma_a^{xe}}{\beta \rho_{xe_0} \Sigma_f \nu V_{core}} X_0$$

In order to evaluate f_2, the BOLD VENTURE computation system was used to evaluate the reactivity loss due to equilibrium xenon and the amount of equilibrium xenon. The results were as follows:

$\rho_{xe_0} = 0.032$

$X_0 = 2.1 \times 10^{16}$

The quantities σ_a^{xe}, Σ_f, and ν are given in table 5.1. Accordingly

$f_2 = 1.2265$

VITA

Name:	Mohammed Abu-Shehadeh
Date of Birth:	December, 25 1957
Place of Birth:	Gazza, Palestine
Education:	-Elementary School (Gazza, Palestine) -Preparatory and Secondary School (Zerka, Jordan) -B.Sc. in Chemistry at Al-Fateh University, Tripoli, Lybia, Started September 1976, graduated June, 1980 with 4.0 average, an honor certificate was granted. -M.S. in Nuclear Engineering at Louisiana State University, Started January 1982, graduated August 1984. -Ph.D. in Nuclear Engineering at the University of Tennessee, Knoxville, Started September 1984, graduated December 1989. An honor certificate was granted in 1985 by the American Nuclear Society upon winning first place in the student design competition, graduate division.